Defense Threat Reduction Agency
8725 John J. Kingman Road, MS-6201
Fort Belvoir, VA 22060-6201

DTRA-TR-24-011

TECHNICAL REPORT

Parameterization of a Systemic Time Dependent Physiological Model for Combined Thermal Burn and Widespread Radiation Injury

DISTRIBUTION A. Approved for public release: distribution unlimited.

March 2024

HDTRA1-14-D-0003

Prepared by:
Applied Research Associates, Inc.
801 N. Quincy Street
Suite 700
Arlington, VA 22203

UNIT CONVERSION TABLE

U.S. customary units to and from international units of measurement*

U.S. Customary Units	Multiply by → / ← Divide by†		International Units
Length/Area/Volume			
inch (in)	2.54	$\times 10^{-2}$	meter (m)
foot (ft)	3.048	$\times 10^{-1}$	meter (m)
yard (yd)	9.144	$\times 10^{-1}$	meter (m)
mile (mi, international)	1.609 344	$\times 10^{3}$	meter (m)
mile (nmi, nautical, U.S.)	1.852	$\times 10^{3}$	meter (m)
barn (b)	1	$\times 10^{-28}$	square meter (m^2)
gallon (gal, U.S. liquid)	3.785 412	$\times 10^{-3}$	cubic meter (m^3)
cubic foot (ft^3)	2.831 685	$\times 10^{-2}$	cubic meter (m^3)
Mass/Density			
pound (lb)	4.535 924	$\times 10^{-1}$	kilogram (kg)
atomic mass unit (AMU)	1.660 539	$\times 10^{-27}$	kilogram (kg)
pound-mass per cubic foot ($lb\ ft^{-3}$)	1.601 846	$\times 10^{1}$	kilogram per cubic meter ($kg\ m^{-3}$)
Pound-force (lbf avoirdupois)	4.448 222		Newton (N)
Energy/Work/Power			
electron volt (eV)	1.602 177	$\times 10^{-19}$	joule (J)
erg	1	$\times 10^{-7}$	joule (J)
kiloton (kT) (TNT equivalent)	4.184	$\times 10^{12}$	joule (J)
British thermal unit (Btu) (thermochemical)	1.054 350	$\times 10^{3}$	joule (J)
foot-pound-force (ft lbf)	1.355 818		joule (J)
calorie (cal) (thermochemical)	4.184		joule (J)
Pressure			
atmosphere (atm)	1.013 250	$\times 10^{5}$	pascal (Pa)
pound force per square inch (psi)	6.984 757	$\times 10^{3}$	pascal (Pa)
Temperature			
degree Fahrenheit (°F)	[T(°F) − 32]/1.8		degree Celsius (°C)
degree Fahrenheit (°F)	[T(°F) + 459.67]/1.8		kelvin (K)
Radiation			
activity of radionuclides [curie (Ci)]	3.7	$\times 10^{10}$	per second (s^{-1}‡)
air exposure [roentgen (R)]	2.579 760	$\times 10^{-4}$	coulomb per kilogram ($C\ kg^{-1}$)
absorbed dose (rad)	1	$\times 10^{-2}$	joule per kilogram ($J\ kg^{-1}$§)
equivalent and effective dose (rem)	1	$\times 10^{-2}$	joule per kilogram ($J\ kg^{-1}$**)

*Specific details regarding the implementation of SI units may be viewed at http://www.bipm.org/en/si/.

†Multiply the U.S. customary unit by the factor to get the international unit. Divide the international unit by the factor to get the U.S. customary unit.

‡The special name for the SI unit of the activity of a radionuclide is the becquerel (Bq). ($1\ Bq = 1\ s^{-1}$).

§The special name for the SI unit of absorbed dose is the gray (Gy). ($1\ Gy = 1\ J\ kg^{-1}$).

**The special name for the SI unit of equivalent and effective dose is the sievert (Sv). ($1\ Sv = 1\ J\ kg^{-1}$).

REPORT DOCUMENTATION PAGE

PLEASE DO NOT RETURN YOUR FORM TO THE ABOVE ORGANIZATION.

1. REPORT DATE	2. REPORT TYPE	3. DATES COVERED	
		START DATE	END DATE
08-03-2024	Technical Report		

4. TITLE AND SUBTITLE

Parameterization of a Systemic Time-Dependent Physiological Model for Combined Thermal Burn and Widespread Radiation Injury

5a. CONTRACT NUMBER	5b. GRANT NUMBER	5c. PROGRAM ELEMENT NUMBER
HDTRA1-14-D-0003		
5d. PROJECT NUMBER	**5e. TASK NUMBER**	**5f. WORK UNIT NUMBER**

6. AUTHOR(S)

Amy Creel, Quintessa Hay, Kyle Gaffney, PhD, Rafael Henriquez-Rivera, PhD, Christina Wagner, PhD

7. PERFORMING ORGANIZATION NAME(S) AND ADDRESS(ES)	8. PERFORMING ORGANIZATION REPORT NUMBER
Applied Research Associates, Inc. 801 N. Quincy Street, Suite 700 Arlington, VA 22203	

9. SPONSORING/MONITORING AGENCY NAME(S) AND ADDRESS(ES)	10. SPONSOR/MONITOR'S ACRONYM(S)	11. SPONSOR/MONITOR'S REPORT NUMBER(S)
Defense Threat Reduction Agency - Nuclear Technologies Department 8725 John J. Kingman Road, Mail Stop 6201 Fort Belvoir, VA 22060-6201	DTRA-RD-NTS	DTRA-TR-24-011

12. DISTRIBUTION/AVAILABILITY STATEMENT

DISTRIBUTION A. Approved for public release: distribution is unlimited.

13. SUPPLEMENTARY NOTES

14. ABSTRACT

Multi-test Extended Fourier Amplitude Sensitivity Test (MeFAST), a global sensitivity analysis method, was applied to a time-dependent physiological model for combined injury following thermal burn and widespread radiation exposure. A reduced parameter space was then sampled to obtain a set of reasonable parameter estimates for implementation of the model in relevant software. The methodology presented herein will be used in future work to parameterize other physiologically driven models of combined injury.

15. SUBJECT TERMS

Combined injury, widespread radiation, thermal burn, modeling, global sensitivity analysis, MeFAST, parameter sampling

16. SECURITY CLASSIFICATION OF:			17. LIMITATION OF ABSTRACT	18. NUMBER OF PAGES
a. REPORT	b. ABSTRACT	C. THIS PAGE		
U	U	U	U	116

19a. NAME OF RESPONSIBLE PERSON	19b. PHONE NUMBER *(Include area code)*
Lee Alleman	+1 (571) 616-2599

PREVIOUS EDITION IS OBSOLETE.

STANDARD FORM 298 (REV. 5/2020)

Prescribed by ANSI Std. Z39.18

This page intentionally left blank.

Parameterization of a Systemic Time-Dependent Physiological Model for Combined Thermal Burn and Widespread Radiation Injury

Table of Contents

Table of Contents i
List of Figures iii
List of Tables xiii
Acknowledgements xiv
Executive Summary 15
Section 1. Introduction 16
Section 2. Model Background 17
2.1 Model Overview 17
2.2 Initial Conditions for Sensitivity Analysis 19
Section 3. Sensitivity Analysis 22
3.1 Methods 22
3.1.1. MeFAST for Parameter Screening 23
3.1.2. MeFAST for Global Sensitivity Analysis of the TDPM 25
3.1.3. Parameter Selection Algorithm 25
3.2 Results 26
3.2.1. Parameter Screening in the Bone Marrow and Thermal Burn Compartments 26
3.2.2. MeFAST for Global Sensitivity Analysis of the TDPM 27
3.2.3. Parameter Selection 28
Section 4. Parameterization 29
4.1 Methods 29
4.1.1. Acceptability Criteria for Brute-Force with Latin Hypercube Sampling 29
4.1.2. Parameter Distributions and Sampling 30
4.1.3. Representative Set 30
4.2 Results 31
4.2.1. Accepted Parameter Combinations 31
4.2.2. Representative Set 35
Section 5. Discussion 39

Section 6. References 40
Appendix A. Model Equations 45
Appendix B. Model Parameters 50
Appendix C. Sensitivity Analysis Plots 61
C.1. MeFAST Plots for Parameter Screening in the Bone Marrow 61
C.1.1. Line Plots of Total Sensitivity Index Rankings 61
C.1.2. Heatmaps of Statistical Significance 74
C.2. MeFAST Plots for Global Sensitivity Analysis of the TDPM 77
C.2.1. Line Plots of Total Sensitivity Index Rankings 77
C.2.2. Heatmaps of Statistical Significance 107
Appendix D. Acronyms and Abbreviations 116

List of Figures

Figure 1. Schematic diagram for the systemic TDPM of combined injury following thermal burn and widespread radiation exposure (Gaffney et al., 2023). This figure shows how immune cells created in the bone marrow from stem cells mature, differentiate, transition to the injury site, and interact with the injury to progress wound healing. 17

Figure 2. Flowchart depicting the updated methodology for performing global sensitivity analysis on the systemic TDPM for combined injury following thermal burn and widespread radiation exposure. The increased number of parameters in state variables in the systemic TDPM significantly increases the computational intensity of GSA. The new methodology includes a screening process which identifies non-influential parameters in the bone marrow and thermal burn compartments and removes them from consideration prior to running GSA on the systemic TDPM, thereby reducing its computational intensity. 22

Figure 3. Flowchart for the algorithm to determine whether a parameter in the bone marrow compartment should be included in global sensitivity analysis (GSA) or fixed at its baseline value. In the first step, if all three of the initial conditions have significance counts less than eight, the parameter is fixed. If two or more of the initial conditions have significance counts greater than or equal to eight, the parameter is included in GSA. If only one of the initial conditions produces a significance count greater than or equal to eight, the algorithm proceeds to the next step. In the next step, only the initial condition with a significance count greater than or equal to eight is considered. If its significance count is also greater than or equal to 16, the parameter is included in GSA. Otherwise, the parameter is fixed. 24

Figure 4. Flowchart for the algorithm to determine whether a parameter of the systemic TDPM should be estimated during parameterization or fixed at its baseline value. In the first step, if all three of the initial conditions have significance counts less than 21, the parameter is fixed. If two or more of the initial conditions have significance counts greater than or equal to 21, the parameter is estimated. If only one of the initial conditions produces a significance count greater than or equal to 21, the algorithm proceeds to the next step. In the next step, only the initial condition with a significance count greater than or equal to 21 is considered. If its significance count is also greater than or equal to 42, the parameter is estimated. Otherwise, the parameter is fixed at its baseline value. 26

Figure 5. Flow chart depicting the method by which a representative set is chosen from the accepted parameter sets. First, the weighted mean square error (MSE) is computed for each parameter set. For the 5% of parameter sets with the smallest weighted MSE, an R^2 value is obtained and then ranked for each state variable. Finally, the overall R^2 rank is computed for each of these sets, and the parameter set with the best overall rank is chosen as the representative set. This method of selection ensures that the representative parameter set not only represents average model dynamics well (indicated by its small weighted MSE), but also most closely reproduces the average dynamics for each individual state variable (indicated by its large R^2). 31

Figure 6. Example dynamics predicted by the TDPM for superficial thermal burn (IC1). The accepted sets were randomly sampled and simulated 100 times to show the diverse model behavior generated by these sets. Observe that the healing dynamics of thermal burn injury do not greatly perturb the systemic populations of immune cells, confirming the collapsibility of the WITBM to the STBM and LITBM. 32

Figure 7. Example dynamics predicted by the TDPM for partial superficial thickness thermal burn (IC2). The accepted sets were randomly sampled and simulated 100 times to show the diverse model behavior generated by these sets. 33

Figure 8. Example dynamics predicted by the TDPM for partial superficial thickness thermal burn (IC2). The accepted sets were randomly sampled and simulated 100 times to show the diverse model behavior generated by these sets. 34

Figure 9. Dynamics of the bone marrow compartment, lymphatic tissue compartment, blood vessel compartment, and thermal burn compartment of the systemic TDPM for combined injury following thermal burn and widespread radiation exposure, as predicted by the representative set for IC1 (superficial thickness burn; solid lines), IC2 (partial superficial thickness burn; dashed lines), and IC3 (deep partial thickness burn; dash-dot lines). 38

Figure 10. Ranked total sensitivity indices for β_{sm} across all 40 MeFAST outputs for (a) IC1, superficial thermal burn; (b) IC2, superficial partial thickness thermal burn; and (c) IC3, deep partial thickness thermal burn. 61

Figure 11. Ranked total sensitivity indices for C_0 across all 40 MeFAST outputs for (a) IC1, superficial thermal burn; (b) IC2, superficial partial thickness thermal burn; and (c) IC3, deep partial thickness thermal burn. 61

Figure 12. Ranked total sensitivity indices for n_s across all 40 MeFAST outputs for (a) IC1, superficial thermal burn; (b) IC2, superficial partial thickness thermal burn; and (c) IC3, deep partial thickness thermal burn. 62

Figure 13. Ranked total sensitivity indices for k_{aIg} across all 40 MeFAST outputs for (a) IC1, superficial thermal burn; (b) IC2, superficial partial thickness thermal burn; and (c) IC3, deep partial thickness thermal burn. 62

Figure 14. Ranked total sensitivity indices for k_{aIm} across all 40 MeFAST outputs for (a) IC1, superficial thermal burn; (b) IC2, superficial partial thickness thermal burn; and (c) IC3, deep partial thickness thermal burn. 63

Figure 15. Ranked total sensitivity indices for k_{aIl} across all 40 MeFAST outputs for (a) IC1, superficial thermal burn; (b) IC2, superficial partial thickness thermal burn; and (c) IC3, deep partial thickness thermal burn. 63

Figure 16. Ranked total sensitivity indices for k_{Irg} across all 40 MeFAST outputs for (a) IC1, superficial thermal burn; (b) IC2, superficial partial thickness thermal burn; and (c) IC3, deep partial thickness thermal burn. 64

Figure 17. Ranked total sensitivity indices for k_{Irm} across all 40 MeFAST outputs for (a) IC1, superficial thermal burn; (b) IC2, superficial partial thickness thermal burn; and (c) IC3, deep partial thickness thermal burn. 64

Figure 18. Ranked total sensitivity indices for k_{Irl} across all 40 MeFAST outputs for (a) IC1, superficial thermal burn; (b) IC2, superficial partial thickness thermal burn; and (c) IC3, deep partial thickness thermal burn. 65

Figure 19. Ranked total sensitivity indices for k_{Irlt} across all 40 MeFAST outputs for (a) IC1, superficial thermal burn; (b) IC2, superficial partial thickness thermal burn; and (c) IC3, deep partial thickness thermal burn. 65

Figure 20. Ranked total sensitivity indices for k_{ag} across all 40 MeFAST outputs for (a) IC1, superficial thermal burn; (b) IC2, superficial partial thickness thermal burn; and (c) IC3, deep partial thickness thermal burn. 66

Figure 21. Ranked total sensitivity indices for I_{∞} across all 40 MeFAST outputs for (a) IC1, superficial thermal burn; (b) IC2, superficial partial thickness thermal burn; and (c) IC3, deep partial thickness thermal burn. 66

Figure 22. Ranked total sensitivity indices for k_{tbd} across all 40 MeFAST outputs for (a) IC1, superficial thermal burn; (b) IC2, superficial partial thickness thermal burn; and (c) IC3, deep partial thickness thermal burn. 67

Figure 23. Ranked total sensitivity indices for k_{tbn} across all 40 MeFAST outputs for (a) IC1, superficial thermal burn; (b) IC2, superficial partial thickness thermal burn; and (c) IC3, deep partial thickness thermal burn. 67

Figure 24. Ranked total sensitivity indices for k_{tbm} across all 40 MeFAST outputs for (a) IC1, superficial thermal burn; (b) IC2, superficial partial thickness thermal burn; and (c) IC3, deep partial thickness thermal burn. 68

Figure 25. Ranked total sensitivity indices for k_{tbl} across all 40 MeFAST outputs for (a) IC1, superficial thermal burn; (b) IC2, superficial partial thickness thermal burn; and (c) IC3, deep partial thickness thermal burn. 68

Figure 26. Ranked total sensitivity indices for k_{QPmax} across all 40 MeFAST outputs for (a) IC1, superficial thermal burn; (b) IC2, superficial partial thickness thermal burn; and (c) IC3, deep partial thickness thermal burn. 69

Figure 27. Ranked total sensitivity indices for n_{kQP} across all 40 MeFAST outputs for (a) IC1, superficial thermal burn; (b) IC2, superficial partial thickness thermal burn; and (c) IC3, deep partial thickness thermal burn. 69

Figure 28. Ranked total sensitivity indices for δ_Q across all 40 MeFAST outputs for (a) IC1, superficial thermal burn; (b) IC2, superficial partial thickness thermal burn; and (c) IC3, deep partial thickness thermal burn. 70

Figure 29. Ranked total sensitivity indices for δ_P across all 40 MeFAST outputs for (a) IC1, superficial thermal burn; (b) IC2, superficial partial thickness thermal burn; and (c) IC3, deep partial thickness thermal burn. 70

Figure 30. Ranked total sensitivity indices for δ_{GS} across all 40 MeFAST outputs for (a) IC1, superficial thermal burn; (b) IC2, superficial partial thickness thermal burn; and (c) IC3, deep partial thickness thermal burn. 71

Figure 31. Ranked total sensitivity indices for δ_{MS} across all 40 MeFAST outputs for (a) IC1, superficial thermal burn; (b) IC2, superficial partial thickness thermal burn; and (c) IC3, deep partial thickness thermal burn. 71

Figure 32. Ranked total sensitivity indices for δ_{LS} across all 40 MeFAST outputs for (a) IC1, superficial thermal burn; (b) IC2, superficial partial thickness thermal burn; and (c) IC3, deep partial thickness thermal burn. 72

Figure 33. Ranked total sensitivity indices for δ_{GSS} across all 40 MeFAST outputs for (a) IC1, superficial thermal burn; (b) IC2, superficial partial thickness thermal burn; and (c) IC3, deep partial thickness thermal burn. 72

Figure 34. Ranked total sensitivity indices for δ_{MSS} across all 40 MeFAST outputs for (a) IC1, superficial thermal burn; (b) IC2, superficial partial thickness thermal burn; and (c) IC3, deep partial thickness thermal burn. 73

Figure 35. Ranked total sensitivity indices for δ_{LSS} across all 40 MeFAST outputs for (a) IC1, superficial thermal burn; (b) IC2, superficial partial thickness thermal burn; and (c) IC3, deep partial thickness thermal burn. 73

Figure 36. Significance results of MeFAST for parameters of the bone marrow compartment with respect to the state variables of the bone marrow compartment for IC1 at days one, three, five, seven, and ten post-injury. A shaded box indicates that the parameter was flagged as statistically significant at the respective state variable and time point by at least two of the three tests performed during MeFAST. These significance results were passed through the algorithm presented in Section 3.1.1.1 to determine which parameters could be fixed during GSA of the systemic TDPM. 74

Figure 37. Significance results of MeFAST for parameters of the bone marrow compartment with respect to the state variables of the bone marrow compartment for IC2 at days one, three, five, seven, and ten post-injury. A shaded box indicates that the parameter was flagged as statistically significant at the respective state variable and time point by at least two of the three tests performed during MeFAST. These significance results were passed through the algorithm presented in Section 3.1.1.1 to determine which parameters could be fixed during GSA of the systemic TDPM. 75

Figure 38. Significance results of MeFAST for parameters of the bone marrow compartment with respect to the state variables of the bone marrow compartment for IC3 at days one, three, five, seven, and ten post-injury. A shaded box indicates that the parameter was flagged as statistically significant at the respective state variable and time point by at least two of the three tests performed during MeFAST. These significance results were passed through the algorithm presented in Section 3.1.1.1 to determine which parameters could be fixed during GSA of the systemic TDPM. 76

Figure 39. Ranked total sensitivity indices for Deb_H across all 105 MeFAST outputs for (a) IC1, superficial thermal burn; (b) IC2, superficial partial thickness thermal burn; and (c) IC3, deep partial thickness thermal burn. 77

Figure 40. Ranked total sensitivity indices for Dam^{∞}_{lvm} across all 105 MeFAST outputs for (a) IC1, superficial thermal burn; (b) IC2, superficial partial thickness thermal burn; and (c) IC3, deep partial thickness thermal burn. 77

Figure 41. Ranked total sensitivity indices for N_1^{∞} across all 105 MeFAST outputs for (a) IC1, superficial thermal burn; (b) IC2, superficial partial thickness thermal burn; and (c) IC3, deep partial thickness thermal burn. 78

Figure 42. Ranked total sensitivity indices for $M1_1^{\infty}$ across all 105 MeFAST outputs for (a) IC1, superficial thermal burn; (b) IC2, superficial partial thickness thermal burn; and (c) IC3, deep partial thickness thermal burn. 78

Figure 43. Ranked total sensitivity indices for $M2_1^{\infty}$ across all 105 MeFAST outputs for (a) IC1, superficial thermal burn; (b) IC2, superficial partial thickness thermal burn; and (c) IC3, deep partial thickness thermal burn. 79

Figure 44. Ranked total sensitivity indices for $M2^{\infty}$ across all 105 MeFAST outputs for (a) IC1, superficial thermal burn; (b) IC2, superficial partial thickness thermal burn; and (c) IC3, deep partial thickness thermal burn. 79

Figure 45. Ranked total sensitivity indices for $M2_E^{\infty}$ across all 105 MeFAST outputs for (a) IC1, superficial thermal burn; (b) IC2, superficial partial thickness thermal burn; and (c) IC3, deep partial thickness thermal burn. 80

Figure 46. Ranked total sensitivity indices for F_1^{∞} across all 105 MeFAST outputs for (a) IC1, superficial thermal burn; (b) IC2, superficial partial thickness thermal burn; and (c) IC3, deep partial thickness thermal burn. 80

Figure 47. Ranked total sensitivity indices for $L2_1^{\infty}$ across all 105 MeFAST outputs for (a) IC1, superficial thermal burn; (b) IC2, superficial partial thickness thermal burn; and (c) IC3, deep partial thickness thermal burn. 81

Figure 48. Ranked total sensitivity indices for $L2_E^{\infty}$ across all 105 MeFAST outputs for (a) IC1, superficial thermal burn; (b) IC2, superficial partial thickness thermal burn; and (c) IC3, deep partial thickness thermal burn. 81

Figure 49. Ranked total sensitivity indices for k_{dnp} across all 105 MeFAST outputs for (a) IC1, superficial thermal burn; (b) IC2, superficial partial thickness thermal burn; and (c) IC3, deep partial thickness thermal burn. 82

Figure 50. Ranked total sensitivity indices for k_{dm1p} across all 105 MeFAST outputs for (a) IC1, superficial thermal burn; (b) IC2, superficial partial thickness thermal burn; and (c) IC3, deep partial thickness thermal burn. 82

Figure 51. Ranked total sensitivity indices for k_{dm2p} across all 105 MeFAST outputs for (a) IC1, superficial thermal burn; (b) IC2, superficial partial thickness thermal burn; and (c) IC3, deep partial thickness thermal burn. 83

Figure 52. Ranked total sensitivity indices for k_{NEmax} across all 105 MeFAST outputs for (a) IC1, superficial thermal burn; (b) IC2, superficial partial thickness thermal burn; and (c) IC3, deep partial thickness thermal burn. 83

Figure 53. Ranked total sensitivity indices for k_{mdE} across all 105 MeFAST outputs for (a) IC1, superficial thermal burn; (b) IC2, superficial partial thickness thermal burn; and (c) IC3, deep partial thickness thermal burn. 84

Figure 54. Ranked total sensitivity indices for k_{nnE} across all 105 MeFAST outputs for (a) IC1, superficial thermal burn; (b) IC2, superficial partial thickness thermal burn; and (c) IC3, deep partial thickness thermal burn. 84

Figure 55. Ranked total sensitivity indices for P_{HN} across all 105 MeFAST outputs for (a) IC1, superficial thermal burn; (b) IC2, superficial partial thickness thermal burn; and (c) IC3, deep partial thickness thermal burn. 85

Figure 56. Ranked total sensitivity indices for n_N across all 105 MeFAST outputs for (a) IC1, superficial thermal burn; (b) IC2, superficial partial thickness thermal burn; and (c) IC3, deep partial thickness thermal burn. 85

Figure 57. Ranked total sensitivity indices for δ_n across all 105 MeFAST outputs for (a) IC1, superficial thermal burn; (b) IC2, superficial partial thickness thermal burn; and (c) IC3, deep partial thickness thermal burn. 86

Figure 58. Ranked total sensitivity indices for d_n across all 105 MeFAST outputs for (a) IC1, superficial thermal burn; (b) IC2, superficial partial thickness thermal burn; and (c) IC3, deep partial thickness thermal burn. 86

Figure 59. Ranked total sensitivity indices for k_{MEmax} across all 105 MeFAST outputs for (a) IC1, superficial thermal burn; (b) IC2, superficial partial thickness thermal burn; and (c) IC3, deep partial thickness thermal burn. 87

Figure 60. Ranked total sensitivity indices for k_{MEmin} across all 105 MeFAST outputs for (a) IC1, superficial thermal burn; (b) IC2, superficial partial thickness thermal burn; and (c) IC3, deep partial thickness thermal burn. 87

Figure 61. Ranked total sensitivity indices for k_{mdE} across all 105 MeFAST outputs for (a) IC1, superficial thermal burn; (b) IC2, superficial partial thickness thermal burn; and (c) IC3, deep partial thickness thermal burn. 88

Figure 62. Ranked total sensitivity indices for k_{mnE} across all 105 MeFAST outputs for (a) IC1, superficial thermal burn; (b) IC2, superficial partial thickness thermal burn; and (c) IC3, deep partial thickness thermal burn. 88

Figure 63. Ranked total sensitivity indices for k_{mm1E} across all 105 MeFAST outputs for (a) IC1, superficial thermal burn; (b) IC2, superficial partial thickness thermal burn; and (c) IC3, deep partial thickness thermal burn. 89

Figure 64. Ranked total sensitivity indices for k_{ml1E} across all 105 MeFAST outputs for (a) IC1, superficial thermal burn; (b) IC2, superficial partial thickness thermal burn; and (c) IC3, deep partial thickness thermal burn. 89

Figure 65. Ranked total sensitivity indices for P_{HM} across all 105 MeFAST outputs for (a) IC1, superficial thermal burn; (b) IC2, superficial partial thickness thermal burn; and (c) IC3, deep partial thickness thermal burn. 90

Figure 66. Ranked total sensitivity indices for n_M across all 105 MeFAST outputs for (a) IC1, superficial thermal burn; (b) IC2, superficial partial thickness thermal burn; and (c) IC3, deep partial thickness thermal burn. 90

Figure 67. Ranked total sensitivity indices for δ_m across all 105 MeFAST outputs for (a) IC1, superficial thermal burn; (b) IC2, superficial partial thickness thermal burn; and (c) IC3, deep partial thickness thermal burn. 91

Figure 68. Ranked total sensitivity indices for d_{m1} across all 105 MeFAST outputs for (a) IC1, superficial thermal burn; (b) IC2, superficial partial thickness thermal burn; and (c) IC3, deep partial thickness thermal burn. 91

Figure 69. Ranked total sensitivity indices for d_{m2} across all 105 MeFAST outputs for (a) IC1, superficial thermal burn; (b) IC2, superficial partial thickness thermal burn; and (c) IC3, deep partial thickness thermal burn. 92

Figure 70. Ranked total sensitivity indices for k_{m1d} across all 105 MeFAST outputs for (a) IC1, superficial thermal burn; (b) IC2, superficial partial thickness thermal burn; and (c) IC3, deep partial thickness thermal burn. 92

Figure 71. Ranked total sensitivity indices for k_{m1l1} across all 105 MeFAST outputs for (a) IC1, superficial thermal burn; (b) IC2, superficial partial thickness thermal burn; and (c) IC3, deep partial thickness thermal burn. 93

Figure 72. Ranked total sensitivity indices for k_{m2m1} across all 105 MeFAST outputs for (a) IC1, superficial thermal burn; (b) IC2, superficial partial thickness thermal burn; and (c) IC3, deep partial thickness thermal burn. 93

Figure 73. Ranked total sensitivity indices for k_{m2l2} across all 105 MeFAST outputs for (a) IC1, superficial thermal burn; (b) IC2, superficial partial thickness thermal burn; and (c) IC3, deep partial thickness thermal burn. 94

Figure 74. Ranked total sensitivity indices for k_{LEmax} across all 105 MeFAST outputs for (a) IC1, superficial thermal burn; (b) IC2, superficial partial thickness thermal burn; and (c) IC3, deep partial thickness thermal burn. 94

Figure 75. Ranked total sensitivity indices for k_{ldE} across all 105 MeFAST outputs for (a) IC1, superficial thermal burn; (b) IC2, superficial partial thickness thermal burn; and (c) IC3, deep partial thickness thermal burn. 95

Figure 76. Ranked total sensitivity indices for k_{lnE} across all 105 MeFAST outputs for (a) IC1, superficial thermal burn; (b) IC2, superficial partial thickness thermal burn; and (c) IC3, deep partial thickness thermal burn. 95

Figure 77. Ranked total sensitivity indices for k_{lm1E} across all 105 MeFAST outputs for (a) IC1, superficial thermal burn; (b) IC2, superficial partial thickness thermal burn; and (c) IC3, deep partial thickness thermal burn. 96

Figure 78. Ranked total sensitivity indices for k_{ll1E} across all 105 MeFAST outputs for (a) IC1, superficial thermal burn; (b) IC2, superficial partial thickness thermal burn; and (c) IC3, deep partial thickness thermal burn. 96

Figure 79. Ranked total sensitivity indices for P_{HL} across all 105 MeFAST outputs for (a) IC1, superficial thermal burn; (b) IC2, superficial partial thickness thermal burn; and (c) IC3, deep partial thickness thermal burn. 97

Figure 80. Ranked total sensitivity indices for n_L across all 105 MeFAST outputs for (a) IC1, superficial thermal burn; (b) IC2, superficial partial thickness thermal burn; and (c) IC3, deep partial thickness thermal burn. 97

Figure 81. Ranked total sensitivity indices for k_{l1} across all 105 MeFAST outputs for (a) IC1, superficial thermal burn; (b) IC2, superficial partial thickness thermal burn; and (c) IC3, deep partial thickness thermal burn. 98

Figure 82. Ranked total sensitivity indices for k_{l2} across all 105 MeFAST outputs for (a) IC1, superficial thermal burn; (b) IC2, superficial partial thickness thermal burn; and (c) IC3, deep partial thickness thermal burn. 98

Figure 83. Ranked total sensitivity indices for δ_l across all 105 MeFAST outputs for (a) IC1, superficial thermal burn; (b) IC2, superficial partial thickness thermal burn; and (c) IC3, deep partial thickness thermal burn. 99

Figure 84. Ranked total sensitivity indices for d_l across all 105 MeFAST outputs for (a) IC1, superficial thermal burn; (b) IC2, superficial partial thickness thermal burn; and (c) IC3, deep partial thickness thermal burn. 99

Figure 85. Ranked total sensitivity indices for n_S across all 105 MeFAST outputs for (a) IC1, superficial thermal burn; (b) IC2, superficial partial thickness thermal burn; and (c) IC3, deep partial thickness thermal burn. 100

Figure 86. Ranked total sensitivity indices for k_{aIm} across all 105 MeFAST outputs for (a) IC1, superficial thermal burn; (b) IC2, superficial partial thickness thermal burn; and (c) IC3, deep partial thickness thermal burn. 100

Figure 87. Ranked total sensitivity indices for k_{aIl} across all 105 MeFAST outputs for (a) IC1, superficial thermal burn; (b) IC2, superficial partial thickness thermal burn; and (c) IC3, deep partial thickness thermal burn. 101

Figure 88. Ranked total sensitivity indices for k_{Irg} across all 105 MeFAST outputs for (a) IC1, superficial thermal burn; (b) IC2, superficial partial thickness thermal burn; and (c) IC3, deep partial thickness thermal burn. 101

Figure 89. Ranked total sensitivity indices for k_{Irl} across all 105 MeFAST outputs for (a) IC1, superficial thermal burn; (b) IC2, superficial partial thickness thermal burn; and (c) IC3, deep partial thickness thermal burn. 102

Figure 90. Ranked total sensitivity indices for k_{Irlt} across all 105 MeFAST outputs for (a) IC1, superficial thermal burn; (b) IC2, superficial partial thickness thermal burn; and (c) IC3, deep partial thickness thermal burn. 102

Figure 91. Ranked total sensitivity indices for k_{ag} across all 105 MeFAST outputs for (a) IC1, superficial thermal burn; (b) IC2, superficial partial thickness thermal burn; and (c) IC3, deep partial thickness thermal burn. 103

Figure 92. Ranked total sensitivity indices for k_{tbl} across all 105 MeFAST outputs for (a) IC1, superficial thermal burn; (b) IC2, superficial partial thickness thermal burn; and (c) IC3, deep partial thickness thermal burn. 103

Figure 93. Ranked total sensitivity indices for k_{QPmax} across all 105 MeFAST outputs for (a) IC1, superficial thermal burn; (b) IC2, superficial partial thickness thermal burn; and (c) IC3, deep partial thickness thermal burn. 104

Figure 94. Ranked total sensitivity indices for r_g across all 105 MeFAST outputs for (a) IC1, superficial thermal burn; (b) IC2, superficial partial thickness thermal burn; and (c) IC3, deep partial thickness thermal burn. 104

Figure 95. Ranked total sensitivity indices for r_l across all 105 MeFAST outputs for (a) IC1, superficial thermal burn; (b) IC2, superficial partial thickness thermal burn; and (c) IC3, deep partial thickness thermal burn. 105

Figure 96. Ranked total sensitivity indices for r_{lt} across all 105 MeFAST outputs for (a) IC1, superficial thermal burn; (b) IC2, superficial partial thickness thermal burn; and (c) IC3, deep partial thickness thermal burn. 105

Figure 97. Ranked total sensitivity indices for δ_P across all 105 MeFAST outputs for (a) IC1, superficial thermal burn; (b) IC2, superficial partial thickness thermal burn; and (c) IC3, deep partial thickness thermal burn. 106

Figure 98. Ranked total sensitivity indices for δ_{GSS} across all 105 MeFAST outputs for (a) IC1, superficial thermal burn; (b) IC2, superficial partial thickness thermal burn; and (c) IC3, deep partial thickness thermal burn. 106

Figure 99. Significance results of MeFAST for parameters of the systemic TDPM with respect to the state variables of the thermal burn compartment for IC1 at days one, three, five, seven, and ten post-injury. A shaded box indicates that the parameter was flagged as statistically significant at the respective state variable and time point by at least two of the three tests performed during MeFAST. These significance results were passed through the algorithm presented in Section 3.1.3 to determine whether each parameter should be estimated or fixed during parameterization. 107

Figure 100. Significance results of MeFAST for parameters of the systemic TDPM with respect to the state variables of the blood vessel and lymphatic tissue compartments for IC1 at days one, three, five, seven, and ten post-injury. A shaded box indicates that the parameter was flagged as statistically significant at the respective state variable and time point by at least two of the three tests performed during MeFAST. These significance results were passed through the algorithm presented in Section 3.1.3 to determine whether each parameter should be estimated or fixed during parameterization. 108

Figure 101. Significance results of MeFAST for parameters of the systemic TDPM with respect to the state variables of the bone marrow compartment for IC1 at days one, three, five, seven, and ten post-injury. A shaded box indicates that the parameter was flagged as statistically significant at the respective state variable and time point by at least two of the three tests performed during MeFAST. These significance results were passed through the algorithm presented in Section 3.1.3 to determine whether each parameter should be estimated or fixed during parameterization. 109

Figure 102. Significance results of MeFAST for parameters of the systemic TDPM with respect to the state variables of the thermal burn compartment for IC2 at days one, three, five, seven, and ten post-injury. A shaded box indicates that the parameter was flagged as

statistically significant at the respective state variable and time point by at least two of the three tests performed during MeFAST. These significance results were passed through the algorithm presented in Section 3.1.3 to determine whether each parameter should be estimated or fixed during parameterization. 110

Figure 103. Significance results of MeFAST for parameters of the systemic TDPM with respect to the state variables of the blood vessel and lymphatic tissue compartments for IC2 at days one, three, five, seven, and ten post-injury. A shaded box indicates that the parameter was flagged as statistically significant at the respective state variable and time point by at least two of the three tests performed during MeFAST. These significance results were passed through the algorithm presented in Section 3.1.3 to determine whether each parameter should be estimated or fixed during parameterization. 111

Figure 104. Significance results of MeFAST for parameters of the systemic TDPM with respect to the state variables of the bone marrow compartment for IC2 at days one, three, five, seven, and ten post-injury. A shaded box indicates that the parameter was flagged as statistically significant at the respective state variable and time point by at least two of the three tests performed during MeFAST. These significance results were passed through the algorithm presented in Section 3.1.3 to determine whether each parameter should be estimated or fixed during parameterization. 112

Figure 105. Significance results of MeFAST for parameters of the systemic TDPM with respect to the state variables of the thermal burn compartment for IC3 at days one, three, five, seven, and ten post-injury. A shaded box indicates that the parameter was flagged as statistically significant at the respective state variable and time point by at least two of the three tests performed during MeFAST. These significance results were passed through the algorithm presented in Section 3.1.3 to determine whether each parameter should be estimated or fixed during parameterization. 113

Figure 106. Significance results of MeFAST for parameters of the systemic TDPM with respect to the state variables of the blood vessel and lymphatic tissue compartments for IC3 at days one, three, five, seven, and ten post-injury. A shaded box indicates that the parameter was flagged as statistically significant at the respective state variable and time point by at least two of the three tests performed during MeFAST. These significance results were passed through the algorithm presented in Section 3.1.3 to determine whether each parameter should be estimated or fixed during parameterization. 114

Figure 107. Significance results of MeFAST for parameters of the systemic TDPM with respect to the state variables of the bone marrow compartment for IC3 at days one, three, five, seven, and ten post-injury. A shaded box indicates that the parameter was flagged as statistically significant at the respective state variable and time point by at least two of the three tests performed during MeFAST. These significance results were passed through the algorithm presented in Section 3.1.3 to determine whether each parameter should be estimated or fixed during parameterization. 115

List of Tables

Table 1. State variables, symbols, definitions, and initial conditions used for performing global sensitivity analysis on the systemic TDPM for combined injury following thermal burn and widespread radiation exposure. 19

Table 2. List of parameters to be included and fixed during GSA of the systemic model as determined by the MeFAST-based selection algorithms discussed in Section 3.1.1. 27

Table 3. List of parameters to be estimated and fixed during parameterization of the systemic TDPM for combined injury following thermal burn and widespread radiation exposure, as determined by the MeFAST-based selection algorithms discussed in Section 3.1.3. 28

Table 4. Acceptability criteria for parameter combinations prescribed under LHS for the systemic TDPM of combined injury following thermal burn and widespread radiation exposure. These criteria were used to identify which sampled parameter sets reproduced biologically observed trends noted in experimental data and literature. 30

Table 5. Parameters descriptions, units, and estimated values assigned by the representative set for each of the 40 parameters chosen to be calibrated by available data. 35

Table 6. Baseline values and ranges for all parameters of the systemic TDPM for combined injury following thermal burn and widespread radiation exposure, given by equations A1 – A41 in Appendix A. Each parameter is assumed to follow a uniform distribution with bounds given by its estimated minimum and estimated maximum. 50

Acknowledgements

We gratefully acknowledge Mr. Lee Alleman, Dr. Lawrence Herskowitz, and DTRA's Nuclear Technologies Survivability Division for programmatic support. This work was performed under DTRA contract HDTRA1-14-D-0003.

Executive Summary

Developed by the Defense Threat Reduction Agency (DTRA), the Health Effects from Nuclear and Radiological Environments (HENRE) engine predicts casualties for given environmental conditions following a nuclear detonation (NUDET) event. As empirical modeling approaches have been unable to produce satisfactory predictions for the effects of combined injuries following a NUDET event, Applied Research Associates (ARA) has developed a framework for quantifying the physiological effects of such injuries on medical outcomes. Previously, a time-dependent physiological model (TDPM) for combined injury following thermal burn and widespread radiation exposure was developed, the first of its kind to incorporate the systemic, synergistic effects of combined injury in this modeling framework. Prior to its implementation in HENRE, the systemic TDPM must be parameterized to ensure that model predictions are biologically sound and model parameters are calibrated to the needs of the HENRE user. This Technical Report (TR) presents the fully parameterized systemic TDPM for combined injury following thermal burn and widespread radiation exposure. The methodology presented herein will also be used in future work to parameterize systemic TDPMs of other combined injuries as they are developed. This not only saves computational time in future model development, but also ensures the compatibility of any future systemic TDPMs to be parameterized and implemented in HENRE, allowing for further expansion of modeling capabilities with respect to the synergistic effects of combined injuries. Future work will include the completion of an insult-to-outcome pipeline of the parameterized systemic TDPM for combined injury following thermal burn and widespread radiation (in which the HENRE user inputs of thermal fluence and prompt dose radiation exposure will be mapped to initial conditions of the systemic TDPM, and the time-series data generated by the systemic TDPM will be mapped to outcomes of interest for combat power, including pain, fatiguability and weakness, and gastrointestinal distress), at which point the fully parametrized systemic TDPM will be implemented into HENRE. In conclusion, the parameterization of the systemic TDPM presented in this document is an important step in both calibrating the TDPM to the needs of the HENRE user and preparing it for its implantation in HENRE.

Section 1. Introduction

Developed by Applied Research Associates (ARA) for the Defense Threat Reduction Agency (DTRA), the Health Effects from Nuclear Radiological Environments (HENRE) engine consists of a library of models used to predict casualties for the given environmental conditions following a nuclear detonation (NUDET) event. Current research efforts are focused on predicting physiological effects from combined injury to support calculations of performance decrement and combat power.

Following a NUDET event, potential injuries can result from air blast related injuries, thermal burns, and/or ionizing radiation exposure (Reeves, 2018). Historical evidence shows that over half of the casualties from a NUDET event are caused by radiation exposure in conjunction with at least one other trauma (Brooks et al., 1952; DiCarlo et al., 2008; Iijima, 1982; Oughterson et al., 1951). Combinations of multiple injuries, such as a combined injury resulting from thermal burn and widespread radiation exposure, have a synergistic effect on depletion of the body's resources (Brooks et al., 1952; Palmer et al., 2011). This results in a systemic wound healing response that impacts performance beyond the extent of the individual injuries themselves (Brooks et al., 1952; Palmer et al., 2011; Pellmar & Ledney, 2005).

Previously, ARA has developed two time-dependent physiological models (TDPMs): (1) a TDPM for local superficial thermal burn injury (Jennings, Hay, et al., 2022); and (2) a TDPM for locally irradiated superficial thermal burn injury (Hay et al., 2022). These local models describe the wound healing process for scenarios in which there is no systemic effect associated with the release of inflammatory mediators at the site of injury (Hettiaratchy & Dziewulski, 2004). However, to account for the potential synergistic effects resulting from a combination of multiple injuries following a NUDET event, a systemic TDPM for combined injury following thermal burn and widespread radiation exposure was developed in DTRA-TR-23-058 (Gaffney et al., 2023) by extending the existing TDPM for local superficial thermal burn (Jennings, Hay, et al., 2022).

The newly developed systemic TDPM for combined injury following thermal burn and widespread radiation exposure must be parameterized before it can be implemented in HENRE. The parameterization process is used to obtain biologically sound estimates of model parameters to ensure the reliability of model predictions. Due to model complexity and lack of empirical data, sensitivity analysis was used to reduce the number of parameters estimated by the available data. This process has been used previously to parameterize the TDPMs for local superficial thermal burn (Creel et al., 2022) and locally irradiated superficial thermal burn (Hay et al., 2023) However, the increase in model equations and number of parameters to be estimated for the systemic TDPM results in a problem space so large that computational time becomes an issue. As such, the methodology used for sensitivity analysis of the systemic TDPM was slightly different than that used for the two local TDPMs – in this case, the number of parameters investigated during sensitivity analysis was reduced by screening the influence of parameters within compartments and removing those which were considered to be non-influential from the analysis.

Section 2. Model Background

2.1 **Model Overview**

A TDPM for combined injury following thermal burn and widespread radiation exposure was developed and presented in DTRA-TR-23-058 (Gaffney et al., 2023). The schematic diagram in Figure 1 depicts the interactions that are encapsulated by the widespread irradiated thermal burn model (WITBM).

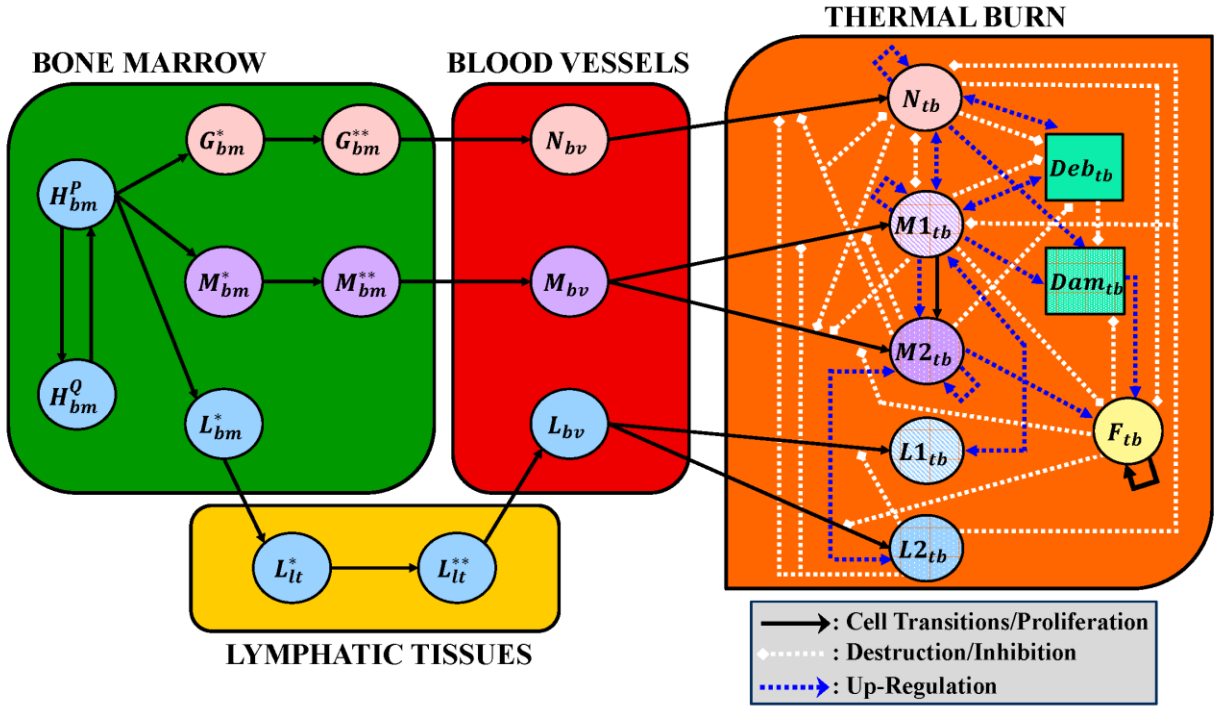


Figure 1. Schematic diagram for the systemic TDPM of combined injury following thermal burn and widespread radiation exposure (Gaffney et al., 2023). This figure shows how immune cells created in the bone marrow from stem cells mature, differentiate, transition to the injury site, and interact with the injury to progress wound healing.

The WITBM is an extension of the local superficial thermal burn model (STBM) with three compartments added to incorporate the systemic effects of more severe thermal burns and combined injury following thermal burn and widespread radiation exposure.

A few modifications have been made to the WITBM since its introduction in DTRA-TR-23-058 (Gaffney et al., 2023). These adjustments were a result of model exploration during the sensitivity analysis and parameterization phase of model development. Modifications include the following[1]:

1. The Hill functions found in the functional extravasation rates of immune cell populations from the blood vessels to the local thermal burn site were removed, and instead replaced with a linear function so that the terms are multiplied by the blood vessel populations directly. For example, the extravasation rate of neutrophils (E_n) was changed from

$$E_n = \mathrm{k}_{\mathrm{NE}_{\max}} \Omega_{\mathrm{i}}(\Omega_H(P_N, n_N, P_{HN}); M2_{tb}, M2_E^{\infty}, L2_{tb}, L2_E^{\infty}) \Omega_H(N_{bv}, y_N, N_H)$$

[1] Model equations and parameters (along with their descriptions) can be found in Appendix A and B, respectively.

to

$$E_n = \mathrm{k}_{\mathrm{NE}_{\max}} \Omega_{\mathrm{i}}(\Omega_H(P_N, n_N, P_{HN}); M2_{tb}, M2_E^{\infty}, L2_{tb}, L2_E^{\infty}) N_{bv}.$$

In model exploration, it was observed that when the blood compartment is near homeostasis, there is little difference between a linear function of the populations and a Hill function of the populations. A linear function is used to reduce complexity of the functional forms for extravasation rates and reduce the number of model parameters.

2. The general extravasation terms in the blood vessels (i.e., $G_n(**)$, $G_m(**)$, and $G_l(**)$) were removed to reduce model complexity during sensitivity analysis and parameterization. The effects of general extravasation will be explored through the inclusion of additional injury types to the systemic TDPM framework in future work.
3. A new term was introduced in the equation for M2 macrophages to describe their removal from the local burn site. As such, the equation for M2 macrophages was changed from

$$\frac{dM2_{tb}}{dt} = E_m(Deb_{tb}, N_{tb}, M1_{tb}, L1_{tb}; M2_{tb}, L2_{tb}) \left(\frac{R_{m2}}{R_{m1} + R_{m2}}\right) + \theta_{m1m2}\left[k_{nm1p} N_{tb} \Omega_i(M1_{tb}; N_{tb}, N_1^{\infty})\right] - d_{m2} M2_{tb}$$

to

$$\frac{dM2_{tb}}{dt} = E_m(Deb_{tb}, N_{tb}, M1_{tb}, L1_{tb}; M2_{tb}, L2_{tb}) \left(\frac{R_{m2}}{R_{m1} + R_{m2}}\right) + \theta_{m1m2}\left[k_{nm1p} N_{tb} \Omega_i(M1_{tb}; N_{tb}, N_1^{\infty})\right] - d_{m2} M2_{tb} - \Omega_i(k_{lvm} M2_{tb}; Dam_{tb}, Dam_{lvm}^{\infty})$$

In model exploration, it was observed that the anti-inflammatory M2 macrophage population was not clearing from the thermal burn site as anticipated. To confront this, a term was added to represent M2 macrophages leaving the injury site, inhibited by damage. This results in an increase of M2 macrophages leaving the thermal burn site following the resolution of damage, thus returning the M2 macrophages back down to their baseline residential population level.

Including these modifications, there are only two differences between the thermal burn compartments of the local STBM and the WITBM:

1. The systemic effects of widespread radiation exposure and combined injury result in dynamic immune cell populations in the bloodstream. As such, the quasi-steady state approximation made for the STBM of constant influx rates into the injury site (Jennings, Creel, et al., 2022a) is no longer applicable. In the WITBM, these constant influx rates were replaced with functional rates dependent on immune cell populations in the blood vessels.
2. As described in (3) of the modifications list above, the WITBM includes a new term for removal of M2 macrophages at the local burn site.

Model equations of the TDPM for combined injury following thermal burn and widespread radiation exposure can be found in Appendix A, and a table of model parameters, descriptions,

ranges, and baseline values can be found in Appendix B. The method by which parameter bounds were calculated can be found in DTRA-TR-21-063 R1 (Creel et al., 2022, Appendix B).

2.2 **Initial Conditions for Sensitivity Analysis**

For sensitivity analysis, a non-dimensional formulation of the WITBM was considered; i.e., to control for the difference in scale between model compartments, initial conditions of the model were set to non-dimensional values to investigate relative change in population sizes. This ensured that the results of sensitivity analysis (i.e., the measures of parameter influence on model output) would not be inadvertently impacted by the discrepancy in scale between compartments.

As shown in Table 1, immune cell populations in the systemic compartments (bone marrow, lymphatic tissues, blood vessels) were initially set to 1 to represent that their populations are at 100% of their baseline value. Note that the initial conditions of quiescent and proliferative hematopoietic stem cells (HSCs) sum to 1, so that the total HSC population is at 100% of its baseline (i.e., $H_{bm}^{Q} + H_{bm}^{P} = 1$). A 90/10 split between quiescent and proliferative HSCs was chosen based on the percentage of quiescent HSCs in the bone marrow ranging from 80% to 95% of the HSC population in the literature (Pietras et al., 2011; Yamada et al., 2013).

Initial conditions of Dam_{tb} and Deb_{tb} are representative of the severity of thermal burn injury. In parameterization of the WITBM, three severities are investigated: (1) superficial thermal burn injury ($Dam_{tb}(0) = Deb_{tb}(0) = 0.1$); (2) superficial partial thickness burn injury ($Dam_{tb}(0) = Deb_{tb}(0) = 0.9$); and (3) partial-thickness burn injury[2] ($Dam_{tb}(0) = Deb_{tb}(0) = 1.8$). The state variables representing immune cell populations and their byproducts at the local thermal burn site (except for $M2_{tb}$ and F_{tb}) are set to zero at the onset of injury because the inflammatory process has not started yet. The initial conditions of $M2_{tb}$ and F_{tb} are set to 0.1 to represent a small residential population present before the wound healing process begins (Franklin, 2021), and are necessary to avoid numerical error of the model.

Table 1. State variables, symbols, definitions, and initial conditions used for performing global sensitivity analysis on the systemic TDPM for combined injury following thermal burn and widespread radiation exposure.

SYMBOL	DESCRIPTION	INITIAL VALUE		
		Superficial Thickness (IC1)	**Superficial Partial Thickness (IC2)**	**Deep Partial Thickness (IC3)**
$\boldsymbol{t}$	Time (in hours)	-	-	-
$\boldsymbol{S_{bm}}$	Environmental HSC signaling molecule	$\frac{\alpha_{sm}}{\beta_{sm}(H_{bm,0}^{Q} + H_{bm,0}^{P})}$	$\frac{\alpha_{sm}}{\beta_{sm}(H_{bm,0}^{Q} + H_{bm,0}^{P})}$	$\frac{\alpha_{sm}}{\beta_{sm}(H_{bm,0}^{Q} + H_{bm,0}^{P})}$

[2] In DTRA-TR-23-030 (Creel et al., 2023), it was found that a thermal fluence of 19 J/cm^2 mapped to an initial condition of $Dam_{tb}(0) = Deb_{tb}(0) = 1.8$, and noted that a thermal fluence of 19 J/cm^2 results in a 50% incidence of second-degree burns in the average unshielded population (Glasstone & Dolan, 1977). Under the system of burn severity classification, the severity of both superficial partial thickness and deep partial thickness burns are encapsulated by the more general term "second-degree burn," with superficial partial thickness burns falling on the less severe end of second-degree burn injuries, and deep partial thickness burns being on the more severe end (Jeschke et al., 2020). Therefore, the initial condition of $Dam_{tb}(0) = Deb_{tb}(0) = 1.8$ is used to represent a more severe second-degree burn injury (i.e., deep partial thickness burn), while the initial condition of $Dam_{tb}(0) = Deb_{tb}(0) = 0.9$ is used to represent a less severe second-degree burn injury (i.e., superficial partial thickness burn), as it was in the STBM (Jennings, Creel, et al., 2022a) and LISTBM (Hay et al., 2022).

SYMBOL	DESCRIPTION	INITIAL VALUE		
		Superficial Thickness (IC1)	**Superficial Partial Thickness (IC2)**	**Deep Partial Thickness (IC3)**
Bone Marrow Compartment				
H_{bm}^{Q}	Quiescent hematopoietic stem cells in the bone marrow	0.9	0.9	0.9
H_{bm}^{P}	Proliferating hematopoietic stem cells in the bone marrow	0.1	0.1	0.1
G_{bm}^{*}	Mitotic granulocyte progenitor cells in the bone marrow	1	1	1
M_{bm}^{*}	Mitotic monocyte progenitor cells in the bone marrow	1	1	1
L_{bm}^{*}	Mitotic lymphocyte progenitor cells in the bone marrow	1	1	1
G_{bm}^{**}	Non-mitotic granulocyte progenitor cells in the bone marrow	1	1	1
M_{bm}^{**}	Non-mitotic monocyte progenitor cells in the bone marrow	1	1	1
Blood Vessels Compartment				
N_{bv}	Circulating neutrophils in the bloodstream	1	1	1
M_{bv}	Circulating monocytes in the bloodstream	1	1	1
L_{bv}	Circulating lymphocytes in the bloodstream	1	1	1
Lymphatic Tissue Compartment				
L_{lt}^{*}	Mitotic lymphocyte progenitor cells in the lymphatic tissues	1	1	1
L_{lt}^{**}	Non-mitotic lymphocyte progenitor cells in the lymphatic tissues	1	1	1
Local Thermal Burn Compartment				
Dam_{tb}	Damaged tissue in the injury site (unitless)	0.1	0.9	1.8
Deb_{tb}	Debris in the injury site (unitless)	0.1	0.9	1.8

SYMBOL	DESCRIPTION	INITIAL VALUE		
		Superficial Thickness (IC1)	Superficial Partial Thickness (IC2)	Deep Partial Thickness (IC3)
N_{tb}	Neutrophils recruited to the injury site	0	0	0
$M1_{tb}$	Pro-inflammatory monocytes activated at the injury site	0	0	0
$M2_{tb}$	Anti-inflammatory monocytes activated at the injury site	0.1	0.1	0.1
$L1_{tb}$	Pro-inflammatory lymphocytes recruited to the injury site	0	0	0
$L2_{tb}$	Anti-inflammatory lymphocytes recruited to the injury site	0	0	0
F_{tb}	Fibroblasts at the injury site	0.1	0.1	0.1

Section 3. Sensitivity Analysis

Due to model complexity and limited data availability, sensitivity analysis (SA) was necessary to ensure effective use of available data to parameterize the WITBM. SA quantifies how variation in model parameters impacts variation in model output, allowing for identification of which parameters contribute most to uncertainty in model predictions (Wu et al., 2013). The parameters which were deemed most influential by the results of sensitivity analysis were then estimated with available data, thus maximizing the utility of data despite its sparse volume (Lenhart et al., 2002).

3.1 **Methods**

Global sensitivity analysis (GSA) of the WITBM was performed using an updated version of the sensitivity analysis methodology previously applied to the STBM (Creel et al., 2022) and LITBM (Hay et al., 2023). Due to the increased number of parameters and state variables in the WITBM, the methodology was updated to include a screening process which: (1) identifies non-influential parameters within individual compartments, and (2) removes them from consideration prior to running GSA on the TDPM. A flowchart of the updated sensitivity analysis methodology is provided in Figure 2.

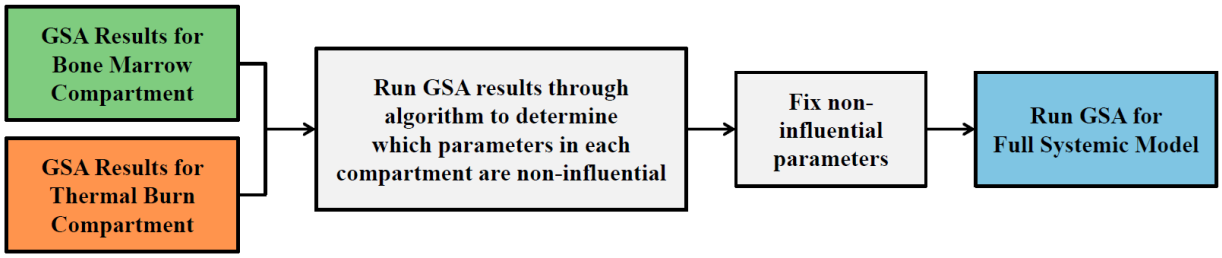


Figure 2. Flowchart depicting the updated methodology for performing global sensitivity analysis on the systemic TDPM for combined injury following thermal burn and widespread radiation exposure. The increased number of parameters in state variables in the systemic TDPM significantly increases the computational intensity of GSA. The new methodology includes a screening process which identifies non-influential parameters in the bone marrow and thermal burn compartments and removes them from consideration prior to running GSA on the systemic TDPM, thereby reducing its computational intensity.

The Extended Fourier Amplitude Sensitivity Test (eFAST) has been shown to be the method best suited to assess the parameters of models with highly non-linear relationships (Marino et al., 2008), such as the WITBM. This method has been used previously to investigate parameters of the STBM and the LITBM (Creel et al., 2022; Hay et al., 2023). As done for the LITBM (Hay et al., 2023), the WITBM will be investigated using MeFAST, which is a slightly modified version of eFAST that includes additional statistical tests during analyses to better determine parameter influence. A total of three tests were used to determine statistical significance of parameter influence: (1) the original t-test used in eFAST (Marino et al., 2008); (2) the ANOVA test followed by the Tukey procedure, introduced in MeFAST (Dela et al., 2022); and (3) the Wilcoxon test, also introduced in MeFAST (Dela et al., 2022). For a more detailed description of MeFAST and its statistical significance tests, see DTRA-TR-23-048 (Hay et al., 2023).

For each use of MeFAST, the WITBM was assessed at five time points: $t = 24$, $t = 72$, $t = 168$, $t = 240$, and $t = 336$ hours, corresponding to days one, three, seven, ten, and fourteen post-injury, respectively. These time points were used previously in the local STBM (Creel et al., 2022) and LITBM (Hay et al., 2023), and are commonly used data points for collection in experimental

models of thermal burn injury (Lateef et al., 2019). The model was simulated for three different initial conditions, referred to as initial condition (IC) 1, IC2, and IC3, as defined in Table 1.

3.1.1. MeFAST for Parameter Screening

For complex models, especially those with many parameters, the computational cost of running a global sensitivity analysis is high. To combat this, a screening method of sensitivity analysis can be used to reduce the number of parameters considered during analysis (Zi, 2011).

Popular conventional methods for screening parameters prior to sensitivity analysis (e.g., the local one-at-a-time method (Link et al., 2018) and the Morris method (Morris, 1991; Wu et al., 2013)) were not applicable to the WITBM due to its high nonlinearity and, in most cases, inability to satisfy their necessary assumptions. Because these techniques were not applicable, a workflow was developed to analyze the influence of parameters on a relatively local level, while still considering interactions between model parameters. First, the model was split by its four compartments (bone marrow, blood vessels, lymphatic tissue, and thermal burn), and MeFAST was applied to one compartment at a time, investigating parameters contained within that compartment only (i.e., not directly used in any other compartment of the model). The table of parameters (Table 6) in Appendix B includes columns marking off which model compartments each parameter can be found in.

Note that the lymphatic tissue and blood vessel compartments each have no more than three state variables (see Table 1) and only three parameters that are contained solely within their compartments; as such, a sensitivity analysis within these compartments would not be an informative task for the purposes of removing parameters prior to GSA of the WITBM. Therefore, all parameters of the lymphatic tissue and blood vessel compartments were included in sensitivity analysis of the full model, and only the bone marrow and thermal burn compartments were screened prior to sensitivity analysis.

3.1.1.1 Parameter Screening in the Bone Marrow Compartment

Results of MeFAST were obtained for 26 parameters in the bone marrow compartment using 1093 samples per search curve, resampled 8 times (i.e., $N_s = 1093$ with $N_r = 8$), for a total of 236,088 iterations per initial condition. For details on the use and significance of these sampling values in the sensitivity analysis algorithm, see DTRA-TR-21-063 R1 (Creel et al., 2022) and (Marino et al., 2008).

The bone marrow compartment contains eight state variables of interest: signaling biomolecules (S_{bm}), quiescent and proliferative hematopoietic stem cells (H_{bm}^{Q} and H_{bm}^{P}, respectively), mitotic and non-mitotic granulocyte progenitor cells (G_{bm}^{*} and G_{bm}^{**}, respectively), mitotic and non-mitotic monocyte progenitor cells (M_{bm}^{*} and M_{bm}^{**}, respectively), and mitotic lymphocyte progenitor cells (L_{bm}^{*}). The influence of parameters in the bone marrow on each of these state variables was assessed for three initial conditions (IC1, IC2, and IC3 in Table 1) at five time points of interest ($t = 24$, $t = 72$, $t = 168$, $t = 240$, $t = 336$), for a total of 120 sensitivity analysis outputs for each parameter (40 per initial condition). For each output, a parameter was determined to be influential if it was deemed statistically significant by at least two of the three significance tests performed. To implement the algorithm for removing parameters from consideration during sensitivity analysis of WITBM, three values were calculated for each parameter:

1. $n_{1,bm}$: the number of times the parameter was found to be statistically significant across all 40 sensitivity outputs of the bone marrow compartment with IC1 for the MeFAST method
2. $n_{2,bm}$: the number of times the parameter was found to be statistically significant across all 40 sensitivity outputs of the bone marrow compartment with IC2 for the MeFAST method
3. $n_{3,bm}$: the number of times the parameter was found to be statistically significant across all 40 sensitivity outputs of the bone marrow compartment with IC3 for the MeFAST method

Observe that by construction $n_{j,bm} \leq 40$ for $j = 1,2,3$.

The algorithm used to determine whether parameters of the bone marrow compartment would be included in sensitivity analysis of the WITBM or fixed at their baseline value is given in Figure 3. A cut-off of at least 8 significant points was used in the algorithm for each parameter based on the results of each method. A value of 8 ensures that the parameter is sensitive in at least two of the bone marrow state variables or at least two of the time points of interest, since each variable has at most five time points and each time point spans 8 total variables.

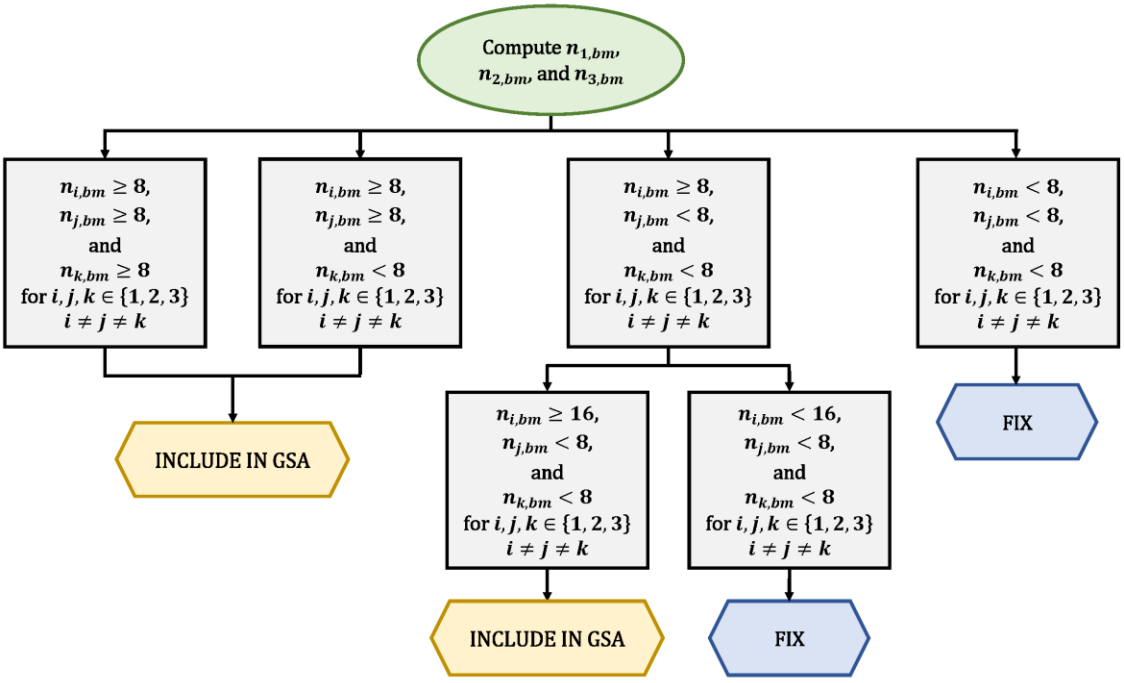


Figure 3. Flowchart for the algorithm to determine whether a parameter in the bone marrow compartment should be included in global sensitivity analysis (GSA) or fixed at its baseline value. In the first step, if all three of the initial conditions have significance counts less than eight, the parameter is fixed. If two or more of the initial conditions have significance counts greater than or equal to eight, the parameter is included in GSA. If only one of the initial conditions produces a significance count greater than or equal to eight, the algorithm proceeds to the next step. In the next step, only the initial condition with a significance count greater than or equal to eight is considered. If its significance count is also greater than or equal to 16, the parameter is included in GSA. Otherwise, the parameter is fixed.

3.1.1.2 Parameter Screening in the Thermal Burn Compartment

The thermal burn compartment contains eight state variables of interest: damaged tissue in the injury site (Dam_{tb}) and debris in the injury site (Deb_{tb}), neutrophils recruited to the injury site (N_{tb}), pro-inflammatory and anti-inflammatory monocytes activated at the injury site ($M1_{tb}$ and $M2_{tb}$, respectively), pro-inflammatory and anti-inflammatory lymphocytes recruited to the injury site ($L1_{tb}$ and $L2_{tb}$, respectively), and fibroblasts at the injury site (F_{tb}). As discussed in Section

2.1, the thermal burn compartment of the WITBM is extremely similar to that of the STBM. Therefore, the results of eFAST obtained for parameterization of the STBM, presented in DTRA-TR-21-063 R1 (Creel et al., 2022), were used to identify which parameters were non-influential and could therefore be removed from consideration.

For the purposes of the current sensitivity analysis, any parameters which were presented as influential in DTRA-TR-21-063 R1 (Creel et al., 2022) were included in GSA of the WITBM. Additionally, any parameters that were introduced into the thermal burn compartment when extending the STBM to the WITBM were also included in GSA. These include parameters related to extravasation from the blood vessels to the burn site and clearance of M2 macrophages from the burn site (see Section 2.1).

3.1.2. MeFAST for Global Sensitivity Analysis of the TDPM

Once the influence of parameters were assessed at a compartment level and those deemed non-influential removed from consideration, MeFAST was used to analyze the full systemic TDPM for combined injury following thermal burn and widespread radiation exposure. A total of 61 parameters were included in GSA.

Results of MeFAST were obtained using 1093 samples per search curve, resampled 8 times (i.e., $N_s = 1093$ with $N_r = 8$), for a total of 542,128 iterations per initial condition. For details on the use and significance of these sampling values in the sensitivity analysis algorithm, see DTRA-TR-21-063 R1 (Creel et al., 2022) and (Marino et al., 2008).

The WITBM was analyzed for all 21 state variables (see Table 1) across three initial conditions (IC1, IC2, and IC3 in Table 1) at five time points of interest ($t = 24$, $t = 72$, $t = 168$, $t = 240$, $t = 336$), for a total of 315 sensitivity analysis outputs for each parameter (105 per initial condition).

3.1.3. Parameter Selection Algorithm

The results of MeFAST were used to determine which parameters should be estimated and which should be held fixed at their baseline value during the parameterization process. To implement the algorithm used to identify whether a parameter should be estimated or held fixed, the 315 sensitivity analysis outputs for each parameter obtained by the method described in section 3.1.2 were used to calculate the following three values for each parameter:

1. $n_{1,all}$: the number of times the parameter was found to be statistically significant across all 105 sensitivity outputs of the TDPM with IC1 for the MeFAST method
2. $n_{2,all}$: the number of times the parameter was found to be statistically significant across all 105 sensitivity outputs of the TDPM with IC1 for the MeFAST method
3. $n_{3,all}$: the number of times the parameter was found to be statistically significant across all 105 sensitivity outputs of the TDPM with IC1 for the MeFAST method

Observe that by construction $n_{j,all} \leq 105$ for $j = 1,2,3$.

The algorithm used to determine whether parameters of the WITBM would be estimated during parameterization or fixed at their baseline value is given in Figure 4. A cut-off of at least 21 significant points was used in the algorithm for each parameter based on the results of each method. A value of 21 ensures that the parameter is sensitive in at least at least four of the state variables

or at least two of the time points of interest, since each variable has at most five time points and each time point spans 21 total variables.

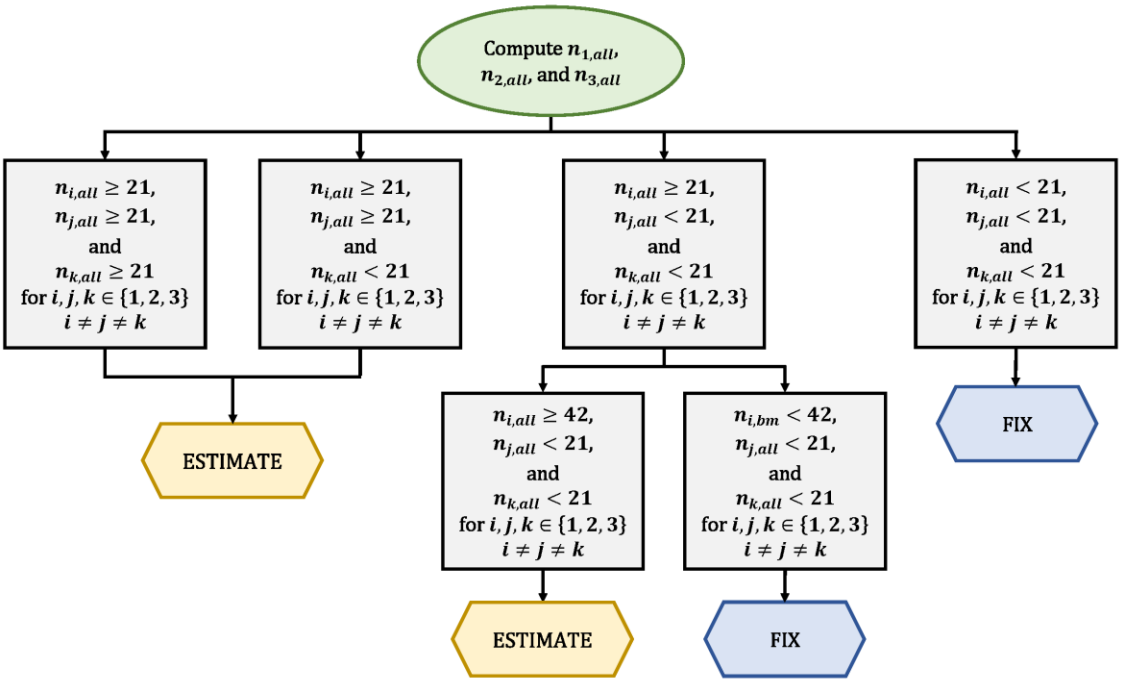


Figure 4. Flowchart for the algorithm to determine whether a parameter of the systemic TDPM should be estimated during parameterization or fixed at its baseline value. In the first step, if all three of the initial conditions have significance counts less than 21, the parameter is fixed. If two or more of the initial conditions have significance counts greater than or equal to 21, the parameter is estimated. If only one of the initial conditions produces a significance count greater than or equal to 21, the algorithm proceeds to the next step. In the next step, only the initial condition with a significance count greater than or equal to 21 is considered. If its significance count is also greater than or equal to 42, the parameter is estimated. Otherwise, the parameter is fixed at its baseline value.

3.2 **Results**

3.2.1. Parameter Screening in the Bone Marrow and Thermal Burn Compartments

For each parameter, MeFAST produced a total sensitivity index (S_{T_i}) with respect to each variable of the bone marrow compartment, at each time point considered, for each initial condition. These sensitivity indices measure the contribution of each parameter and its interactions with all other model parameters to overall output variation (Saltelli et al., 1999), with a high value of S_{T_i} indicating high influence on output.

For each state variable, time point, and initial condition, the S_{T_i} values of all parameters were ranked from 1 to 26, with 1 being assigned to the highest S_{T_i} value, and 26 assigned to the lowest. Line plots of each parameter's ranked total sensitivity indices over time, with respect to each variable, for each initial condition, are provided in Figure 10 in Appendix C.

Significance results obtained via MeFAST for parameters in the bone marrow compartment for each initial condition (IC1, IC2, and IC3) are shown in Figure 36 in Appendix C. Of the 26 parameters in the bone marrow compartment, 15 were deemed non-influential by the algorithm depicted in Figure 3, and therefore fixed during GSA of the WITBM.

Significance results for the parameters of the thermal burn compartment can be found in DTRA-TR-21-063 R1 (Creel et al., 2022).Of the 44 parameters in the thermal burn compartment, 21 were previously deemed non-influential by the algorithm in DTRA-TR-21-063 R1 (Creel et al., 2022), and therefore fixed during GSA of the systemic TDPM.

In total, 36 of the 112 systemic TDPM parameters were removed from consideration during GSA after screening the bone marrow and thermal burn compartments. Of the 76 remaining parameters, 61 were included in GSA; the other 15 are dependent upon the values of other parameters (see Appendix A), and therefore were not directly varied in GSA. Table 2 provides a summary of which category each model parameter falls into (i.e., whether it was included or fixed during GSA).

Table 2. List of parameters to be included and fixed during GSA of the systemic model as determined by the MeFAST-based selection algorithms discussed in Section 3.1.1.

PARAMETERS TO INCLUDE IN GSA	PARAMETERS TO FIX DURING GSA
Inhibition	
Deb_H, Dam_{lvm}^{∞}, N_1^{∞}, $M1_1^{\infty}$, $M1_2^{\infty}$, $M2^{\infty}$, $M2_E^{\infty}$, $L2_1^{\infty}$, $L2_E^{\infty}$	Deb_{dam}^{∞}, N_2^{∞}, F^{∞}, $L2_2^{\infty}$
Damage and Debris	
k_{dnp}, k_{dm1p}, k_{dm2p}	k_{dn}, σ_{dm1}, N_H, $M1_H$, ρ_{dam}, k_{df}, d_{deb}
Neutrophils	
$k_{NE_{max}}$, k_{ndE}, k_{nnE}, P_{HN}, n_N, δ_n, d_n	k_{nm1p}, k_{nm2p}
Macrophages	
$k_{ME_{max}}$, $k_{ME_{min}}$, k_{mdE}, k_{mnE}, k_{mm1E}, k_{ml1E}, P_{HM}, n_M, δ_m, d_{m1}, d_{m2}, k_{m1d}, k_{m1l1}, k_{m2m1}, k_{m2l2}, k_{lvm}	k_{m1n}, k_{m1m1}, k_{m2m2}, θ_{m1m2}
T Lymphocytes	
$k_{LE_{max}}$, k_{ldE}, k_{lnE}, k_{lm1E}, k_{ll1E}, P_{HL}, n_L, k_{l1}, k_{l2}, δ_l, d_l	
Fibroblasts	
	s_f, d_f, k_f, α_{dam}
Bone Marrow and Lymphatic Tissue	
n_S, k_{aIm}, k_{aIl}, k_{Irg}, k_{Irl}, k_{Irlt}, k_{ag}, k_{tbl}, k_{QPmax}, r_g, r_m, r_l, r_{lt}, δ_P, δ_{GSS}	β_{sm}, C_0, k_{aIg}, k_{Irm}, I_{∞}, k_{tbd}, k_{tbn}, k_{tbm}, n_{kQP}, δ_P, δ_{GS}, δ_{MS}, δ_{LS}, δ_{MSS}, δ_{LSS}

3.2.2. MeFAST for Global Sensitivity Analysis of the TDPM

For each parameter, MeFAST produced a total sensitivity index (S_{T_i}) with respect to each variable of the WITBM, at each time point considered, for each initial condition. These sensitivity indices measure the contribution of each parameter and its interactions with all other model parameters to overall output variation (Saltelli et al., 1999), with a high value of S_{T_i} indicating high influence on output.

For each state variable, time point, and initial condition, the S_{T_i} values of all parameters were ranked from 1 to 61, with 1 being assigned to the highest S_{T_i} value, and 61 assigned to the lowest.

Line plots of each parameter's ranked total sensitivity indices over time, with respect to each variable, for each initial condition, are provided in Figures Figure 39 in Appendix C.

Significance results obtained via MeFAST for parameters of the systemic TDPM for each initial condition (IC1, IC2, and IC3) are shown in Figure 100 in Appendix C.

3.2.3. Parameter Selection

Of the 61 parameters investigated by GSA, 40 were deemed influential and therefore chosen to be estimated during parameterization. The remaining parameters were fixed at their baseline values during parameter estimation. Table 3 summarizes which parameters fall into each category.

Table 3. List of parameters to be estimated and fixed during parameterization of the systemic TDPM for combined injury following thermal burn and widespread radiation exposure, as determined by the MeFAST-based selection algorithms discussed in Section 3.1.3.

PARAMETERS TO ESTIMATE	PARAMETERS TO FIX
Inhibition	
Deb_H, $M1_1^\infty$, $M1_2^\infty$, $M2^\infty$, $M2_E^\infty$, F_1^∞, $L2_E^\infty$	Dam_{lvm}^∞, N_1^∞, $L2_1^\infty$
Damage and Debris	
k_{dnp}, k_{dm1p}, k_{dm2p}	
Neutrophils	
k_{nnE}, P_{HN}	$k_{NE_{max}}$, k_{ndE}, n_N, δ_n, d_n
Macrophages	
$k_{ME_{max}}$, $k_{ME_{min}}$, k_{mdE}, k_{mnE}, P_{HM}, n_M, δ_m, k_{m1d}, k_{m1l1}, k_{m2m1}, k_{m2l2}	k_{mm1E}, k_{ml1E}, d_{m1}, d_{m2}
T Lymphocytes	
k_{lnE}, k_{lm1E}, k_{ll1E}, k_{l1}, k_{l2}, δ_l	$k_{LE_{max}}$, k_{ldE}, P_{HL}, n_L, d_l
Fibroblasts	
Bone Marrow and Lymphatic Tissue	
k_{aIm}, k_{aIl}, k_{Irg}, k_{Irl}, k_{tbl}, k_{QPmax}, r_g, r_l, r_{lt}, δ_P, δ_{GSS}	n_S, k_{Irlt}, k_{ag}, r_m

Section 4. Parameterization

4.1 **Methods**

Parameter estimation for the WITBM was conducted using the same method employed for the STBM (Jennings, Creel, et al., 2022b) and the LITBM (Hay et al., 2023). Estimation was performed only for the set of parameters selected in Section 3.2.3, ensuring computational effort was allocated properly to influential model parameters.

Brute-force with Latin Hypercube Sampling (LHS) was used to generate potential parameter sets following the methods described in DTRA-TR-22-026 for the STBM (Jennings, Creel, et al., 2022b) and in DTRA-TR-23-048 for the LITBM (Hay et al., 2023). Acceptability criteria were then used to determine whether the parameter sets reproduced biologically observed trends for the various initial conditions (IC1, IC2, and IC3, as defined in Table 1). Accepted parameter sets exhibited a wide range of model behavior similar to what would be observed across a population. These accepted sets were then used to select a representative set, which is the set of parameters that most closely reproduce the average dynamics of each state variable across all accepted sets.

4.1.1. Acceptability Criteria for Brute-Force with Latin Hypercube Sampling

The acceptability criteria applied to the samples obtained via Brute-Force with LHS were derived from trends noted in experimental data and literature. Efforts were also made to ensure that the WITBM produces results consistent with the STBM and LITBM for superficial thermal burns in the absence of radiation to ensure collapsibility of the models. This was done by comparing the healing times of superficial thermal burns predicted by the WITBM to those predicted by the STBM and LITBM (see AC2). All criteria used in the selection of parameter sets are included in Table 4.

Table 4. Acceptability criteria for parameter combinations prescribed under LHS for the systemic TDPM of combined injury following thermal burn and widespread radiation exposure. These criteria were used to identify which sampled parameter sets reproduced biologically observed trends noted in experimental data and literature.

CRITERIA	BIOLOGICAL DESCRIPTION	MATHEMATICAL REPRESENTATION	REFS.
AC1	Debris must be removed before damaged tissue can be repaired (follows from the definition of the inflammatory phase)	• $\tau_{deb} < \tau_{dam}$	(Goldberg & Diegelmann, 2010; Schultz et al., 2011)
AC2	In the absence of radiation, the systemic model for combined injury following thermal burn and widespread radiation exposure collapses to the superficial thermal burn model	• For a superficial thickness burn (IC1), ▪ $\tau_{dam} = 4.667 \pm 0.5$ days ▪ $\left\|\boldsymbol{X}_{0.1}^{tail} - \boldsymbol{X}^{*}\right\|_2 < 0.3$ ** • For a minor superficial partial thickness burn (IC2), ▪ $\tau_{dam} = 7.833 \pm 0.5$ days ▪ $\left\|\boldsymbol{X}_{0.9}^{tail} - \boldsymbol{X}^{*}\right\|_2 < 0.3$ **	(Abazari et al., 2020; Evers et al., 2010; Jeschke et al., 2020; Peng et al., 2006; Reeves, 2018)
AC3	In the absence of radiation, superficial burns heal without scarring	• $\left\|\boldsymbol{X}_{0.1}^{tail} - \boldsymbol{X}^{*}\right\|_2 < 0.3$ • $\left\|\boldsymbol{X}_{0.9}^{tail} - \boldsymbol{X}^{*}\right\|_2 < 0.3$	(Finnerty et al., 2016)

Notation: Let τ_{dam} and τ_{deb} be the time points such that $Dam(\tau_{dam}) < 0.01$ and $Deb(\tau_{deb}) < 0.01$, respectively.

** $\|\cdot\|_2$ represents the 2-norm of a matrix, which computes the maximum absolute row sum. $\boldsymbol{X}_{0.1}^{tail}$ and $\boldsymbol{X}_{0.9}^{tail}$ represent the "tail" numerical solution over $t \in [0, 100 * 24]$ (in hours) of all state variables under superficial thickness burn (IC1) and superficial partial thickness burn (IC2), respectively (see Table 1).

4.1.2. Parameter Distributions and Sampling

To use LHS for parameterization, each estimated parameter first must be assigned a distribution. Parameters of the WITBM were assumed to be uniformly distributed[3] on a closed interval. The bounds for each parameter can be found in Table 6 of Appendix B.

For the WITBM, certain conditions must be met to ensure that sampled parameters satisfy the assumption that all parameters are positive, real numbers. These conditions are listed in Equations A57 – A71 of Appendix A. Sampling was performed such that all conditions were met.

4.1.3. Representative Set

A representative parameter set was chosen from the accepted sets using the method introduced in DTRA-TR-23-048 (Hay et al., 2023), which employs the parameter sets' weighted mean squared errors and R^2 values calculated with respect to each state variable.

The process for obtaining a representative set, depicted visually in Figure 5, is as follows: First, the weighted mean squared error (MSE) for each parameter set was calculated. These weighted

[3] A uniform distribution is recommended when little is known about the parameter values and their respective distributions (Marino et al., 2008), as in the current model.

MSEs were then ranked from smallest to largest, with a smaller MSE indicating a better fit to the average model dynamics seen across all accepted sets. Next, for the 5% of parameter sets with the smallest weighted MSE, R^2 values were calculated with respect to each state variable. These values were then ranked from largest to smallest, with a larger R^2 value indicating a better fit to the average dynamics for each individual state variable. Finally, the representative set was chosen by finding the best ranked parameter set in terms of R^2. This ensured that the representative set not only represented average model dynamics well (indicated by its small weighted MSE), but also most closely reproduced the average dynamics for each individual state variable (indicated by its large R^2).

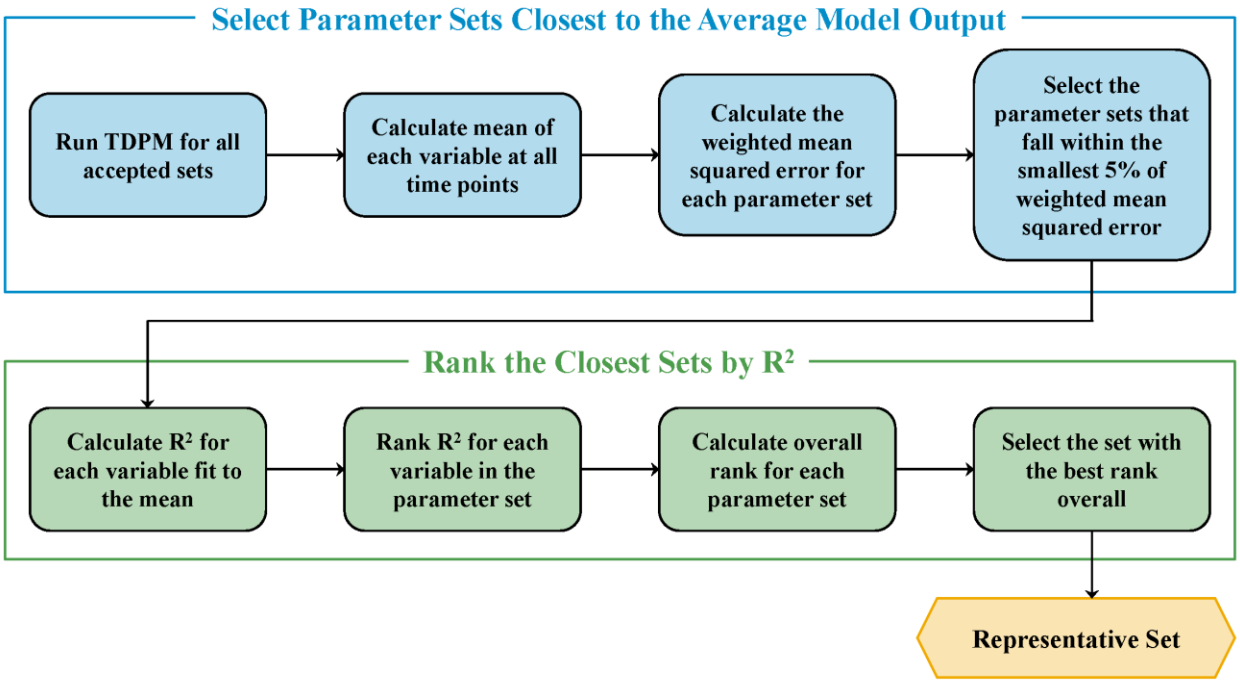


Figure 5. Flow chart depicting the method by which a representative set is chosen from the accepted parameter sets. First, the weighted mean square error (MSE) is computed for each parameter set. For the 5% of parameter sets with the smallest weighted MSE, an R^2 value is obtained and then ranked for each state variable. Finally, the overall R^2 rank is computed for each of these sets, and the parameter set with the best overall rank is chosen as the representative set. This method of selection ensures that the representative parameter set not only represents average model dynamics well (indicated by its small weighted MSE), but also most closely reproduces the average dynamics for each individual state variable (indicated by its large R^2).

4.2 **Results**

4.2.1. Accepted Parameter Combinations

Of the 400,000 parameter sets generated by LHS and simulated, a total of 65,000 sets were accepted by the criteria outlined in Table 4. Figure 6 depict model trends produced by an arbitrarily chosen sample of 100 of the accepted parameter sets for IC1, IC2, and IC3, respectively.

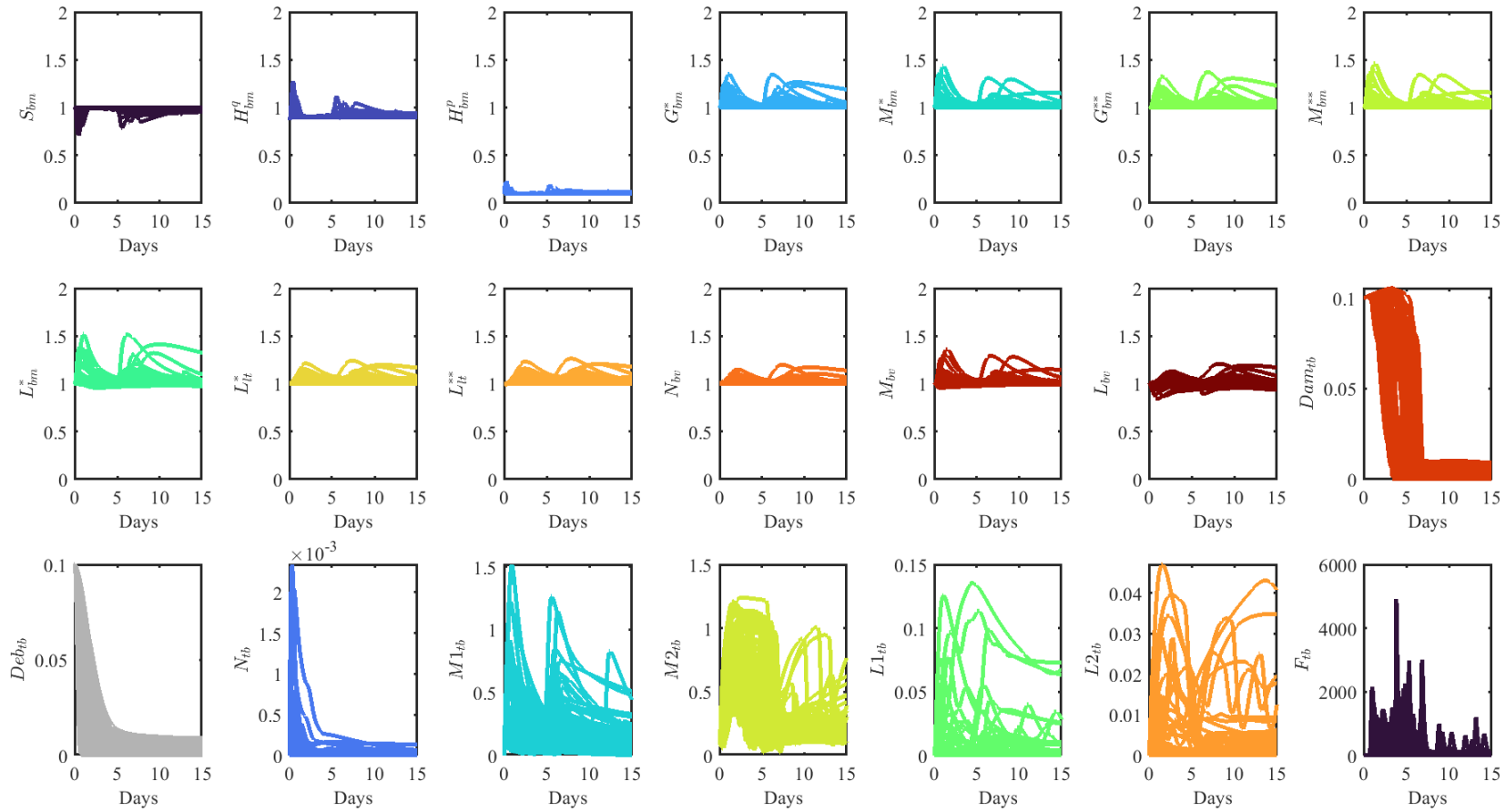


Figure 6. Example dynamics predicted by the TDPM for superficial thermal burn (IC1). The accepted sets were randomly sampled and simulated 100 times to show the diverse model behavior generated by these sets. Observe that the healing dynamics of thermal burn injury do not greatly perturb the systemic populations of immune cells, confirming the collapsibility of the WITBM to the STBM and LITBM.

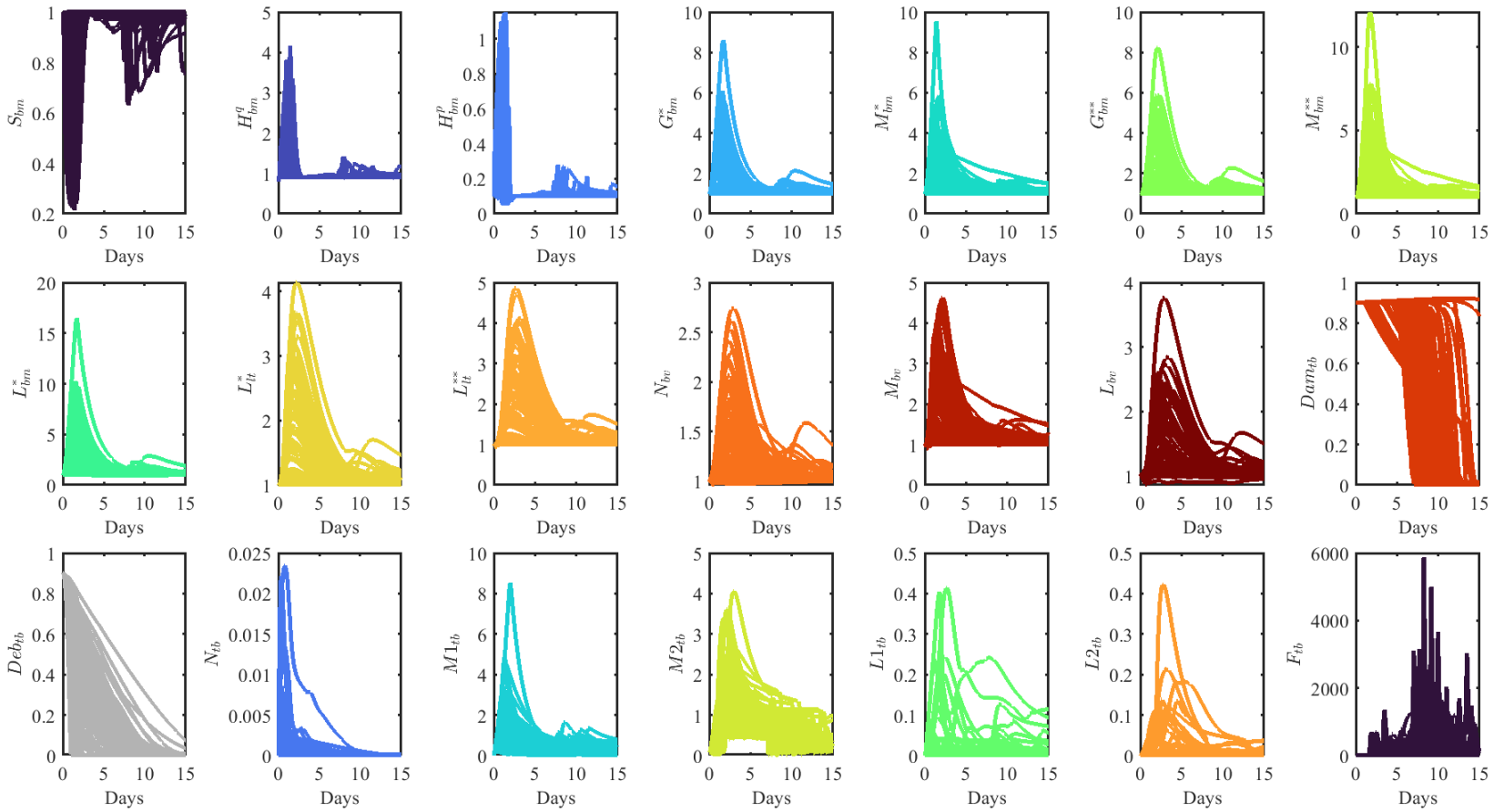


Figure 7. Example dynamics predicted by the TDPM for partial superficial thickness thermal burn (IC2). The accepted sets were randomly sampled and simulated 100 times to show the diverse model behavior generated by these sets.

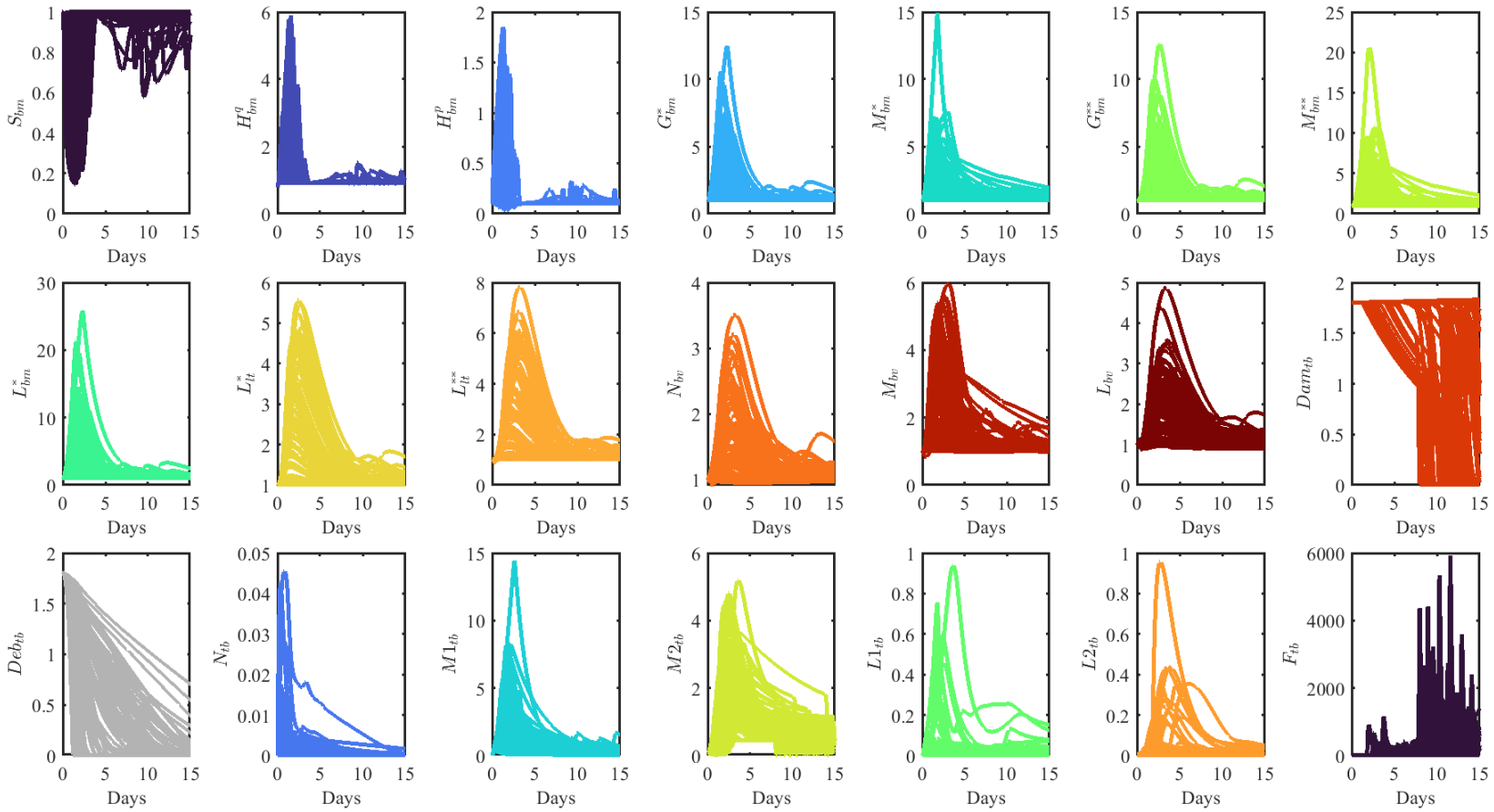


Figure 8. Example dynamics predicted by the TDPM for partial superficial thickness thermal burn (IC2). The accepted sets were randomly sampled and simulated 100 times to show the diverse model behavior generated by these sets.

Observe that the healing dynamics of superficial thermal burn injury do not perturb systemic populations of immune cells (Figure 6), confirming collapsibility of the WITBM to the STBM and LITBM. As burn severity increases (Figure 7), systemic immune cell populations are recruited to the thermal burn injury site, and the rate of recruitment increases with severity.

4.2.2. Representative Set

The representative set was chosen by comparing each of the 65,000 accepted parameter sets with the temporal means of each variable across all model simulations, as described in Section 4.1.3. The estimated value of each parameter assigned by the representative set is given inTable 5. Parameters descriptions, units, and estimated values assigned by the representative set for each of the 40 parameters chosen to be calibrated by available data. Table 5, and plots of the representative set simulated for each initial condition are shown in Figure 9.

Table 5. Parameters descriptions, units, and estimated values assigned by the representative set for each of the 40 parameters chosen to be calibrated by available data.

PARAMETER		DESCRIPTION	UNITS	ESTIMATE VALUE
Inhibition	Deb_H	Constant controlling the effectiveness of Deb_{tb} at inhibiting phagocytic removal of debris by N_{tb}, $M1_{tb}$, and $M2_{tb}$	D-units	0.066965043
	$M1_1^\infty$	Constant controlling the effectiveness of $M1_{tb}$ at inhibiting activation of $M2_{tb}$	M-units	3
	$M1_2^\infty$	Constant controlling the effectiveness of $M1_{tb}$ at inhibiting proliferation and activation of F_{tb}	M-units	0.149045726
	$M2^\infty$	Constant controlling the effectiveness of $M2_{tb}$ at inhibiting activation of N_{tb} and $M1_{tb}$	M-units	0.109999431
	$M2_E^\infty$	Constant controlling the effectiveness of $M2_{tb}$ at inhibiting extravasation of N_{bv} , M_{bv} and L_{bv}	M-units	51.78081041
	F_1^∞	Constant controlling the effectiveness of F_{tb} at inhibiting the activation of $L2_{tb}$	F-units	135.7530498
	$L2_E^\infty$	Constant controlling the effectiveness of $L2_{tb}$ at inhibiting extravasation of N_{bv} , M_{bv} and L_{bv}	L-units	16.76029829
Damage and Debris	k_{dnp}	Phagocytosis rate of Deb_{tb} by N_{tb}	D-units/(N-units·h)	0.004777946
	k_{dm1p}	Phagocytosis rate of Deb_{tb} by $M1_{tb}$	D-units/(M-units·h)	0.019335205
	k_{dm2p}	Phagocytosis rate of Deb_{tb} by $M2_{tb}$	D-units/(M-units·h)	0.003801554
	k_{nnE}	Extravasation rate of N_{bv} to N_{tb} by N_{tb} and its byproducts	N-units/(N-units·h)	0.058598516

PARAMETER		DESCRIPTION	UNITS	ESTIMATE VALUE
	P_{HN}	Hill constant for biomolecular signaling effect on extravasation of N_{bv} to N_{tb}	N-units	312.7369349
Macrophages	$k_{ME_{max}}$	Maximum extravasation rate of M_{bv}	M-units/h	5.5
	$k_{ME_{min}}$	Minimum extravasation rate of M_{bv} to maintain homeostatic resident macrophages	M-units/(D-units·h)	0.08
	k_{mdE}	Extravasation rate of M_{bv} to injury site by Deb_{tb}	M-units/(N-units·h)	0.059745292
	k_{mnE}	Extravasation rate of M_{bv} to injury site by N_{tb}	M-units/(M-units·h)	0.148629024
	P_{HM}	Hill constant for biomolecular signaling effect on extravasation of M_{bv} to $M1_{tb}, M2_{tb}$	M-units	97.55789853
	n_M	Hill exponent for biomolecular signaling effect on extravasation of M_{bv} to $M1_{tb}, M2_{tb}$	M-units/h	0.921677385
	δ_m	Decay rate of M_{bv}	1/h	0.138843772
	k_{m1d}	Activation rate of resting monocytes and tissue-resident macrophages to $M1_{tb}$ by Deb_{tb}	1/(D-units·h)	0.49651044
	k_{m1l1}	Activation rate of resting monocytes and tissue-resident macrophages to $M1_{tb}$ by $L1_{tb}$ and its byproducts	1/(L-units·h)	4.90412E-11
	k_{m2m1}	Activation rate of resting monocytes and tissue-resident macrophages to $M2_{tb}$ by $M1_{tb}$ and its byproducts	1/(M-units·h)	0.004823564
	k_{m2l2}	Activation rate of resting monocytes and tissue-resident macrophages to $M2_{tb}$ by $L2_{tb}$ and its byproducts	1/(L-units·h)	6.20594E-11
Lymphocytes	k_{lnE}	Extravasation rate of L_{bv} to injury site by N_{tb}	L-units/(N-units·h)	0.014206901
	k_{lm1E}	Extravasation rate of L_{bv} to injury site by $M1_{tb}$	L-units/(M-units·h)	0.301046349
	k_{ll1E}	Extravasation rate of L_{bv} to injury site by $L1_{tb}$	L-units/(L-units·h)	0.0477098
	k_{l1}	Induction rate of activated (effector) T lymphocytes to $L1_{tb}$ by $M1_{tb}$	1/(M-units·h)	0.062144088
	k_{l2}	Induction rate of activated (effector) T lymphocytes to $L2_{tb}$ by $M2_{tb}$	1/(M-units·h)	0.076432745

PARAMETER		DESCRIPTION	UNITS	ESTIMATE VALUE
	δ_l	Decay rate of L_{bv}	1/h	0.13926453
Bone Marrow and Lymphatic Tissues	k_{aIm}	Injury signal weight factor for differentiation towards non-mitogenic monocyte progenitors	Unitless	1.448394895
	k_{aIl}	Injury signal weight factor for differentiation towards non-mitogenic lymphocyte progenitors	Unitless	1
	k_{Irg}	Injury signal weight factor for transfer of granulocytes from the bone marrow to the bloodstream	Unitless	1.619490519
	k_{Irl}	Injury signal weight factor for transfer of lymphocytes from the bone marrow to the lymphatic tissue	Unitless	1.620493739
	k_{tbl}	Lymphocyte chemokine surrogate weight factor for biomolecular injury signal from the thermal burn site	Unitless	0.01
	k_{QPmax}	Maximum rate of entrance into the proliferative cell cycle for quiescent HSCs	1/h	0.7294
	r_g	Maximum transfer rate of non-mitogenic progenitor granulocytes into neutrophils in the bloodstream	N-units/h	0.15
	r_l	Maximum transfer rate of mitogenic progenitor lymphocytes into the lymphatic tissues	L-units/h	0.07655822
	r_{lt}	Maximum transfer rate of non-mitogenic progenitor lymphocytes into the bloodstream	L-units/h	0.142170906
	δ_P	Decay rate of H_{bm}^P	1/h	0.12
	δ_{GSS}	Decay rate of G_{bm}^{**}	1/h	0.08

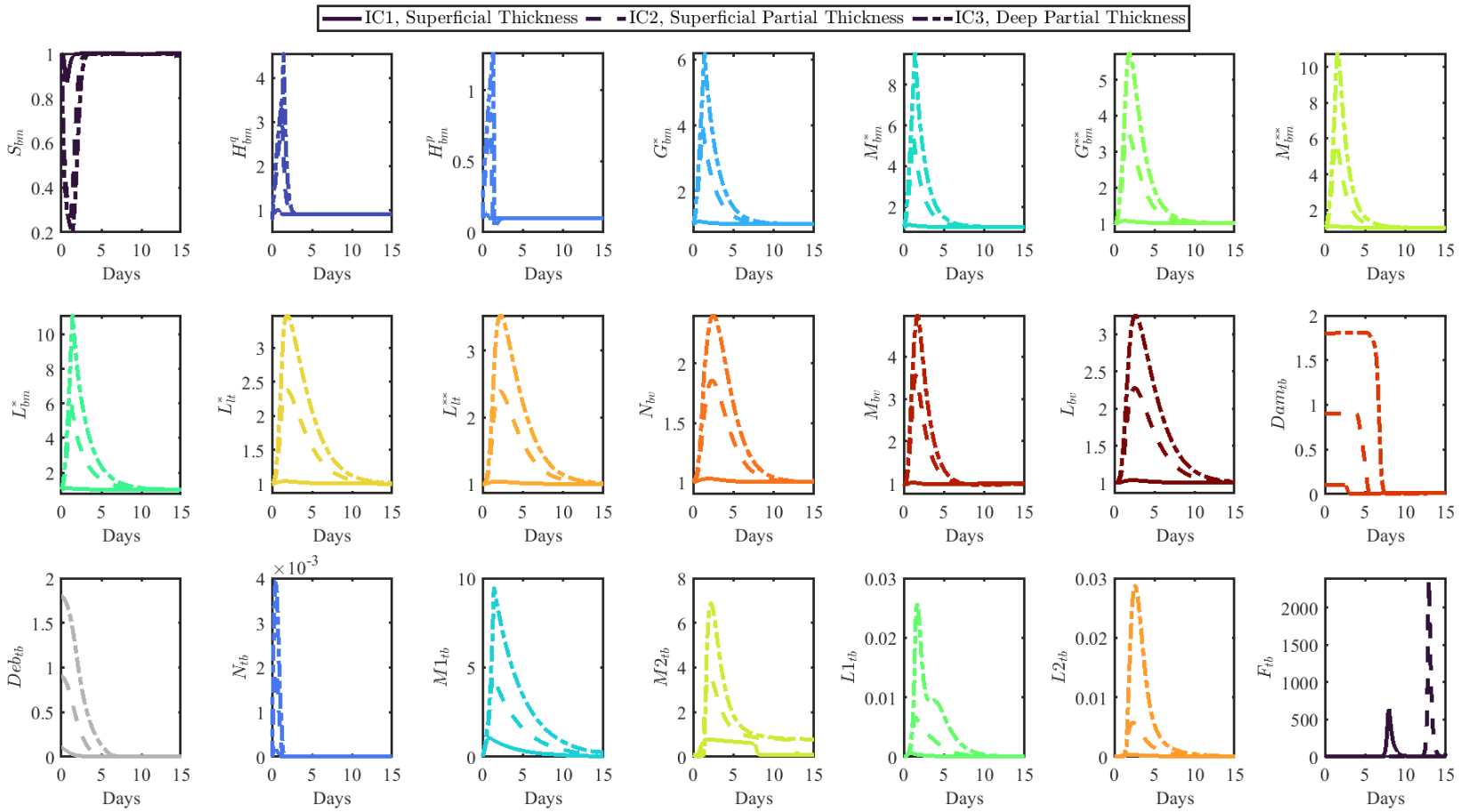


Figure 9. Dynamics of the bone marrow compartment, lymphatic tissue compartment, blood vessel compartment, and thermal burn compartment of the systemic TDPM for combined injury following thermal burn and widespread radiation exposure, as predicted by the representative set for IC1 (superficial thickness burn; solid lines), IC2 (partial superficial thickness burn; dashed lines), and IC3 (deep partial thickness burn; dash-dot lines).

Section 5. Discussion

The large number of parameters in the TDPM for systemic thermal burn and widespread radiation exposure, along with the limited data available for NUDET events, warrant the use of sensitivity analysis to identify the most influential model parameters prior to parameter estimation. Of the 112 parameters in the WITBM, 40 were identified as significantly influential by the results of sensitivity analysis, and therefore included in parameter estimation. The use of this methodology reduces uncertainty of model predictions by ensuring the limited available data is used to calibrate highly influential model parameters.

Due to the significant increase in number of parameters in the WITBM as compared to the previously parameterized local STBM and LITBM, some parameters of the WITBM were screened to remove those which were non-influential prior to sensitivity analysis, thereby reducing its computational intensity. Although the results of sensitivity analysis would be more comprehensive if the parameters which were deemed non-influential during the screening process were instead included in sensitivity analysis, any benefit would be outweighed by the additional computational intensity.

It should be noted that any update to the WITBM, including the addition of a new compartment to incorporate a new type of combined injury, requires a new sensitivity analysis to be performed and for the model to be re-parameterized. The parameterized WITBM presented in this TR is only applicable to combined injuries following thermal burn and widespread radiation exposure, where the severity of thermal burn does not result in damage to the blood vessels and the widespread radiation exposure is not severe enough to promptly cause significant damage to other body systems than hematopoiesis.

The methodology presented herein will be used in future work to parameterize other systemic TDPMs for combined injury. Furthermore, because the bone marrow and thermal burn compartments will remain the same in future systemic TDPMs, the results obtained in screening the bone marrow and thermal burn compartments can be re-used in future parameterization efforts, thus reducing the computational intensity of sensitivity analysis in future work.

Parameterization of the systemic TDPM for combined injury following thermal burn and widespread radiation exposure is a large step towards its implementation in HENRE. Future work will include completion of the insult-to-outcome pipeline by mapping HENRE user inputs to initial conditions of the WITBM, and time-series data generated by the systemic WITBM to outcomes that are of interest to the HENRE user, such as pain, fatiguability and weakness, and gastrointestinal distress. This TR marks the first work in parametrization of a TDPM that investigates the systemic, synergistic effects of combined injury, and once the insult-to-outcome pipeline is completed, this parameterized TDPM will be the first of its kind to be implemented into HENRE.

Section 6. References

Abazari, M., Ghaffari, A., Rashidzadeh, H., Badeleh, S. M., & Maleki, Y. (2020). A systematic review on classification, identification, and healing process of burn wound healing. *International Journal of Lower Extremity Wounds*, 1–13.

Brooks, J. W., Evans, E. I., Ham, W. T., & Reid, J. D. (1952). The Influence of External Body Radiation on Mortality from Thermal Burns. *Annals of Surgery*, *136*(3), 533–544.

Creel, A., Gaffney, K., & Brun, O. (2023). *Implementation of an Insult-to-Outcome Pipeline for Modeling Superficial Thermal Burns in HENRE* (DTRA-TR-23-030). Defense Threat Reduction Agency, Fort Belvoir, VA.

Creel, A., Jennings, R., & Reynolds, A. (2022). *Sensitivity Analysis for a Time-Dependent Physiological Model of Superficial Thermal Burns* (DTRA-TR-21-063 R1). Defense Threat Reduction Agency, Fort Belvoir, VA.

Dela, A., Shtylla, B., & de Pillis, L. (2022). Multi-method global sensitivity analysis of mathematical models. *Journal of Theoretical Biology*, *546*, 111159. https://doi.org/10.1016/j.jtbi.2022.111159

DiCarlo, A. L., Hatchett, R. J., Kaminski, J. M., Ledney, G. D., Pellmar, T. C., Okunieff, P., & Ramakrishnan, N. (2008). Medical Countermeasures for Radiation Combined Injury: Radiation with Burn, Blast, Trauma and/or Sepsis. Report of an NIAID Workshop, March 26–27, 2007. *Radiation Research*, *169*(6), 712–721. https://doi.org/10.1667/RR1295.1

Evers, L. H., Bhavsar, D., & Mailänder, P. (2010). The biology of burn injury. *Experimental Dermatology*, *19*(9), 777–783. https://doi.org/10.1111/j.1600-0625.2010.01105.x

Finnerty, C. C., Jeschke, M. G., Branski, L. K., Barret, J. P., Dziewulski, P., & Herndon, D. N. (2016). Hypertrophic scarring: The greatest unmet challenge following burn injury. *Lancet*

(London, England), *388*(10052), 1427–1436. https://doi.org/10.1016/S0140-6736(16)31406-4

Franklin, R. A. (2021). Fibroblasts and macrophages: Collaborators in tissue homeostasis. *Immunological Reviews*, *302*(1), 86–103. https://doi.org/10.1111/imr.12989

Gaffney, K., Creel, A., Chughtai, N., Hay, Q., & Brun, O. (2023). *Systemic Combined Injury TDPM of Thermal Burn and Widespread Radiation Exposure* (DTRA-TR-23-058). Defense Threat Reduction Agency, Fort Belvoir, VA.

Glasstone, S., & Dolan, P. J. (1977). *The Effects of Nuclear Weapons*. U.S. Department of Defense.

Goldberg, S. R., & Diegelmann, R. F. (2010). Wound Healing Primer. *Surgical Clinics of North America*, *90*(6), 1133–1146. https://doi.org/10.1016/j.suc.2010.08.003

Hay, Q., Gaffney, K., & Creel, A. (2023). *Parameterization of a Time-Dependent Physiological Model of Combined Injury for a Locally Irradiated Superficial Thermal Burn* (DTRA-TR-23-048). Defense Threat Reduction Agency, Fort Belvoir, VA.

Hay, Q., Jennings, R., Reynolds, A. M., & Creel, A. (2022). *A TDPM of Healing Initiated by an Irradiated Superficial Thermal Burn* (DTRA-TR-22-067). Defense Threat Reduction Agency, Fort Belvoir, VA.

Hettiaratchy, S., & Dziewulski, P. (2004). Pathophysiology and types of burns. *BMJ : British Medical Journal*, *328*(7453), 1427–1429.

Iijima, S. (1982). Pathology of atomic bomb casualties. *Acta Pathologica Japonica*, *32 Suppl 2*, 237–270.

Jennings, R., Creel, A., & Reynolds, A. (2022a). *A Time-Dependent Physiological Model of Innate and Adaptive Immune Responses Activated by Superficial Thermal Burns* (DTRA-TR-21-032 R1). Defense Threat Reduction Agency, Fort Belvoir, VA.

Jennings, R., Creel, A., & Reynolds, A. (2022b). *Estimation of Inflammation and Repair Parameters for a Superficial Thermal Burn* (DTRA-TR-22-026). Defense Threat Reduction Agency, Fort Belvoir, VA.

Jennings, R., Hay, Q., Creel, A., & Reynolds, A. (2022). *A Time-Dependent Physiological Model of Innate and Adaptive Immune Responses Activated by Irradiated Superficial Thermal Burns* (DTRA-TR-22-067). Defense Threat Reduction Agency, Fort Belvoir, VA.

Jeschke, M. G., van Baar, M. E., Choudhry, M. A., Chung, K. K., Gibran, N. S., & Logsetty, S. (2020). Burn injury. *Nature Reviews. Disease Primers*, *6*(1), 11. https://doi.org/10.1038/s41572-020-0145-5

Lateef, Z., Stuart, G., Jones, N., Mercer, A., Fleming, S., & Wise, L. (2019). The Cutaneous Inflammatory Response to Thermal Burn Injury in a Murine Model. *International Journal of Molecular Sciences*, *20*(3), Article 3. https://doi.org/10.3390/ijms20030538

Lenhart, T., Eckhardt, K., Fohrer, N., & Frede, H.-G. (2002). Comparison of two different approaches of sensitivity analysis. *Physics and Chemistry of the Earth, Parts A/B/C*, *27*(9), 645–654. https://doi.org/10.1016/S1474-7065(02)00049-9

Link, K. G., Stobb, M. T., Paola, J. D., Neeves, K. B., Fogelson, A. L., Sindi, S. S., & Leiderman, K. (2018). A local and global sensitivity analysis of a mathematical model of coagulation and platelet deposition under flow. *PLOS ONE*, *13*(7), e0200917. https://doi.org/10.1371/journal.pone.0200917

Marino, S., Hogue, I. B., Ray, C. J., & Kirschner, D. E. (2008). A Methodology For Performing Global Uncertainty And Sensitivity Analysis In Systems Biology. *Journal of Theoretical Biology*, *254*(1), 178–196. https://doi.org/10.1016/j.jtbi.2008.04.011

Morris, M. D. (1991). Factorial Sampling Plans for Preliminary Computational Experiments. *Technometrics*, *33*(2). https://www.jstor.org/stable/1269043

Oughterson, A. W., LeRoy, G. V., Liebow, A. A., Hammond, E. C., Barnett, H. L., Rosenbaum, J. D., & Schneider, B. A. (1951). *Medical Effects Of Atomic Bombs The Report Of The Joint Commission For The Investigation Of The Effects Of The Atomic Bomb In Japan Volume 1* (NP-3036; AM-2837(vol. I)). Army Inst. of Pathology, Washington, DC (United States). https://doi.org/10.2172/4421057

Palmer, J. L., Deburghgraeve, C. R., Bird, M. D., Hauer-Jensen, M., & Kovacs, E. J. (2011). Development of a Combined Radiation and Burn Injury Model. *Journal of Burn Care & Research : Official Publication of the American Burn Association*, *32*(2), 317–323. https://doi.org/10.1097/BCR.0b013e31820aafa9

Pellmar, T. C., & Ledney, G. D. (2005). *Combined Injury: Radiation in Combination with Trauma, Infectious Disease, or Chemical Exposures*. d

Peng, D., Huang, W., Ai, S., & Wang, S. (2006). Clinical significance of leukocyte infiltrative response in deep wound of patients with major burns. *Burns*, *32*(8), 946–950. https://doi.org/10.1016/j.burns.2006.03.003

Pietras, E. M., Warr, M. R., & Passegué, E. (2011). Cell cycle regulation in hematopoietic stem cells. *Journal of Cell Biology*, *195*(5), 709–720. https://doi.org/10.1083/jcb.201102131

Reeves, G. I. (2018). Chapter 14: Effects on Personnel. In *EM-1: Capabilities of Nuclear Weapons*.

Saltelli, A., Tarantola, S., & Chan, K. P.-S. (1999). A Quantitative Model-Independent Method for Global Sensitivity Analysis of Model Output. *Technometrics*, *41*(1), 39–56. https://doi.org/10.1080/00401706.1999.10485594

Schultz, G. S., Chin, G. A., Moldawer, L., & Diegelmann, R. F. (2011). Principles of Wound Healing. In *Mechanisms of Vascular Disease: A Reference Book for Vascular Specialists*. University of Adelaide Press. https://www.ncbi.nlm.nih.gov/books/NBK534261/

Wu, J., Dhingra, R., Gambhir, M., & Remais, J. V. (2013). Sensitivity analysis of infectious disease models: Methods, advances and their application. *Journal of The Royal Society Interface*, *10*(86), 20121018. https://doi.org/10.1098/rsif.2012.1018

Yamada, T., Park, C. S., & Lacorazza, H. D. (2013). Genetic control of quiescence in hematopoietic stem cells. *Cell Cycle*, *12*(15), 2376–2383. https://doi.org/10.4161/cc.25416

Zi, Z. (2011). Sensitivity analysis approaches applied to systems biology models. *IET Systems Biology*, *5*(6), 336–336. https://doi.org/10.1049/iet-syb.2011.0015

Appendix A. Model Equations

The systemic TDPM for combined thermal burn and widespread radiation injury is governed by the following system of ODEs, separated by compartment:

Bone Marrow

$$\frac{dS_{bm}}{dt} = \alpha_{sm} - \beta_{sm} S_{bm}\left(H_{bm}^{Q} + H_{bm}^{P}\right) \tag{A1}$$

$$\frac{dH_{bm}^{Q}}{dt} = 2\sigma_P(S_{bm})H_{bm}^{P} + \gamma_P(S_{bm})H_{bm}^{P} - k_{QP}(*)H_{bm}^{Q} - \delta_Q H_{bm}^{Q} \tag{A2}$$

$$\frac{dH_{bm}^{P}}{dt} = k_{QP}(*)H_{bm}^{Q} - \sigma_P(S_{bm})H_{bm}^{P} - \gamma_P(S_{bm})H_{bm}^{P} - \delta_P H_{bm}^{P} \tag{A3}$$

$$\frac{dG_{bm}^{*}}{dt} = \gamma_{PG}(*)H_{bm}^{P} - \delta_{GS} G_{bm}^{*} \tag{A4}$$

$$\frac{dM_{bm}^{*}}{dt} = \gamma_{PM}(*)H_{bm}^{P} - \delta_{MS} M_{bm}^{*} \tag{A5}$$

$$\frac{dL_{bm}^{*}}{dt} = \gamma_{PL}(*)H_{bm}^{P} - \delta_{LS} L_{bm}^{*} - \Delta_{Lbm}(*)L_{bm}^{*} \tag{A6}$$

$$\frac{dG_{bm}^{**}}{dt} = \gamma_{GS} G_{bm}^{*} - \Delta_{Nbm}(*)G_{bm}^{**} - \delta_{GSS} G_{bm}^{**} \tag{A7}$$

$$\frac{dM_{bm}^{**}}{dt} = \gamma_{MS} M_{bm}^{*} - \Delta_{Mbm}(*)M_{bm}^{**} - \delta_{MSS} M_{bm}^{**} \tag{A8}$$

Lymphatic Tissues

$$\frac{dL_{lt}^{*}}{dt} = \Delta_{Lbm}(*)L_{bm}^{*} - \delta_{LS} L_{lt}^{*} \tag{A9}$$

$$\frac{dL_{lt}^{**}}{dt} = \gamma_{LS} L_{lt}^{*} - \Delta_{Llt}(*)L_{lt}^{**} - \delta_{LSS} L_{lt}^{**} \tag{A10}$$

Blood Vessels

$$\frac{dN_{bv}}{dt} = \Delta_{Nbm}(*)G_{bm}^{**} - E_n(Deb_{tb}, N_{tb}, M1_{tb}; M2_{tb}, L2_{tb}) - \delta_n N_{bv} \tag{A11}$$

$$\frac{dM_{bv}}{dt} = \Delta_{Mbm}(*)M_{bm}^{**} - E_m(Deb_{tb}, N_{tb}, M1_{tb}, L1_{tb}; M2_{tb}, L2_{tb}) - \delta_m M_{bv} \tag{A12}$$

$$\frac{dL_{bv}}{dt} = \Delta_{Llt}(*)L_{lt}^{**} - E_l(Deb_{tb}, N_{tb}, M1_{tb}, L1_{tb}; M2_{tb}, L2_{tb}) - \delta_l L_{bv} \tag{A13}$$

Thermal Burn Injury Site

$$\frac{dDam_{tb}}{dt} = k_{dn}\Omega_H(\Omega_i(N_{tb}; L2_{tb}, L2_2^{\infty}), 6, N_H) + \sigma_{dm1}k_{dn}\Omega_H(\Omega_i(M1_{tb}; L2_{tb}, L2_2^{\infty}), 6, M1_H) - \rho_{dam}\Omega_i(Dam_{tb}; Deb_{tb}, Deb_{dam}^{\infty}) - k_{df}F_{tb}\Omega_i(Dam_{tb}; Deb_{tb}, Deb_{dam}^{\infty}) \quad (A14)$$

$$\frac{dDeb_{tb}}{dt} = k_{dn}\Omega_H(\Omega_i(N_{tb}; L2_{tb}, L2_2^{\infty}), 6, N_H) + \sigma_{dm1}k_{dn}\Omega_H(\Omega_i(M1_{tb}; L2_{tb}, L2_2^{\infty}), 6, M1_H) - k_{dnp}N_{tb}\Omega_H(Deb_{tb}, 1, Deb_H) - k_{dm1p}\Omega_i(M1_{tb}; N_{tb}, N_1^{\infty})\Omega_H(Deb_{tb}, 1, Deb_H) - k_{dm2p}\Omega_i(M2_{tb}; N_{tb}, N_1^{\infty})\Omega_H(Deb_{tb}, 1, Deb_H) - d_{deb}Deb_{tb} \quad (A15)$$

$$\frac{dN_{tb}}{dt} = E_n(Deb_{tb}, N_{tb}, M1_{tb}; M2_{tb}, L2_{tb}) - k_{nm1p}N_{tb}\Omega_{\mathrm{i}}(M1_{tb}; N_{tb}, N_1^{\infty}) - k_{nm2p}N_{tb}\Omega_{\mathrm{i}}(M2_{tb}; N_{tb}, N_1^{\infty}) - d_nN_{tb} \quad (A16)$$

$$\frac{dM1_{tb}}{dt} = E_m(Deb_{tb}, N_{tb}, M1_{tb}, L1_{tb}; M2_{tb}, L2_{tb})\left(\frac{R_{m1}}{R_{m1}+R_{m2}}\right) - \theta_{m1m2}\left[k_{nm1p}N_{tb}\Omega_i(M1_{tb}; N_{tb}, N_1^{\infty})\right] - d_{m1}M1_{tb} \quad (A17)$$

$$\frac{dM2_{tb}}{dt} = E_m(Deb_{tb}, N_{tb}, M1_{tb}, L1_{tb}; M2_{tb}, L2_{tb})\left(\frac{R_{m2}}{R_{m1}+R_{m2}}\right) + \theta_{m1m2}\left[k_{nm1p}N_{tb}\Omega_i(M1_{tb}; N_{tb}, N_1^{\infty})\right] - d_{m2}M2_{tb} - \Omega_i(k_{lvm}M2_{tb}; Dam_{tb}, Dam_{lvm}^{\infty}) \quad (A18)$$

$$\frac{dL1_{tb}}{dt} = E_l(Deb_{tb}, N_{tb}, M1_{tb}, L1_{tb}; M2_{tb}, L2_{tb})\left(\frac{R_{l1}}{R_{l1}+R_{l2}}\right) - d_lL1_{tb} \quad (A19)$$

$$\frac{dL2_{tb}}{dt} = E_l(Deb_{tb}, N_{tb}, M1_{tb}, L1_{tb}; M2_{tb}, L2_{tb})\left(\frac{R_{l2}}{R_{l1}+R_{l2}}\right) - d_lL2_{tb} \quad (A20)$$

$$\frac{dF_{tb}}{dt} = s_f + \Omega_i(F_{tb}; N_{tb}, N_2^{\infty}, M1_{tb}, M1_2^{\infty})\left(k_f + \alpha_{dam}Dam_{tb} + \alpha_{m2}M2_{tb}\right) - d_fF_{tb} \quad (A21)$$

where

$$\Omega_i(X; Y_1, Y_1^{\infty}, \ldots, Y_m, Y_m^{\infty}) = \frac{X}{1 + \left(\frac{Y_1}{Y_1^{\infty}}\right)^2 + \ldots + \left(\frac{Y_m}{Y_m^{\infty}}\right)^2} \quad (A22)$$

$$\Omega_H(X, n, X_H) = \frac{X^n}{X_H^n + X^n} \quad (A23)$$

$$\sigma_P(S_{bm}) = C_0 + (C_d - C_0)\Omega_H(S_{bm}, n_S, S_{bmh}) \quad (A24)$$

$$\gamma_P(S_{bm}) = C_d - \sigma_P(S_{bm}) = \gamma_{pg}(*) + \gamma_{pm}(*) + \gamma_{pl}(*) \quad (A25)$$

$$\gamma_{PX}(*) = \gamma_P(S_{bm})\left(\frac{a_X}{a_g + a_m + a_l}\right) \tag{A26}$$

$$a_X = \frac{1 + k_{aIX} I_{tb}}{1 + k_{aX} X^*_{bm}} \tag{A27}$$

$$I_{tb} = \frac{k_{tbd} Dam_{tb} + k_{tbn} N_{tb} + k_{tbm} M1_{tb} + k_{tbl} L1_{tb}}{1 + \left(\frac{M2_{tb}}{M2_\infty}\right)^2 + \left(\frac{L2}{L2_\infty}\right)^2} \tag{A28}$$

$$k_{QP}(*) = k_{QPmax}\left(1 - \Omega_H\left(\Omega_I\left(\left(H^Q_{bm} + H^P_{bm}\right); I_{tb}, I_\infty\right), n_{kQP}, H_{kqp}\right)\right) \tag{A29}$$

$$E_n = k_{NE_{max}} \Omega_i(\Omega_H(P_N, n_N, P_{HN}); M2_{tb}, M2^\infty_E, L2_{tb}, L2^\infty_E) N_{bv} \tag{A30}$$

$$E_m = \left[\left(k_{ME_{max}} - k_{ME_{min}}\right)[\Omega_i(\Omega_H(P_M, n_M, P_{HM}); M2_{tb}, M2^\infty_E, L2_{tb}, L2^\infty_E)] + k_{ME_{min}}\right] M_{bv} \tag{A31}$$

$$E_l = k_{LE_{max}} \Omega_i(\Omega_H(P_L, n_L, P_{HL}); M2_{tb}, M2^\infty_E, L2_{tb}, L2^\infty_E) L_{bv} \tag{A32}$$

$$P_N = k_{ndE} \mathrm{Deb}_{tb} + k_{nnE} N_{tb} \tag{A33}$$

$$P_M = k_{mdE} Deb_{tb} + k_{mnE} N_{tb} + k_{mm1E} M1_{tb} + k_{ml1E} L1_{tb} \tag{A34}$$

$$P_L = k_{ldE} \mathrm{Deb}_{tb} + k_{lnE} N_{tb} + k_{lm1E} \mathrm{M1}_{tb} + k_{ll1E} \mathrm{L1}_{tb} \tag{A35}$$

$$R_{m1} = \Omega_i(k_{m1d} Deb_{tb} + k_{m1n} N_{tb} + k_{m1m1} M1_{tb} + k_{m1l1} L1_{tb}; M2_{tb}, M2^\infty, L2_{tb}, L2^\infty_1) \tag{A36}$$

$$R_{m2} = \Omega_i(k_{m2m1} M1_{tb} + k_{m2m2} M2_{tb} + k_{m2l2} L2_{tb}; N_{tb}, N^\infty_1, M1_{tb}, M1^\infty_1, F_{tb}, F^\infty) \tag{A37}$$

$$R_{l1} = \frac{k_{l1} M1_{tb}}{1 + \left(\frac{L2_{tb}}{L2^\infty_1}\right)^2} \tag{A38}$$

$$R_{l2} = \frac{k_{l2} M2_{tb}}{1 + \left(\frac{F_{tb}}{F^\infty_1}\right)^2} \tag{A39}$$

$$\Delta_{Xbm}(*) = \frac{r_X}{1 + \beta_{rX} X_{bv}\left(\frac{1}{1 + k_{IrX} I_{tb}}\right)} \tag{A40}$$

$$\Delta_{Xlt}(*) = \frac{r_{Xt}}{1 + \beta_{rXt} X_{bv}\left(\frac{1}{1 + k_{IrXt} I_{tb}}\right)} \tag{A41}$$

All parameters are assumed to be non-negative.

To ensure the TDPM maintains homeostasis under the proper conditions, the following parameters must be expressed as a function of other model parameters:

$$\alpha_{sm} = \beta_{sm} \tag{A42}$$

$$C_d = 10\left(\delta_{gs} + \delta_{ms} + 2\delta_{ls}\right) + \delta_p + 9\delta_q \tag{A43}$$

$$S_{bmH} = \left(\frac{C_d - C_0}{\delta_p + 9\delta_q - C_0}\right)^{1/n_s} \tag{A44}$$

$$H_{kqp} = \left(\frac{1}{\frac{9k_{qpmax}}{C_d + \delta_p} - 1}\right)^{1/n_{kqp}} \tag{A45}$$

$$k_{am} = \frac{\delta_{gs}\left(1 + k_{ag}\right)}{\delta_{ms}} - 1 \tag{A46}$$

$$k_{al} = \frac{\delta_{gs}\left(1 + k_{ag}\right)}{2\delta_{ls}} - 1 \tag{A47}$$

$$\gamma_{gs} = \delta_{gss} + \delta_n \tag{A48}$$

$$\gamma_{ms} = \delta_{mss} + k_{ME_{min}} + \delta_m \tag{A49}$$

$$\gamma_{ls} = \delta_{lss} + \delta_l \tag{A50}$$

$$\beta_{rg} = \frac{r_g}{\gamma_{gs} - \delta_{gss}} - 1 \tag{A51}$$

$$\beta_{rm} = \frac{r_m}{\gamma_{ms} - \delta_{mss}} - 1 \tag{A52}$$

$$\beta_{rl} = \frac{r_l}{\gamma_{ls}} - 1 \tag{A53}$$

$$\beta_{rlt} = \frac{r_{lt}}{\gamma_{ls} - \delta_{lss}} - 1 \tag{A54}$$

$$k_{lvm} = 10k_{ME_{min}} - d_{m2} \tag{A55}$$

$$\alpha_{m2} = 10d_f - 100s_f - 10k_f \tag{A56}$$

Additionally, to guarantee that all parameters are positive, real numbers, the following conditions must be satisfied:

$$k_{ME_{min}} > \frac{d_{m2}}{10} \tag{A57}$$

$$k_{ME_{max}} > k_{ME_{min}} \tag{A58}$$

$$C_d \geq C_0 \tag{A59}$$

$$C_d > \delta_p + 9\delta_q \tag{A60}$$

$$k_{qpmax} > \frac{C_d + \delta_p}{9} = \frac{10\left(\delta_{gs} + \delta_{ms} + 2\delta_{ls}\right) + 2\delta_p + 9\delta_q}{9} \tag{A61}$$

$$\delta_{gs} > \frac{2\delta_{ls}}{1 + k_{ag}} \tag{A62}$$

$$\delta_{gs} > \frac{\delta_{ms}}{1 + k_{ag}} \tag{A63}$$

$$\gamma_{gs} > \delta_{gss} \tag{A64}$$

$$\gamma_{ms} > \delta_{mss} \tag{A65}$$

$$\gamma_{ls} > \delta_{lss} \tag{A66}$$

$$r_g > \gamma_{gs} - \delta_{gss} = \delta_n \tag{A67}$$

$$r_m > \gamma_{ms} - \delta_{mss} = k_{ME_{min}} + \delta_m \tag{A68}$$

$$r_l > \delta_{ls} \tag{A69}$$

$$r_{lt} > \gamma_{ls} - \delta_{lss} = \delta_l \tag{A70}$$

$$d_f > 100s_f + 10k_f \tag{A71}$$

Appendix B. Model Parameters

Table 6. Baseline values and ranges for all parameters of the systemic TDPM for combined injury following thermal burn and widespread radiation exposure, given by equations A1 – A41 in Appendix A. Each parameter is assumed to follow a uniform distribution with bounds given by its estimated minimum and estimated maximum.

PARAMETER		DESCRIPTION	UNITS	BASELINE VALUE	ESTIMATED MINIMUM	ESTIMATED MAXIMUM	COMPARTMENT(S)			
							BM	LT	BV	TB
Inhibition	Deb_{dam}^{∞}	Constant controlling the effectiveness of Deb_{tb} at inhibiting damage repair	D-units	0.01	0.001	0.019				X
	Deb_H	Constant controlling the effectiveness of Deb_{tb} at inhibiting phagocytic removal of debris by N_{tb}, $M1_{tb}$, and $M2_{tb}$	D-units	0.1	0.01	0.19				X
	Dam_{lvm}^{∞}	Constant controlling the effectiveness of Dam_{tb} at inhibiting clearance of $M2_{tb}$	D-units	0.01	0.001	0.019				X
	N_1^{∞}	Constant controlling the effectiveness of N_{tb} at inhibiting the activity on other immune cells	N-units	2	0.2	3.8				X
	N_2^{∞}	Constant controlling the effectiveness of N_{tb} at inhibiting proliferation and activation of F_{tb}	N-units	0.1	0.01	0.19				X
	$M1_1^{\infty}$	Constant controlling the effectiveness of $M1_{tb}$ at inhibiting activation of $M2_{tb}$	M-units	3	0.3	5.7				X
	$M1_2^{\infty}$	Constant controlling the effectiveness of $M1_{tb}$ at inhibiting proliferation and activation of F_{tb}	M-units	0.1	0.01	0.19				X
	$M2^{\infty}$	Constant controlling the effectiveness of $M2_{tb}$ at inhibiting activation of N_{tb} and $M1_{tb}$	M-units	0.125	0.0125	0.2375				X

PARAMETER		DESCRIPTION	UNITS	BASELINE VALUE	ESTIMATED MINIMUM	ESTIMATED MAXIMUM	COMPARTMENT(S)			
							BM	LT	BV	TB
	$M2_E^{\infty}$	Constant controlling the effectiveness of $M2_{tb}$ at inhibiting extravasation of N_{bv} , M_{bv} and L_{bv}	M-units	65	0.33200295	106.9379514			X	X
	F^{∞}	Constant controlling the effectiveness of F_{tb} at inhibiting the activation of $M2_{tb}$	F-units	100	10	190				X
	F_1^{∞}	Constant controlling the effectiveness of F_{tb} at inhibiting the activation of $L2_{tb}$	F-units	100	10	190				X
	$L2_1^{\infty}$	Constant controlling the effectiveness of $L2_{tb}$ at inhibiting the activation of N_{tb}, $M1_{tb}$, and $L1_{tb}$	L-units	0.05	0.005	0.095				X
	$L2_2^{\infty}$	Constant controlling the effectiveness of $L2_{tb}$ at inhibiting collateral damage associated with N_{tb} and $M1_{tb}$	L-units	0.12	0.012	0.228				X
	$L2_E^{\infty}$	Constant controlling the effectiveness of $L2_{tb}$ at inhibiting extravasation of N_{bv} , M_{bv} and L_{bv}	L-units	10	1.29407154	17.1622908			X	X
Damage & Debris	k_{dn}	Maximum collateral tissue damage rate caused by N_{tb} at the local burn site	D-units/h	0.000175	0.0000175	0.0003325				X
	σ_{dm1}	Tissue damage scaling coefficient for $M1_{tb}$	Unitless	0.5	0.05	0.95				X
	N_H	Hill constant for tissue damage associated with N_{tb}	N-units	0.06	0.006	0.114				X
	$M1_H$	Hill constant for tissue damage associated with $M1_{tb}$	M-units	0.06	0.006	0.114				X

PARAMETER		DESCRIPTION	UNITS	BASELINE VALUE	ESTIMATED MINIMUM	ESTIMATED MAXIMUM	COMPARTMENT(S)			
							BM	LT	BV	TB
	ρ_{dam}	Baseline tissue damage repair rate via a combination of repair, resolution, and regeneration	1/h	0.004	0.0004	0.0076				X
	k_{df}	Repair rate on Dam_{tb} by F_{tb}	1/(F-units·h)	0.0005	0.00005	0.00095				X
	k_{dnp}	Phagocytosis rate of Deb_{tb} by N_{tb}	D-units/(N-units·h)	0.005	0.0005	0.0095				X
	k_{dm1p}	Phagocytosis rate of Deb_{tb} by $M1_{tb}$	D-units/(M-units·h)	0.016726659	0.001672666	0.031780652				X
	k_{dm2p}	Phagocytosis rate of Deb_{tb} by $M2_{tb}$	D-units/(M-units·h)	0.003422271	0.000342227	0.006502315				X
	d_{deb}	Decay rate of Deb_{tb}	1/h	0.0001	0.00001	0.00019				X
Neutrophils	$k_{NE_{max}}$	Maximum extravasation rate of N_{bv} to N_{tb}	N-units/h	0.3	0.104429455	0.466557311			X	X
	k_{ndE}	Extravasation rate of N_{bv} to N_{tb} by Deb_{tb}	N-units/(D-units·h)	0.3	1×10^{-10}	0.505865303			X	X
	k_{nnE}	Extravasation rate of N_{bv} to N_{tb} by N_{tb} and its byproducts	N-units/(N-units·h)	0.1	0.044737581	0.167142326			X	X
	P_{HN}	Hill constant for biomolecular signaling effect on extravasation of N_{bv} to N_{tb}	N-units	200	12.24669767	337.7596216			X	X
	n_N	Hill exponent for biomolecular signaling effect on extravasation of N_{bv} to N_{tb}	N-units	1	0.372745731	1.604135991			X	X
	δ_n	Decay rate of N_{bv}	1/h	0.0318	0.00320909	0.050331903			X	
	d_n	Decay rate of N_{tb}	1/h	0.1	0.01	0.19				X
	k_{nm1p}	Phagocytosis rate of N_{tb} by $M1_{tb}$	1/(M-units·h)	0.12075	0.012075	0.229425				X
	k_{nm2p}	Phagocytosis rate of N_{tb} by $M2_{tb}$	1/(M-units·h)	0.362833333	0.036283333	0.689383333				X

PARAMETER		DESCRIPTION	UNITS	BASELINE VALUE	ESTIMATED MINIMUM	ESTIMATED MAXIMUM	COMPARTMENT(S)			
							BM	LT	BV	TB
Macrophages	$k_{ME_{max}}$	Maximum extravasation rate of M_{bv}	M-units/h	1	0.088426473	9.043016004			X	X
	$k_{ME_{min}}$	Minimum extravasation rate of M_{bv} to maintain homeostatic resident macrophages	M-units/(D-units·h)	0.0725	0.048095335	0.130303183			X	X
	k_{mdE}	Extravasation rate of M_{bv} to injury site by Deb_{tb}	M-units/(N-units·h)	0.1	0.033096941	0.163255366			X	X
	k_{mnE}	Extravasation rate of M_{bv} to injury site by N_{tb}	M-units/(M-units·h)	0.1	0.001735034	0.172674197			X	X
	k_{mm1E}	Extravasation rate of M_{bv} to injury site by $M1_{tb}$	M-units/(L-units·h)	0.1	0.019821087	0.17742944			X	X
	k_{ml1E}	Extravasation rate of M_{bv} to injury site by $L1_{tb}$	M-units	0.01	0.004125794	0.018953821			X	X
	P_{HM}	Hill constant for biomolecular signaling effect on extravasation of M_{bv} to $M1_{tb}, M2_{tb}$	M-units	100	52.96597012	180.1424672			X	X
	n_M	Hill exponent for biomolecular signaling effect on extravasation of M_{bv} to $M1_{tb}, M2_{tb}$	M-units/h	1	0.859491518	1.835619433			X	X
	δ_m	Decay rate of M_{bv}	1/h	0.1	0.038609004	0.173562288			X	
	d_{m1}	Decay rate of $M1_{tb}$	1/h	0.058220519	0.005822052	0.110618986				X
	d_{m2}	Decay rate of $M2_{tb}$	1/h	0.105786803	0.01057868	0.200994926				X
	k_{m1d}	Activation rate of resting monocytes and tissue-resident macrophages to $M1_{tb}$ by Deb_{tb}	1/(D-units·h)	0.3	0.03	0.57				X

PARAMETER		DESCRIPTION	UNITS	BASELINE VALUE	ESTIMATED MINIMUM	ESTIMATED MAXIMUM	COMPARTMENT(S)			
							BM	LT	BV	TB
	k_{m1n}	Activation rate of resting monocytes and tissue-resident macrophages to $M1_{tb}$ by N_{tb} and its byproducts	1/(N-units·h)	0.03	0.003	0.057				X
	k_{m1m1}	Activation rate of resting monocytes and tissue-resident macrophages to $M1_{tb}$ by $M1_{tb}$ and its byproducts	1/(M-units·h)	0.3	1×10^{-10}	0				X
	k_{m1l1}	Activation rate of resting monocytes and tissue-resident macrophages to $M1_{tb}$ by $L1_{tb}$ and its byproducts	1/(L-units·h)	0.03	1×10^{-10}	0				X
	k_{m2m1}	Activation rate of resting monocytes and tissue-resident macrophages to $M2_{tb}$ by $M1_{tb}$ and its byproducts	1/(M-units·h)	0	0.001542892	0.029314941				X
	k_{m2m2}	Activation rate of resting monocytes and tissue-resident macrophages to $M2_{tb}$ by $M2_{tb}$ and its byproducts	1/(M-units·h)	0	6.76667E-05	0.001285667				X
	k_{m2l2}	Activation rate of resting monocytes and tissue-resident macrophages to $M2_{tb}$ by $L2_{tb}$ and its byproducts	1/(L-units·h)	0.015428916	1×10^{-10}	0				X
	θ_{m1m2}	Transition rate of $M1_{tb}$ to $M2_{tb}$	M-units/N-units	0.000676667	0.069008333	1.311158333				X
	k_{lvm}	Clearance rate of $M2_{tb}$	1/h	Appendix A, Eq. (A55)	n/a	n/a				X
Fibroblasts	s_f	Non-injury recruitment rate of fibroblasts to the local burn site	F-units/h	0.001388889	0.000138889	0.002638889				X
	d_f	Decay rate of F_{tb}	1/h	0.195	0.0195	0.3705				X
	k_f	Baseline proliferation and activation rate of F_{tb}	1/h	0.005333333	0.000533333	0.010133333				X

PARAMETER		DESCRIPTION	UNITS	BASELINE VALUE	ESTIMATED MINIMUM	ESTIMATED MAXIMUM	COMPARTMENT(S)			
							BM	LT	BV	TB
	α_{m2}	Constant controlling the up-regulation of F_{tb} proliferation and activation by $M2_{tb}$	1/(M-units·h)	Appendix A, Eq. (A56)	n/a	n/a				X
	α_{dam}	Constant controlling the up-regulation of F_{tb} proliferation and activation by Dam_{tb}	1/(M-units·h)	0.066666667	0.006666667	0.126666667				X
Lymphocytes	$k_{LE_{max}}$	Maximum extravasation rate of L_{bv}	L-units/h	0.25	0.111501697	0.436484211			X	X
	k_{ldE}	Extravasation rate of L_{bv} to injury site by Deb_{tb}	L-units/(D-units·h)	0.01	0.004321226	0.016836409			X	X
	k_{lnE}	Extravasation rate of L_{bv} to injury site by N_{tb}	L-units/(N-units·h)	0.01	0.003455026	0.018015701			X	X
	k_{lm1E}	Extravasation rate of L_{bv} to injury site by $M1_{tb}$	L-units/(M-units·h)	0.25	0.089282907	0.424946785			X	X
	k_{ll1E}	Extravasation rate of L_{bv} to injury site by $L1_{tb}$	L-units/(L-units·h)	0.1	0.018808045	0.160930686			X	X
	P_{HL}	Hill constant for biomolecular signaling effect on extravasation of L_{bv} to $L1_{tb}, L2_{tb}$	L-units	100	1.242245567	161.6314532			X	X
	n_L	Hill exponent for biomolecular signaling effect on extravasation of L_{bv} to $L1_{tb}, L2_{tb}$	L-units	1	0.48874409	1.78347253			X	X
	k_{l1}	Induction rate of activated (effector) T lymphocytes to $L1_{tb}$ by $M1_{tb}$	1/(M-units·h)	0.097773944	0.009777394	0.185770493				X
	k_{l2}	Induction rate of activated (effector) T lymphocytes to $L2_{tb}$ by $M2_{tb}$	1/(M-units·h)	0.05	0.005	0.095				X
	δ_l	Decay rate of L_{bv}	1/h	0.101469096	0.037060911	0.175459584			X	

PARAMETER		DESCRIPTION	UNITS	BASELINE VALUE	ESTIMATED MINIMUM	ESTIMATED MAXIMUM	COMPARTMENT(S)			
							BM	LT	BV	TB
	d_ℓ	Decay rate of $L1_{tb}$ and $L2_{tb}$	1/h	0.101469096	0.01014691	0.192791282				X
Bone Marrow & Lymphatic Tissue	α_{sm}	Production rate of growth factor-like environmental mediator	S-units/h	Appendix A, Eq. (A42)	n/a	n/a	X			
	β_{sm}	Consumption rate of growth factor-like environmental mediator by HSCs	1/(S-units·h)	0.5	0.069339101	0.913134476	X			
	C_d	Maximum proliferating HSC division rate	1/h	Appendix A, Eq. (A43)	n/a	n/a	X			
	C_0	Minimum proliferating HSC division rate	1/h	0.25	0.06107176	0.476934376	X			
	γ_{GS}	Transition rate from G_{bm}^{*} to G_{bm}^{**}	1/h	Appendix A, Eq. (A48)	n/a	n/a	X			
	γ_{MS}	Transition rate from M_{bm}^{*} to M_{bm}^{**}	1/h	Appendix A, Eq. (A49)	n/a	n/a	X			
	γ_{LS}	Transition rate from L_{lt}^{*} to L_{lt}^{**}	1/h	Appendix A, Eq. (A50)	n/a	n/a		X		
	S_{bmH}	Hill constant for mathematical saturation effect of S_{bm} on the symmetric HSC division rate	S-units	Appendix A, Eq. (A44)	n/a	n/a	X			
	n_S	Hill exponent for mathematical saturation effect of S_{bm} on the symmetric HSC division rate	S-units	2	0.715097858	3.184064273	X			
	k_{aIg}	Injury signal weight factor for differentiation towards non-mitogenic granulocyte progenitors	Unitless	0.7	0.147221393	1.134065648	X			

PARAMETER	DESCRIPTION	UNITS	BASELINE VALUE	ESTIMATED MINIMUM	ESTIMATED MAXIMUM	COMPARTMENT(S)			
						BM	LT	BV	TB
k_{aIm}	Injury signal weight factor for differentiation towards non-mitogenic monocyte progenitors	Unitless	1	0.33048928	1.717415408	X			
k_{aIl}	Injury signal weight factor for differentiation towards non-mitogenic lymphocyte progenitors	Unitless	1	0.373079403	1.642410303	X			
k_{Irg}	Injury signal weight factor for transfer of granulocytes from the bone marrow to the bloodstream	Unitless	1	0.22388986	1.847699842	X		X	
k_{Irm}	Injury signal weight factor for transfer of monocytes from the bone marrow to the bloodstream	Unitless	1	0.244587509	1.779108836	X		X	
k_{Irl}	Injury signal weight factor for transfer of lymphocytes from the bone marrow to the lymphatic tissue	Unitless	1	0.02656503	1.932898071	X	X		
k_{Irlt}	Injury signal weight factor for transfer of lymphocytes from the lymphatic tissue to the bloodstream	Unitless	1	0.025165462	1.894736066		X	X	
k_{ag}	Population signal weight factor for differentiation towards mitogenic granulocyte progenitors	Unitless	0.7491	0.12254113	0.908114474	X			
k_{am}	Population signal weight factor for differentiation towards mitogenic monocyte progenitors	Unitless	Appendix A, Eq. (A46)	n/a	n/a	X			
k_{al}	Population signal weight factor for differentiation towards mitogenic lymphocyte progenitors	Unitless	Appendix A, Eq. (A47)	n/a	n/a	X			

PARAMETER	DESCRIPTION	UNITS	BASELINE VALUE	ESTIMATED MINIMUM	ESTIMATED MAXIMUM	COMPARTMENT(S)			
						BM	LT	BV	TB
I_∞	Constant controlling the effectiveness of injury signal I_{tb} at awakening quiescent HSCs	I-units	0.05	0.015846307	0.080359609	X			
k_{tbd}	Damage DAMP surrogate weight factor for biomolecular injury signal from the thermal burn injury site	Unitless	0.25	0.106204677	0.408478393	X	X	X	
k_{tbn}	Neutrophil chemokine surrogate weight factor for biomolecular injury signal from the thermal burn site	Unitless	0.05	1×10^{-10}	0.087496605	X	X	X	
k_{tbm}	Macrophage chemokine surrogate weight factor for biomolecular injury signal from the thermal burn site	Unitless	0.05	0.010227734	0.079044923	X	X	X	
k_{tbl}	Lymphocyte chemokine surrogate weight factor for biomolecular injury signal from the thermal burn site	Unitless	0.01	0.00308396	0.014920331	X	X	X	
k_{QPmax}	Maximum rate of entrance into the proliferative cell cycle for quiescent HSCs	1/h	0.7294	0.252924471	1.143748524	X			
n_{kQP}	Hill exponent for mathematical saturation effect of injury signal on the transition of quiescent HSCs to proliferation	H-units	2	0.24677091	3.49698711	X			
H_{kQP}	Hill constant for mathematical saturation effect of injury signal on the transition of quiescent HSCs to proliferation	H-units	Appendix A, Eq. (A45)	n/a	n/a	X			
r_g	Maximum transfer rate of non-mitogenic progenitor granulocytes into neutrophils in the bloodstream	N-units/h	0.15	0.048672905	0.232227109	X		X	

PARAMETER	DESCRIPTION	UNITS	BASELINE VALUE	ESTIMATED MINIMUM	ESTIMATED MAXIMUM	COMPARTMENT(S)			
						BM	LT	BV	TB
r_m	Maximum transfer rate of non-mitogenic progenitor granulocytes into monocytes in the bloodstream	M-units/h	0.2	0.140450967	0.324305804	X		X	
r_l	Maximum transfer rate of mitogenic progenitor lymphocytes into the lymphatic tissues	L-units/h	0.15	0.050038385	0.262677101	X	X		
r_{lt}	Maximum transfer rate of non-mitogenic progenitor lymphocytes into the bloodstream	L-units/h	0.11	0.078194616	0.208866552		X	X	
β_{rg}	Population weight factor on neutrophil transfer from bone marrow to the bloodstream	Unitless	Appendix A, Eq. (A51)	n/a	n/a	X		X	
β_{rm}	Population weight factor on monocyte transfer from bone marrow to the bloodstream	Unitless	Appendix A, Eq. (A52)	n/a	n/a	X		X	
β_{rl}	Population weight factor on lymphocyte transfer from bone marrow to the bloodstream	Unitless	Appendix A, Eq. (A53)	n/a	n/a	X	X		
β_{rlt}	Population weight factor on lymphocyte transfer from lymphatic tissue to the bloodstream	Unitless	Appendix A, Eq. (A54)	n/a	n/a	X	X	X	
δ_Q	Decay rate of H_{bm}^Q	1/h	0.09	0.023284453	0.146842352	X			
δ_P	Decay rate of H_{bm}^P	1/h	0.12	0.01397316	0.198232359	X			
δ_{GS}	Decay rate of G_{bm}^*	1/h	0.025	0.021208498	0.053787695	X			
δ_{MS}	Decay rate of M_{bm}^*	1/h	0.025	0.003098367	0.041457586	X			
δ_{LS}	Decay rate of L_{bm}^* and L_{lt}^*	1/h	0.019	0.003330836	0.030567537	X	X		
δ_{GSS}	Decay rate of G_{bm}^{**}	1/h	0.08	0.017820702	0.131148161	X			

PARAMETER		DESCRIPTION	UNITS	BASELINE VALUE	ESTIMATED MINIMUM	ESTIMATED MAXIMUM	COMPARTMENT(S)			
							BM	LT	BV	TB
	δ_{MSS}	Decay rate of M_{bm}^{**}	1/h	0.08	0.02078252	0.116699289	X			
	δ_{LSS}	Decay rate of L_{lt}^{**}	1/h	0.05	0.025058728	0.085999772		X		

Appendix C. Sensitivity Analysis Plots

C.1. MeFAST Plots for Parameter Screening in the Bone Marrow

C.1.1. Line Plots of Total Sensitivity Index Rankings

Plots display the ranked total sensitivity indices for each parameter across all 40 sensitivity indices for (a) superficial thermal burn (IC1, $Dam_{tb}(0) = Deb_{tb}(0) = 0.1$); (b) superficial partial thickness burn (IC2, $Dam_{tb}(0) = Deb_{tb}(0) = 0.9$); and (c) deep partial thickness burn (IC3, $Dam_{tb}(0) = Deb_{tb}(0) = 1.8$).

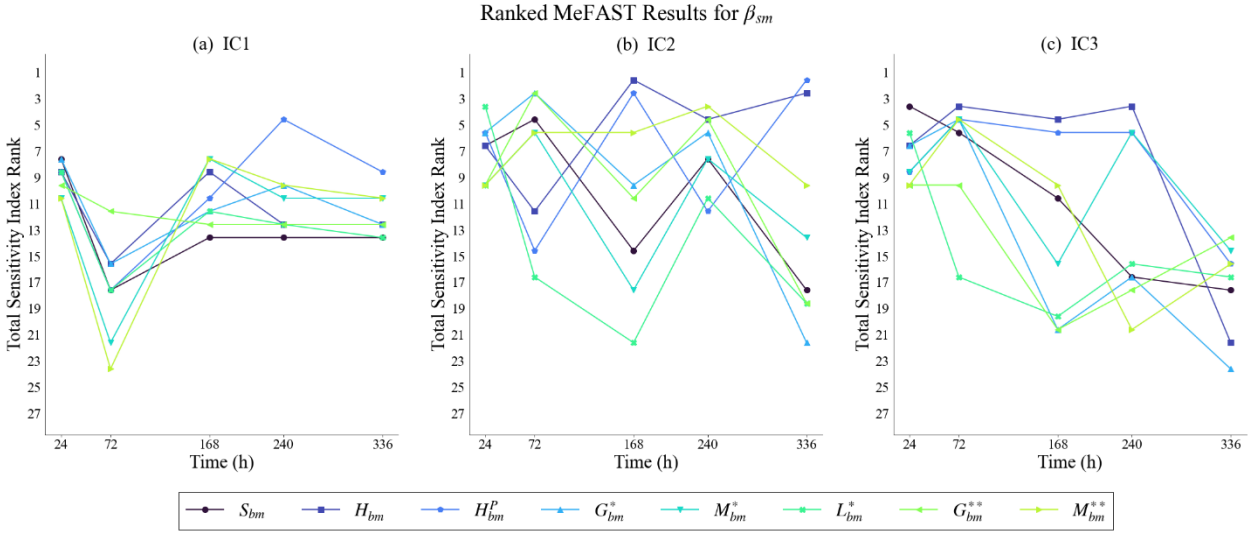


Figure 10. Ranked total sensitivity indices for β_{sm} across all 40 MeFAST outputs for (a) IC1, superficial thermal burn; (b) IC2, superficial partial thickness thermal burn; and (c) IC3, deep partial thickness thermal burn.

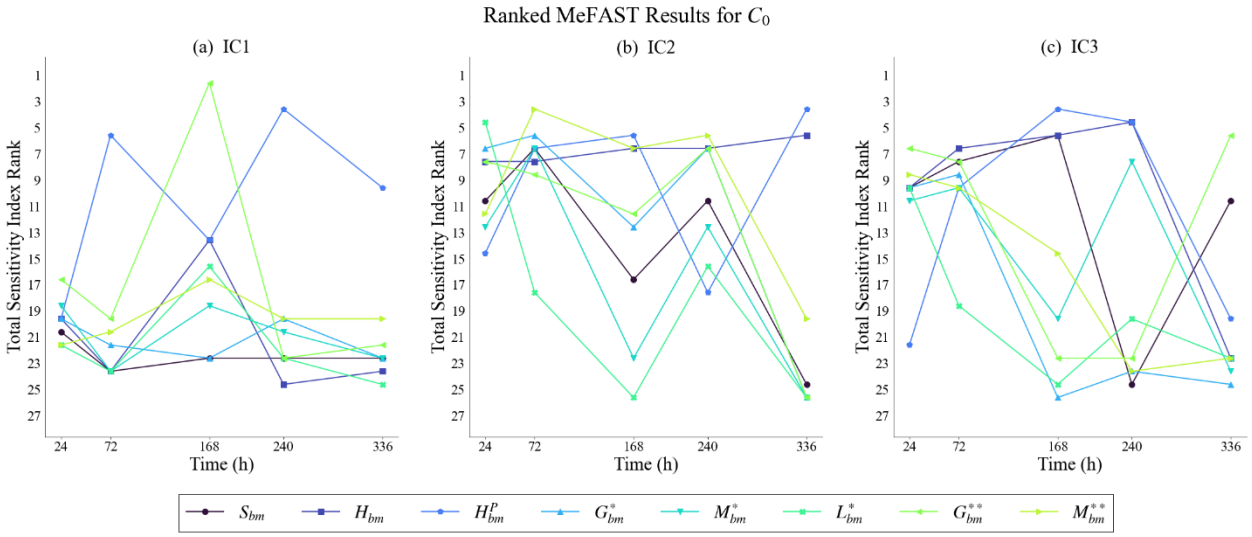


Figure 11. Ranked total sensitivity indices for C_0 across all 40 MeFAST outputs for (a) IC1, superficial thermal burn; (b) IC2, superficial partial thickness thermal burn; and (c) IC3, deep partial thickness thermal burn.

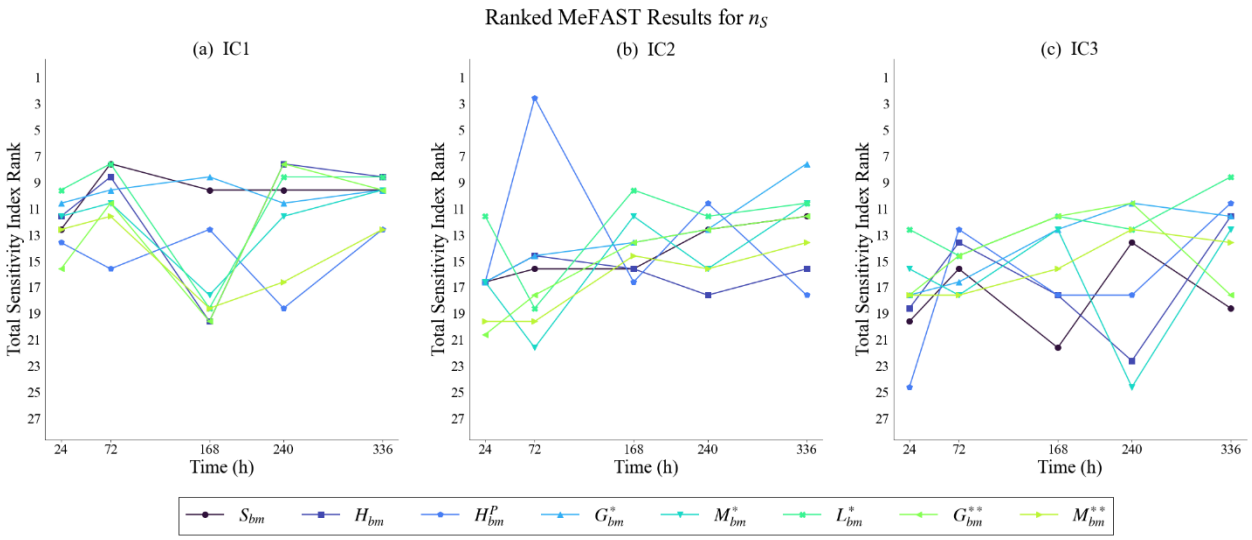


Figure 12. Ranked total sensitivity indices for n_s across all 40 MeFAST outputs for (a) IC1, superficial thermal burn; (b) IC2, superficial partial thickness thermal burn; and (c) IC3, deep partial thickness thermal burn.

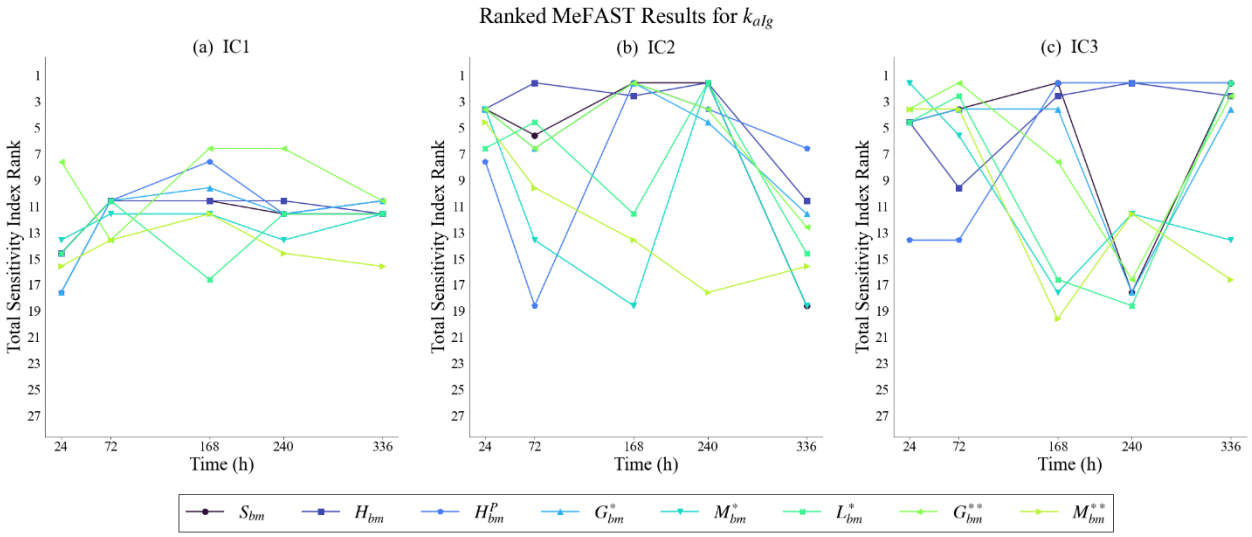


Figure 13. Ranked total sensitivity indices for k_{aIg} across all 40 MeFAST outputs for (a) IC1, superficial thermal burn; (b) IC2, superficial partial thickness thermal burn; and (c) IC3, deep partial thickness thermal burn.

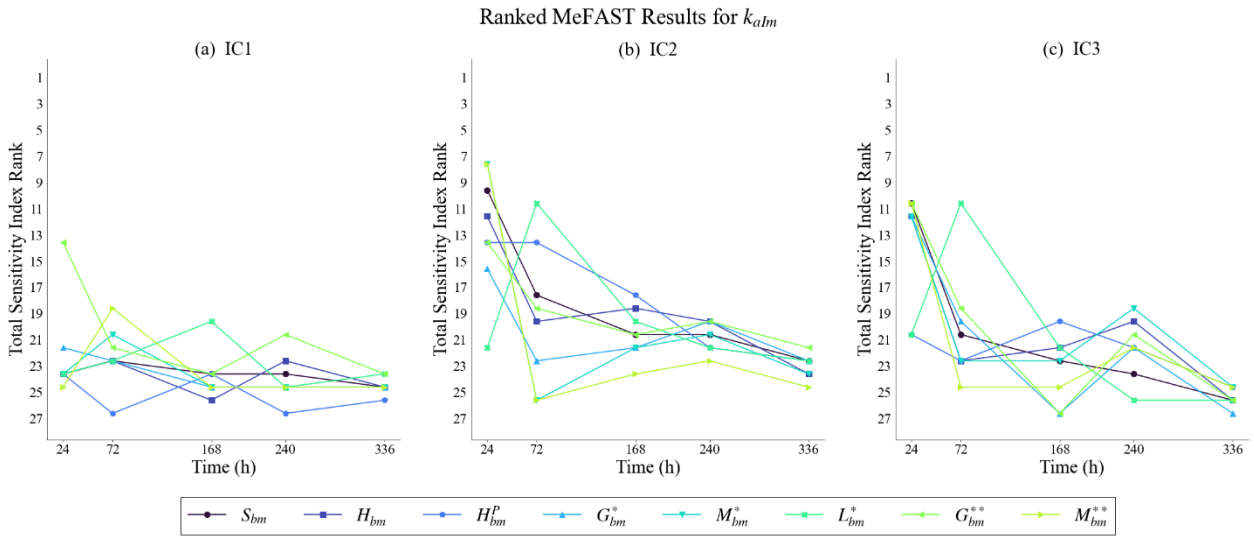


Figure 14. Ranked total sensitivity indices for k_{aIm} across all 40 MeFAST outputs for (a) IC1, superficial thermal burn; (b) IC2, superficial partial thickness thermal burn; and (c) IC3, deep partial thickness thermal burn.

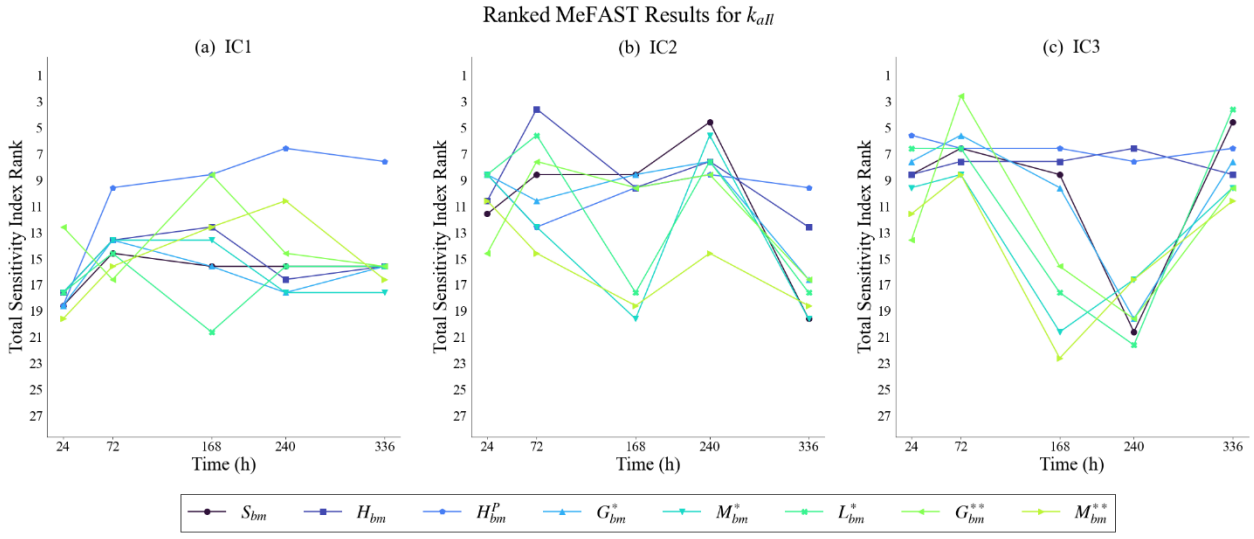


Figure 15. Ranked total sensitivity indices for k_{aII} across all 40 MeFAST outputs for (a) IC1, superficial thermal burn; (b) IC2, superficial partial thickness thermal burn; and (c) IC3, deep partial thickness thermal burn.

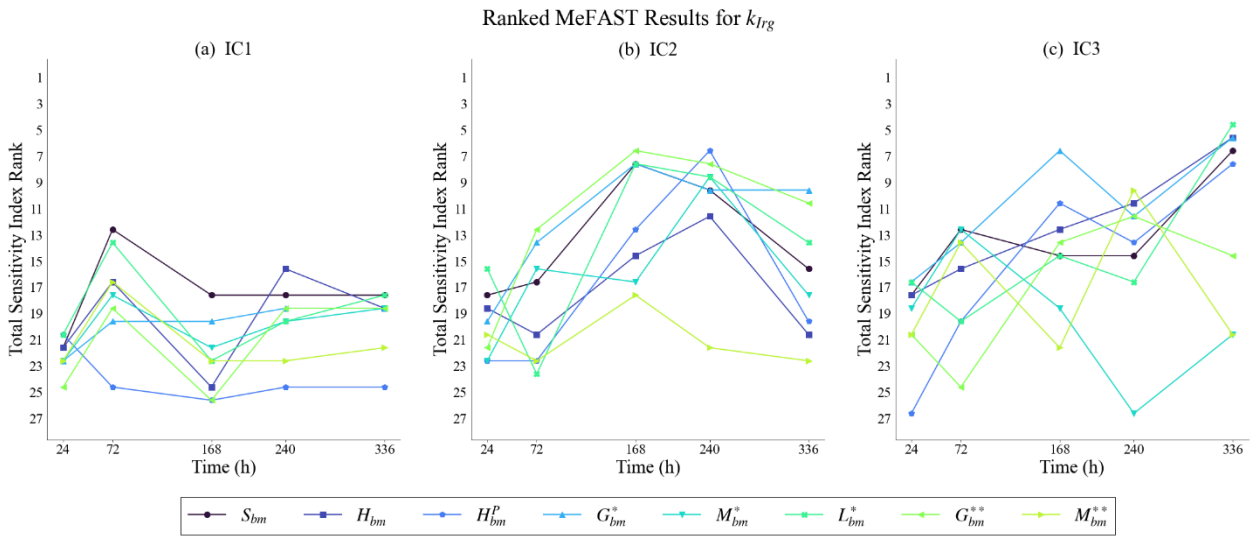


Figure 16. Ranked total sensitivity indices for k_{Irg} across all 40 MeFAST outputs for (a) IC1, superficial thermal burn; (b) IC2, superficial partial thickness thermal burn; and (c) IC3, deep partial thickness thermal burn.

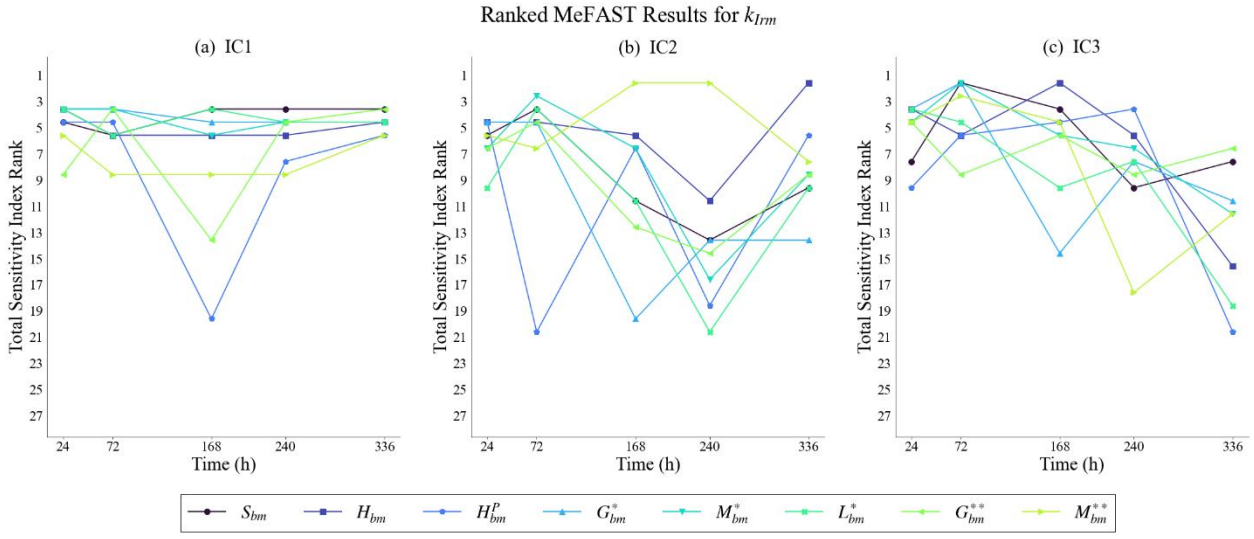


Figure 17. Ranked total sensitivity indices for k_{Irm} across all 40 MeFAST outputs for (a) IC1, superficial thermal burn; (b) IC2, superficial partial thickness thermal burn; and (c) IC3, deep partial thickness thermal burn.

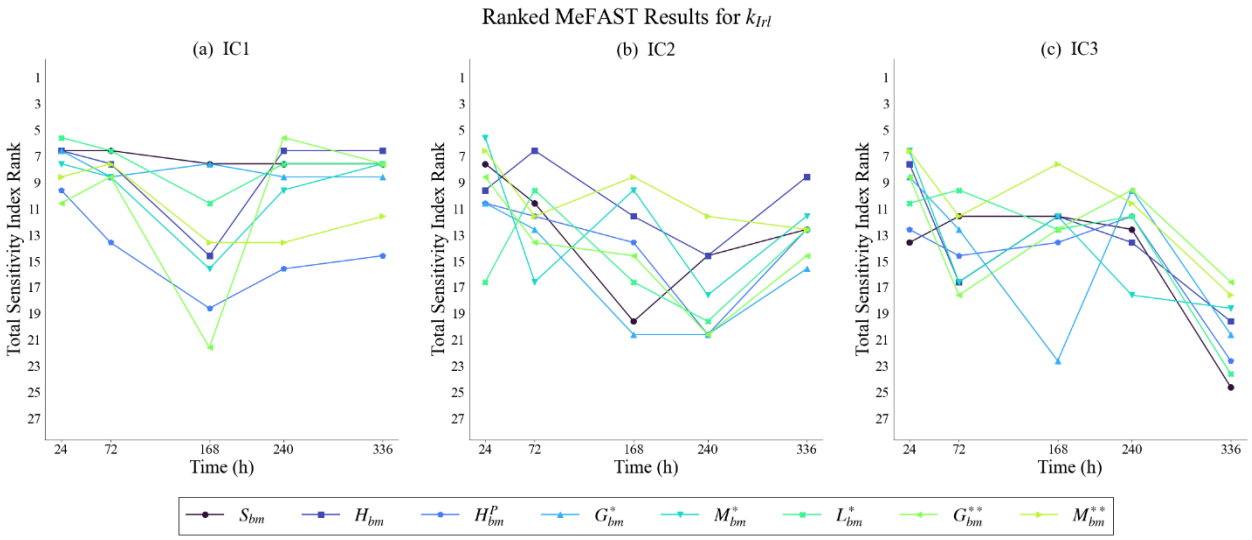


Figure 18. Ranked total sensitivity indices for k_{Irl} across all 40 MeFAST outputs for (a) IC1, superficial thermal burn; (b) IC2, superficial partial thickness thermal burn; and (c) IC3, deep partial thickness thermal burn.

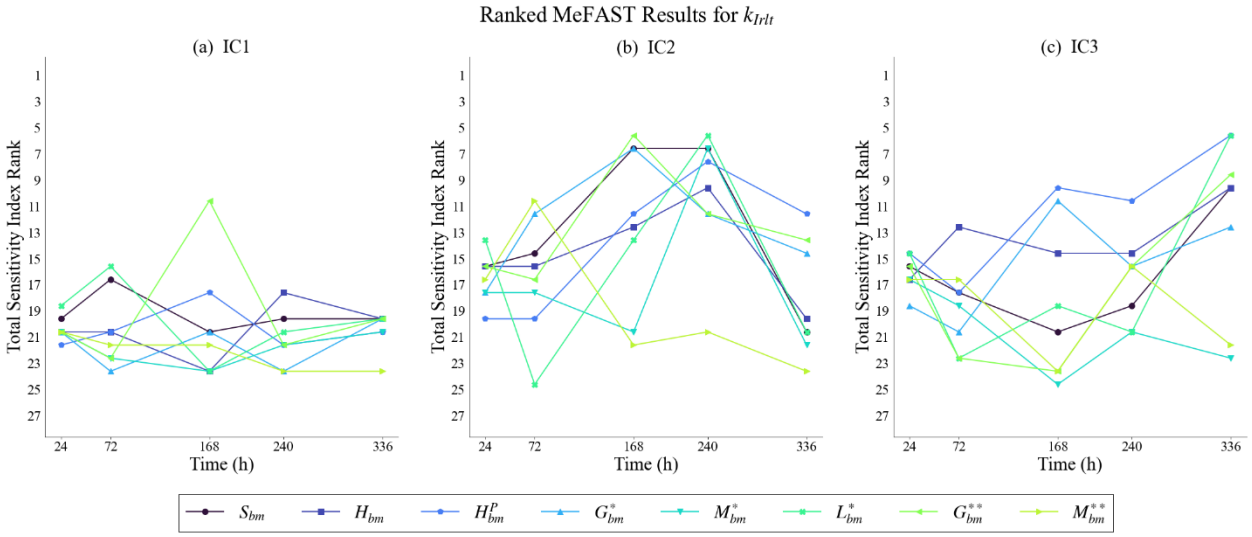


Figure 19. Ranked total sensitivity indices for k_{Irlt} across all 40 MeFAST outputs for (a) IC1, superficial thermal burn; (b) IC2, superficial partial thickness thermal burn; and (c) IC3, deep partial thickness thermal burn.

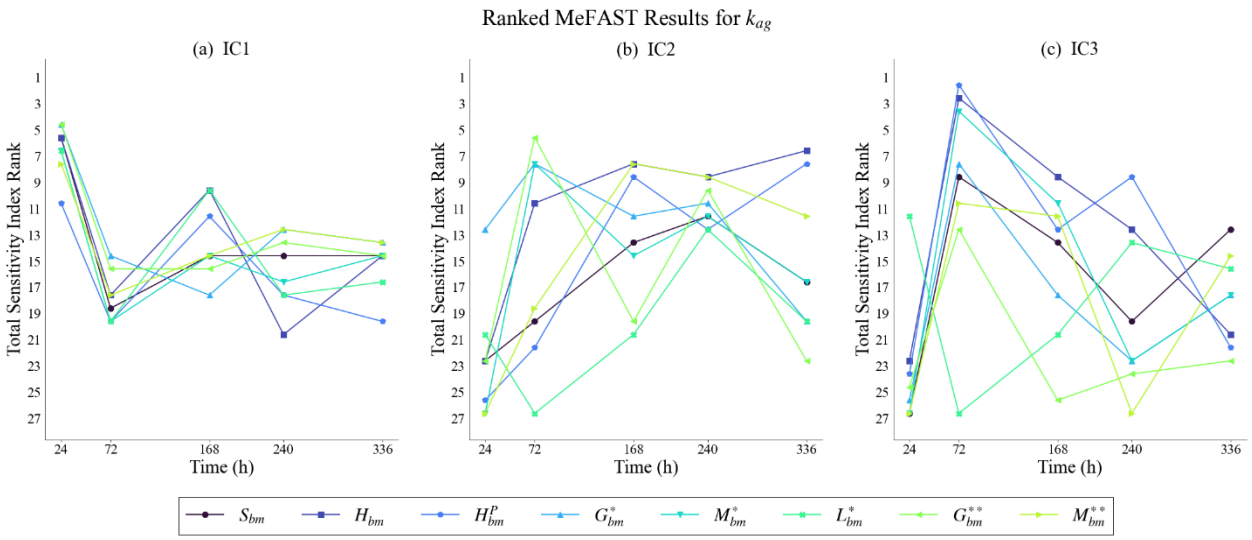


Figure 20. Ranked total sensitivity indices for k_{ag} across all 40 MeFAST outputs for (a) IC1, superficial thermal burn; (b) IC2, superficial partial thickness thermal burn; and (c) IC3, deep partial thickness thermal burn.

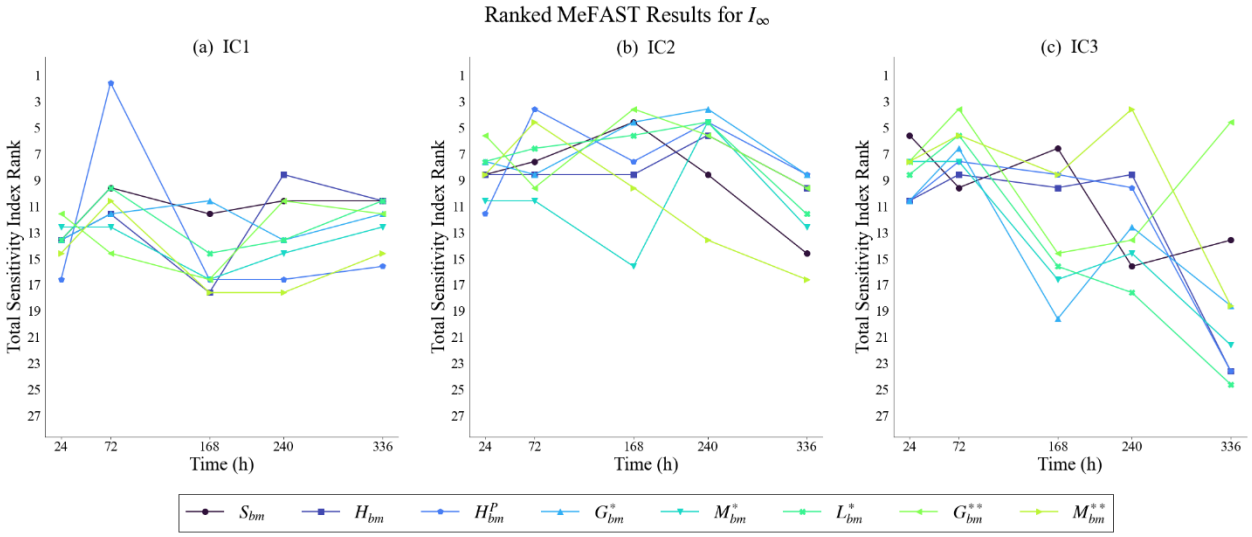


Figure 21. Ranked total sensitivity indices for I_∞ across all 40 MeFAST outputs for (a) IC1, superficial thermal burn; (b) IC2, superficial partial thickness thermal burn; and (c) IC3, deep partial thickness thermal burn.

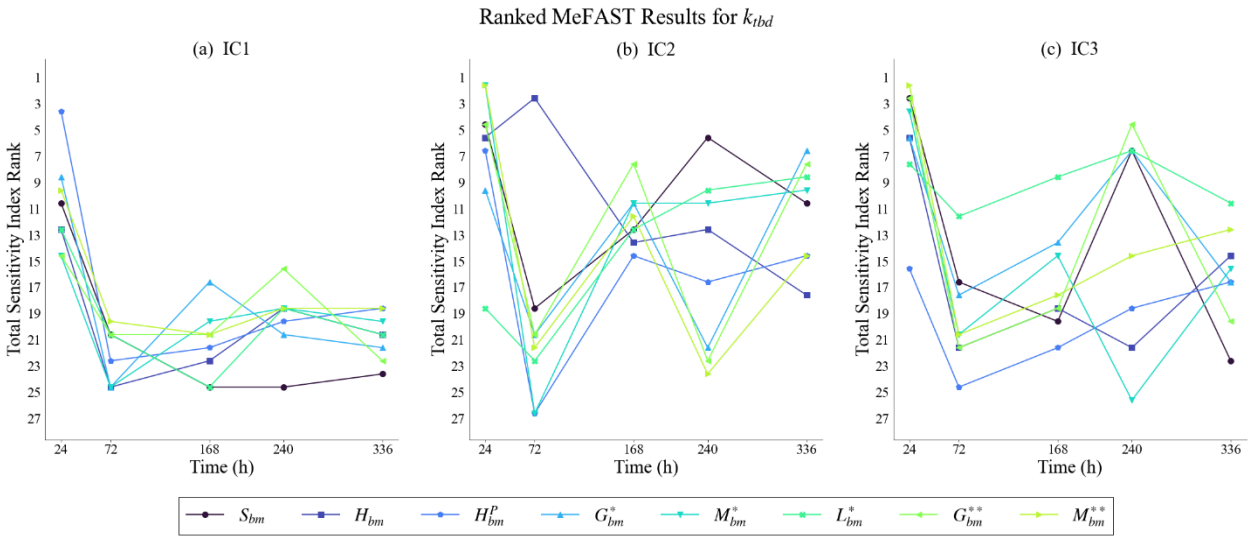


Figure 22. Ranked total sensitivity indices for k_{tbd} across all 40 MeFAST outputs for (a) IC1, superficial thermal burn; (b) IC2, superficial partial thickness thermal burn; and (c) IC3, deep partial thickness thermal burn.

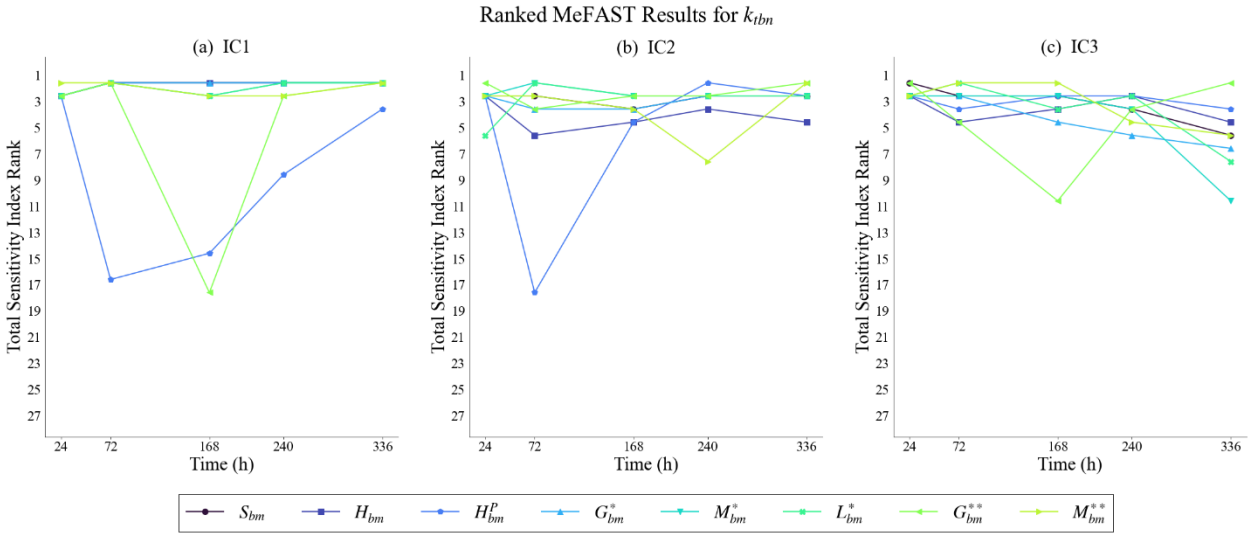


Figure 23. Ranked total sensitivity indices for k_{tbn} across all 40 MeFAST outputs for (a) IC1, superficial thermal burn; (b) IC2, superficial partial thickness thermal burn; and (c) IC3, deep partial thickness thermal burn.

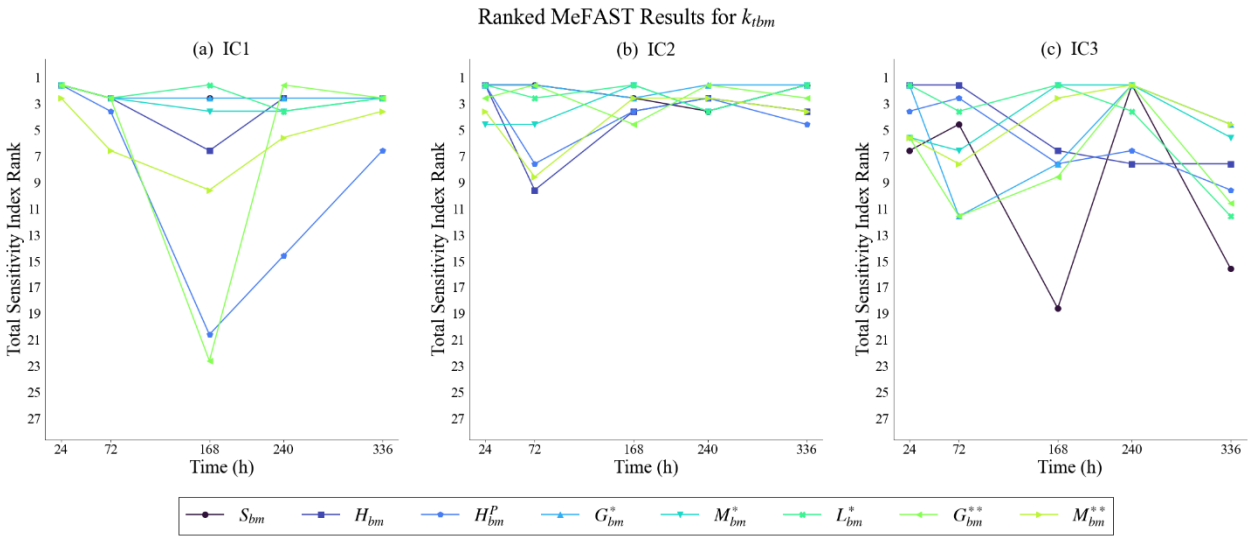


Figure 24. Ranked total sensitivity indices for k_{tbm} across all 40 MeFAST outputs for (a) IC1, superficial thermal burn; (b) IC2, superficial partial thickness thermal burn; and (c) IC3, deep partial thickness thermal burn.

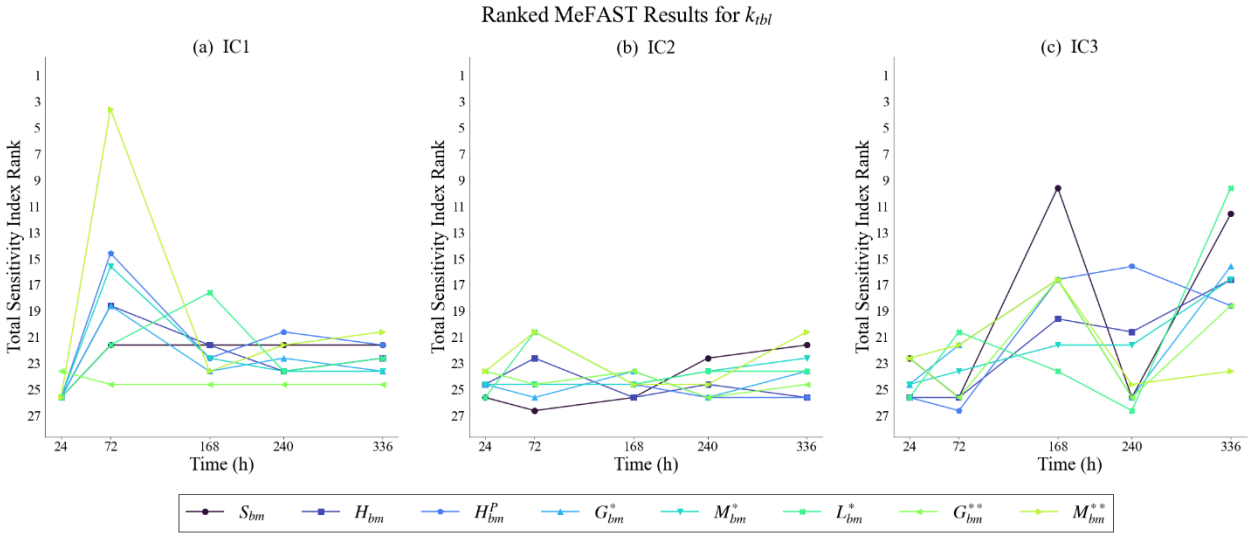


Figure 25. Ranked total sensitivity indices for k_{tbl} across all 40 MeFAST outputs for (a) IC1, superficial thermal burn; (b) IC2, superficial partial thickness thermal burn; and (c) IC3, deep partial thickness thermal burn.

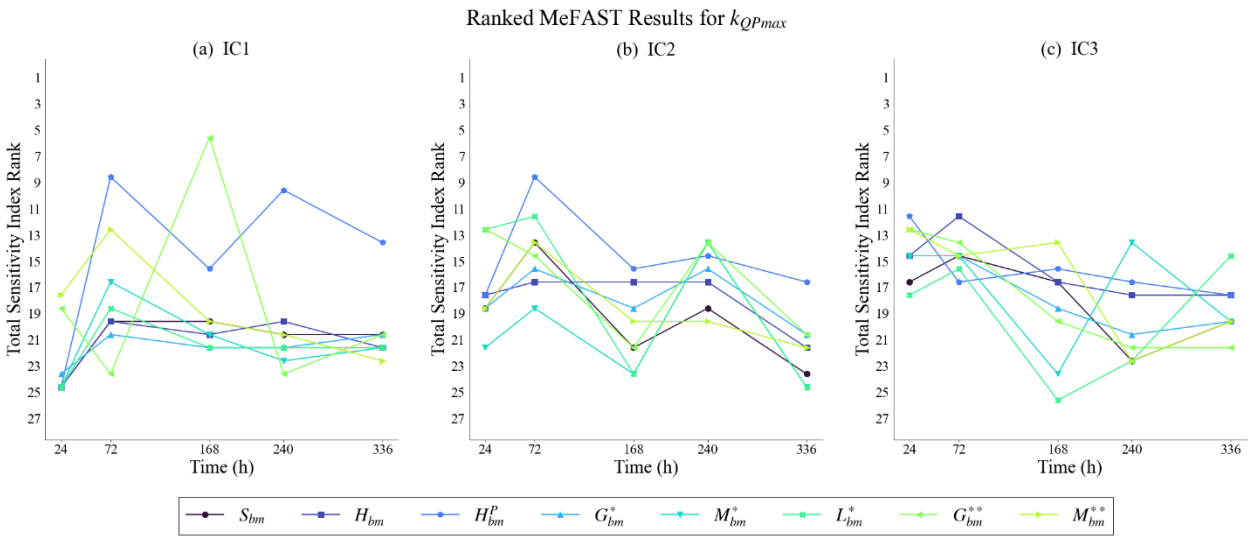


Figure 26. Ranked total sensitivity indices for k_{QPmax} across all 40 MeFAST outputs for (a) IC1, superficial thermal burn; (b) IC2, superficial partial thickness thermal burn; and (c) IC3, deep partial thickness thermal burn.

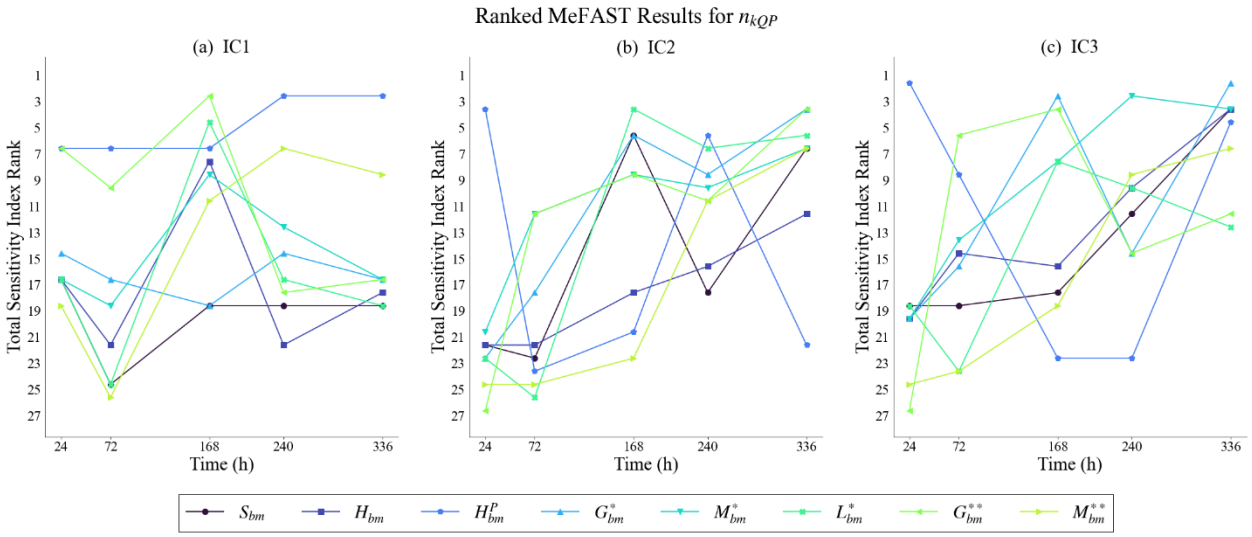


Figure 27. Ranked total sensitivity indices for n_{kQP} across all 40 MeFAST outputs for (a) IC1, superficial thermal burn; (b) IC2, superficial partial thickness thermal burn; and (c) IC3, deep partial thickness thermal burn.

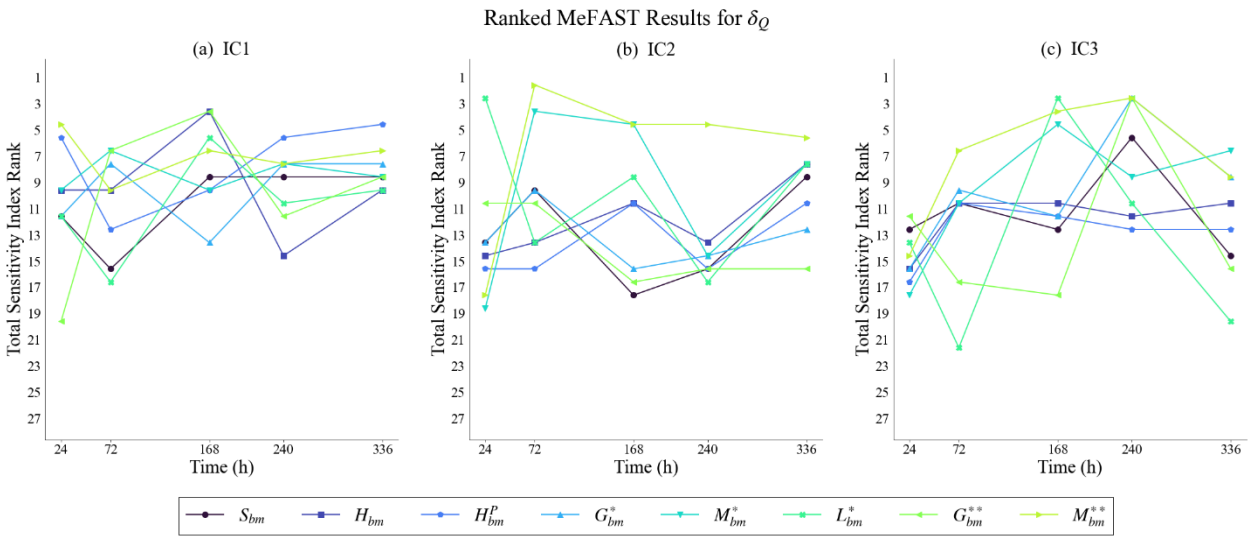


Figure 28. Ranked total sensitivity indices for δ_Q across all 40 MeFAST outputs for (a) IC1, superficial thermal burn; (b) IC2, superficial partial thickness thermal burn; and (c) IC3, deep partial thickness thermal burn.

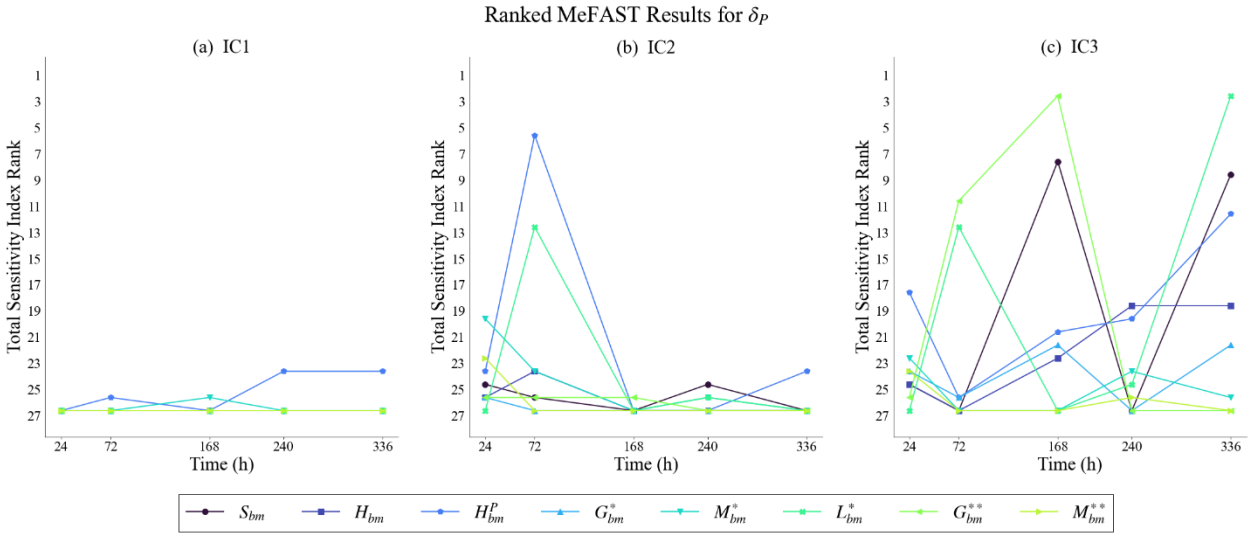


Figure 29. Ranked total sensitivity indices for δ_P across all 40 MeFAST outputs for (a) IC1, superficial thermal burn; (b) IC2, superficial partial thickness thermal burn; and (c) IC3, deep partial thickness thermal burn.

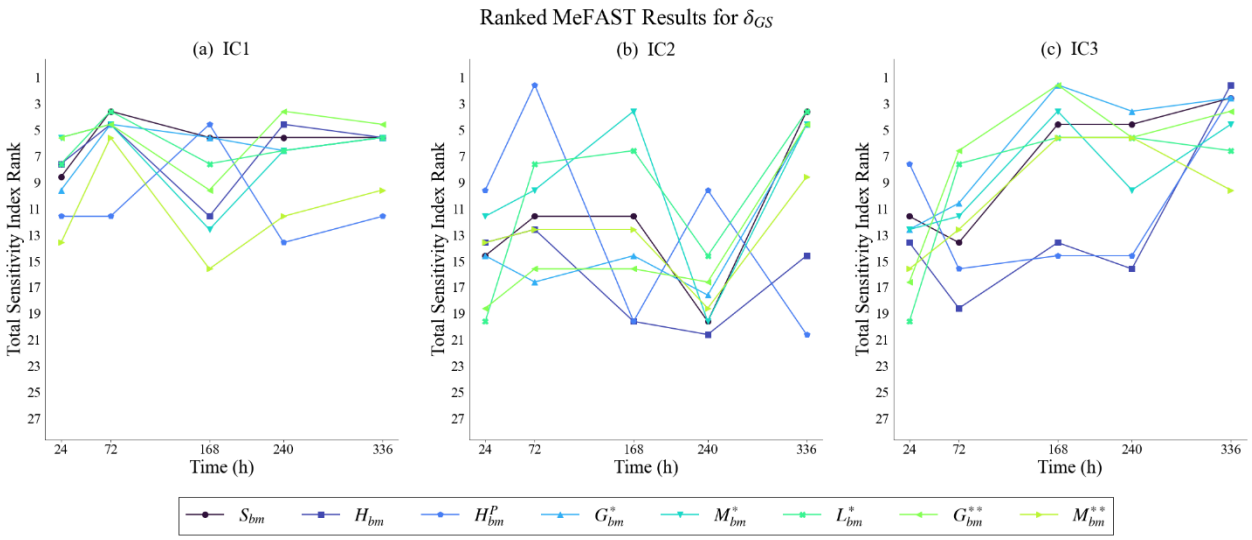


Figure 30. Ranked total sensitivity indices for δ_{GS} across all 40 MeFAST outputs for (a) IC1, superficial thermal burn; (b) IC2, superficial partial thickness thermal burn; and (c) IC3, deep partial thickness thermal burn.

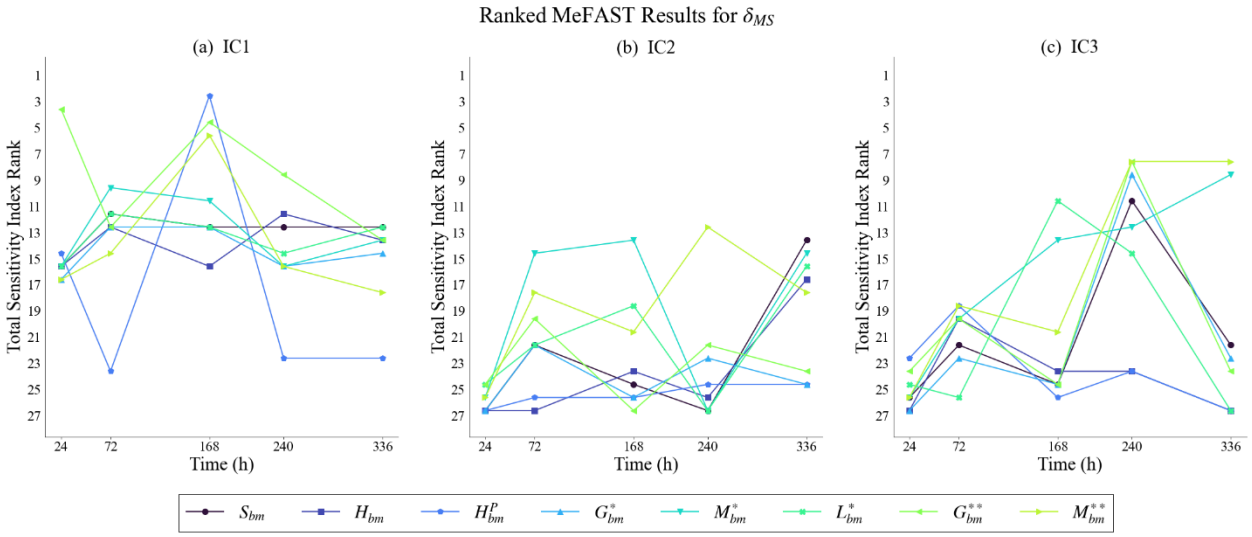


Figure 31. Ranked total sensitivity indices for δ_{MS} across all 40 MeFAST outputs for (a) IC1, superficial thermal burn; (b) IC2, superficial partial thickness thermal burn; and (c) IC3, deep partial thickness thermal burn.

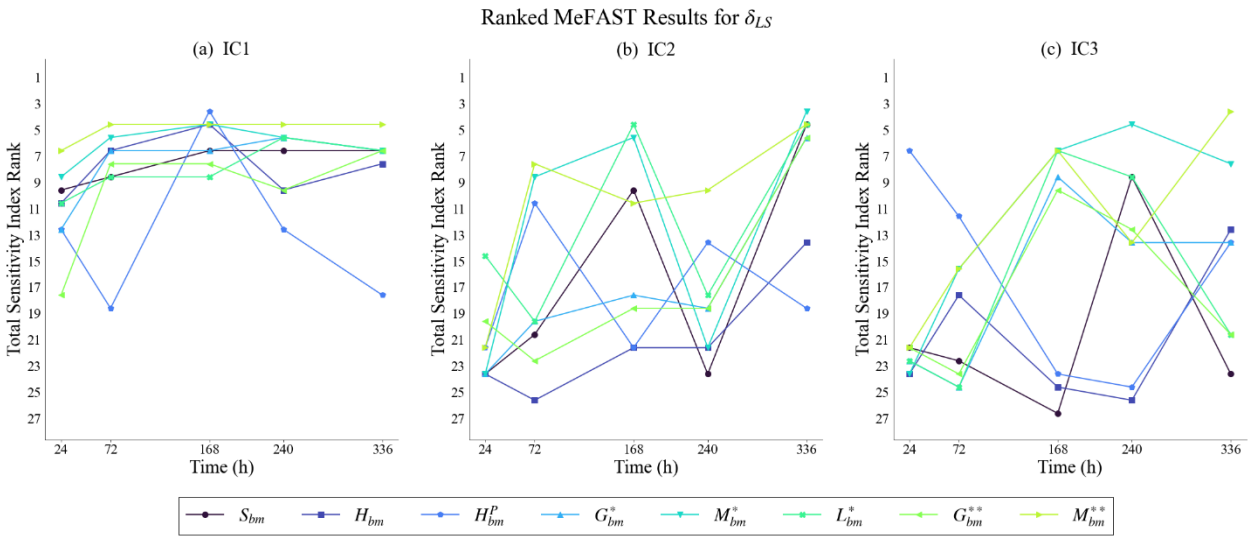


Figure 32. Ranked total sensitivity indices for δ_{LS} across all 40 MeFAST outputs for (a) IC1, superficial thermal burn; (b) IC2, superficial partial thickness thermal burn; and (c) IC3, deep partial thickness thermal burn.

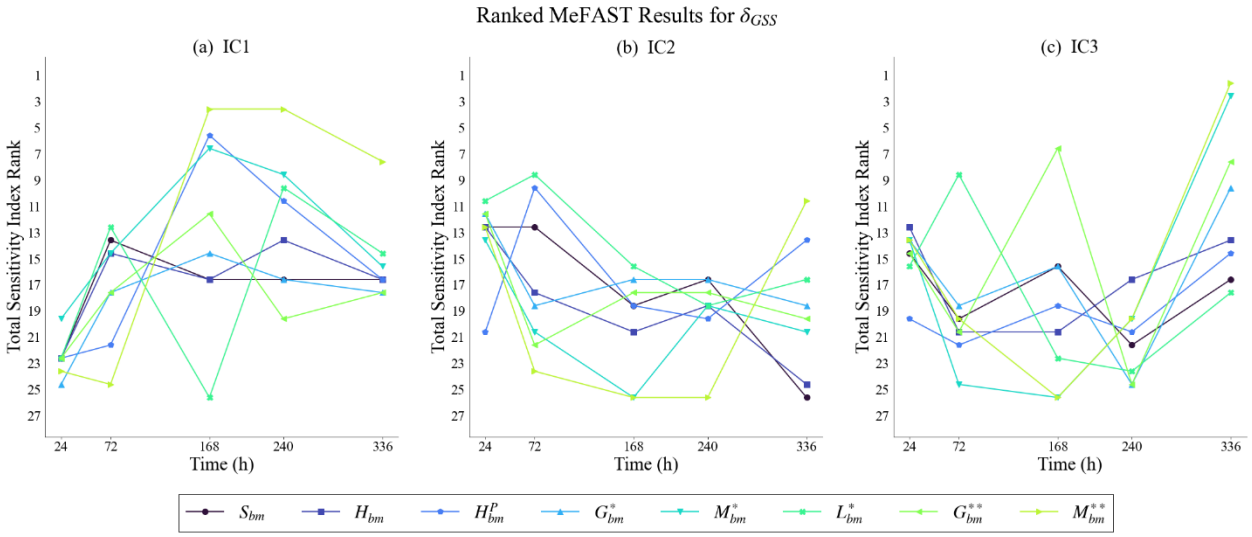


Figure 33. Ranked total sensitivity indices for δ_{GSS} across all 40 MeFAST outputs for (a) IC1, superficial thermal burn; (b) IC2, superficial partial thickness thermal burn; and (c) IC3, deep partial thickness thermal burn.

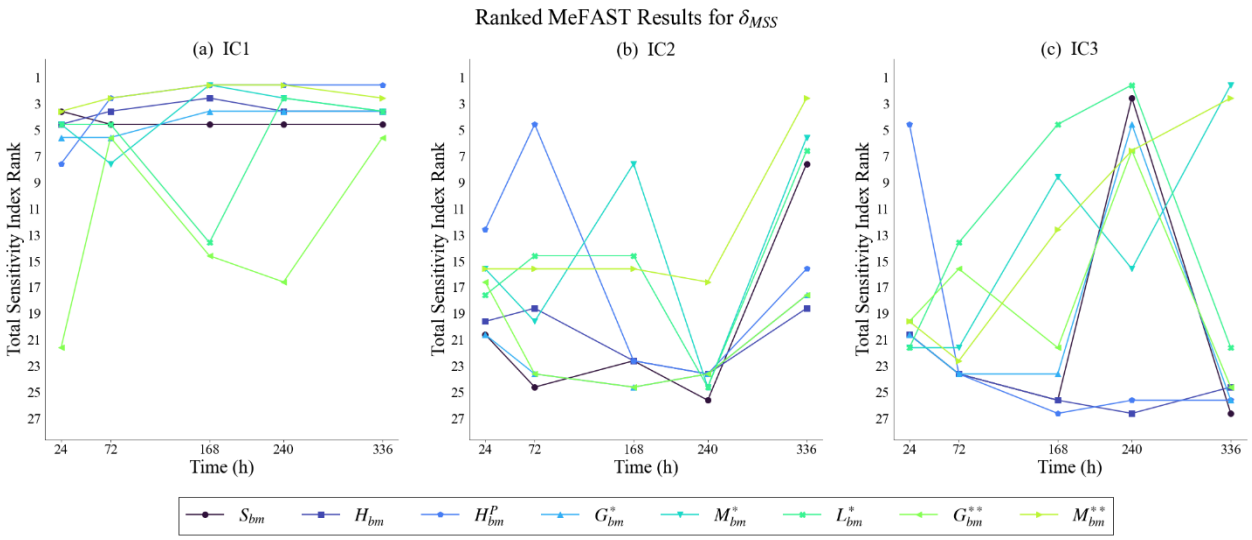


Figure 34. Ranked total sensitivity indices for δ_{MSS} across all 40 MeFAST outputs for (a) IC1, superficial thermal burn; (b) IC2, superficial partial thickness thermal burn; and (c) IC3, deep partial thickness thermal burn.

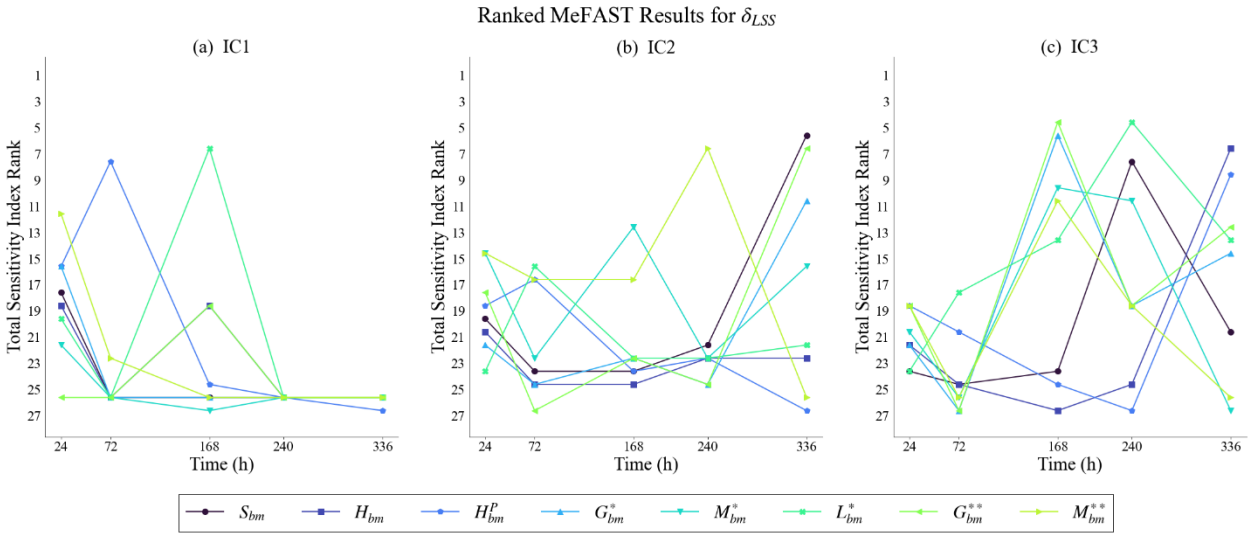


Figure 35. Ranked total sensitivity indices for δ_{LSS} across all 40 MeFAST outputs for (a) IC1, superficial thermal burn; (b) IC2, superficial partial thickness thermal burn; and (c) IC3, deep partial thickness thermal burn.

C.1.2. Heatmaps of Statistical Significance

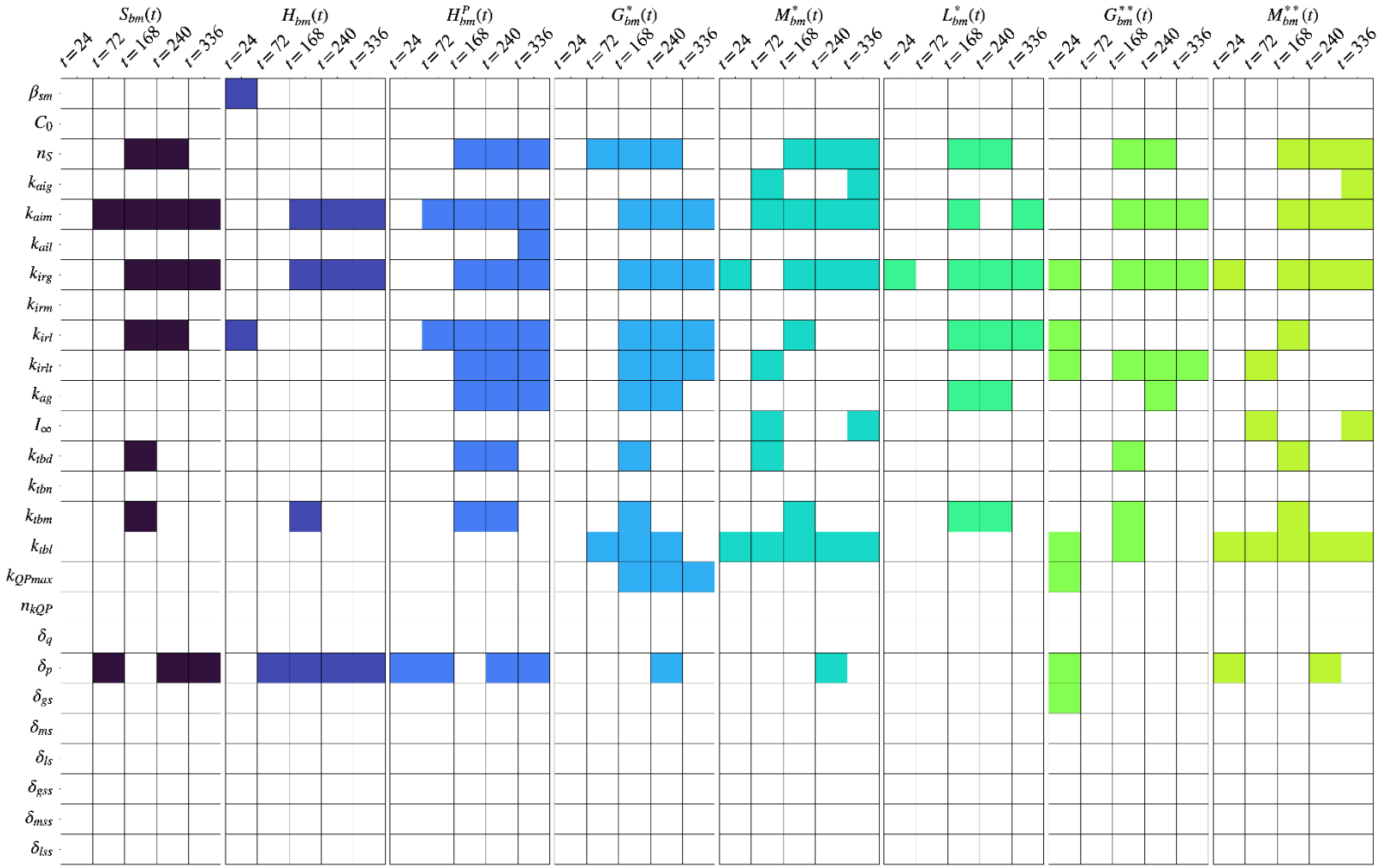


Figure 36. Significance results of MeFAST for parameters of the bone marrow compartment with respect to the state variables of the bone marrow compartment for IC1 at days one, three, five, seven, and ten post-injury. A shaded box indicates that the parameter was flagged as statistically significant at the respective state variable and time point by at least two of the three tests performed during MeFAST. These significance results were passed through the algorithm presented in Section 3.1.1.1 to determine which parameters could be fixed during GSA of the systemic TDPM.

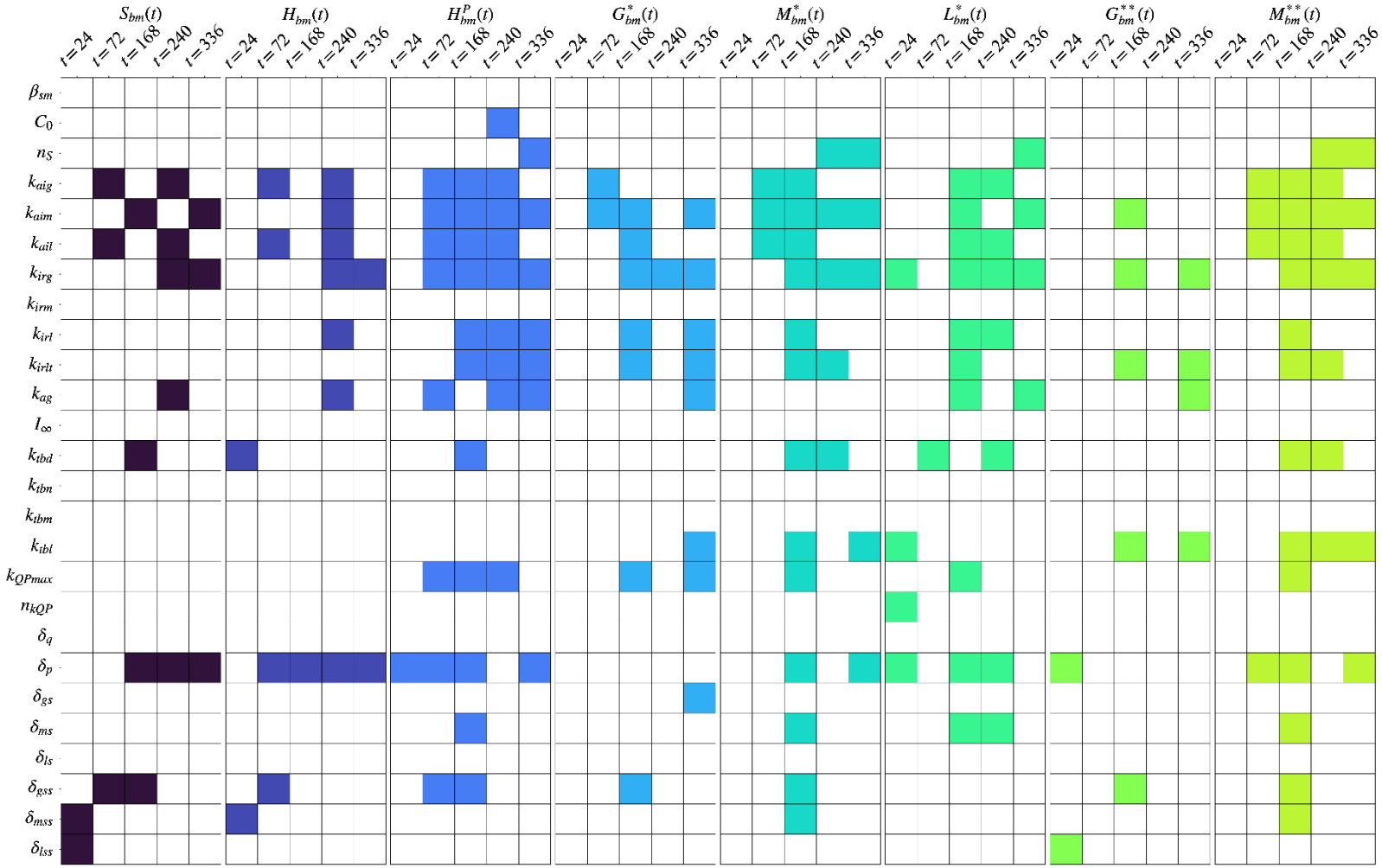


Figure 37. Significance results of MeFAST for parameters of the bone marrow compartment with respect to the state variables of the bone marrow compartment for IC2 at days one, three, five, seven, and ten post-injury. A shaded box indicates that the parameter was flagged as statistically significant at the respective state variable and time point by at least two of the three tests performed during MeFAST. These significance results were passed through the algorithm presented in Section 3.1.1.1 to determine which parameters could be fixed during GSA of the systemic TDPM.

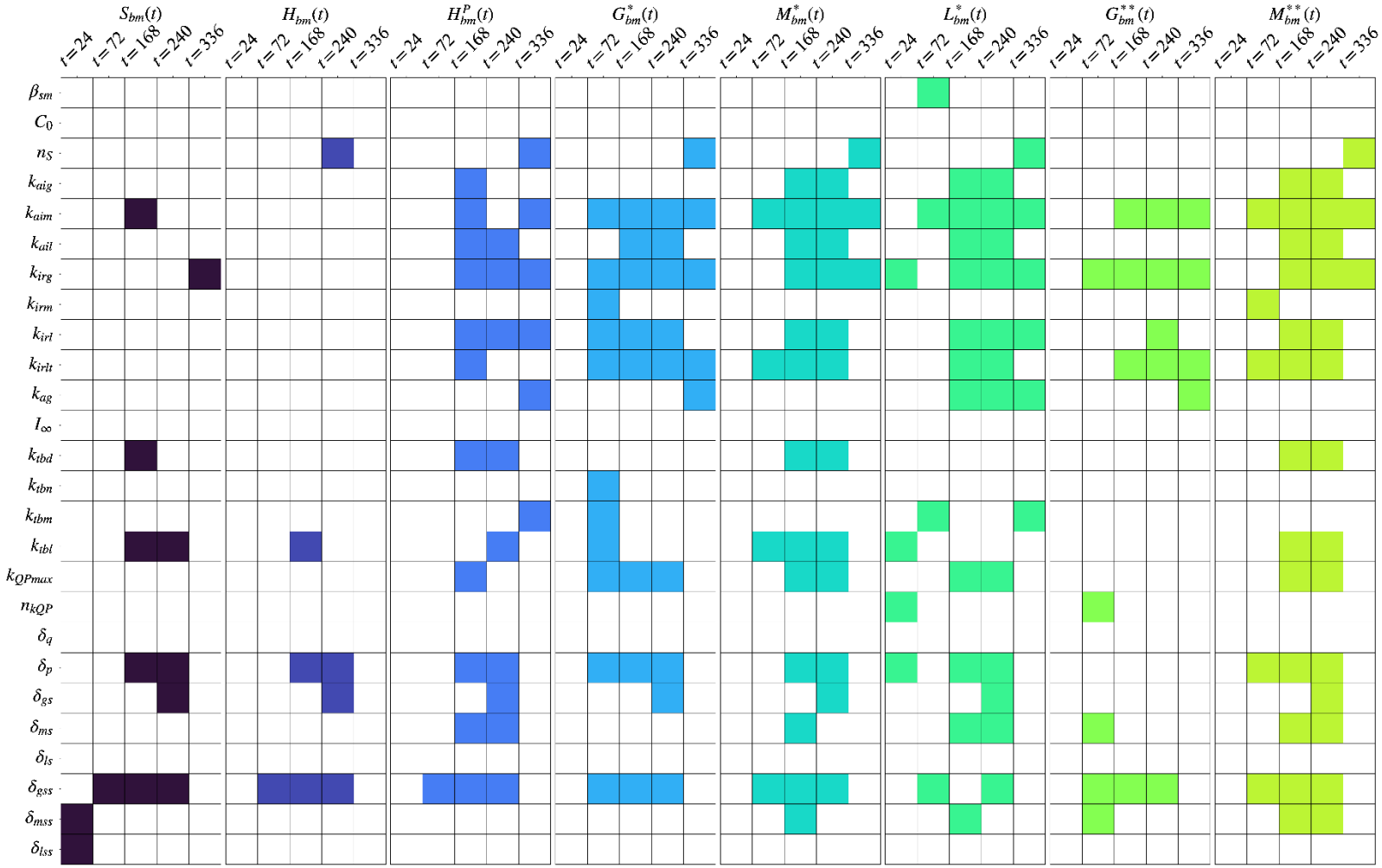


Figure 38. Significance results of MeFAST for parameters of the bone marrow compartment with respect to the state variables of the bone marrow compartment for IC3 at days one, three, five, seven, and ten post-injury. A shaded box indicates that the parameter was flagged as statistically significant at the respective state variable and time point by at least two of the three tests performed during MeFAST. These significance results were passed through the algorithm presented in Section 3.1.1.1 to determine which parameters could be fixed during GSA of the systemic TDPM.

C.2. MeFAST Plots for Global Sensitivity Analysis of the TDPM

C.2.1. Line Plots of Total Sensitivity Index Rankings

Plots display the ranked total sensitivity indices for each parameter across all 105 sensitivity indices for (a) superficial thermal burn (IC1, $Dam_{tb}(0) = Deb_{tb}(0) = 0.1$); (b) superficial partial thickness burn (IC2, $Dam_{tb}(0) = Deb_{tb}(0) = 0.9$); and (c) deep partial thickness burn (IC3, $Dam_{tb}(0) = Deb_{tb}(0) = 1.8$).

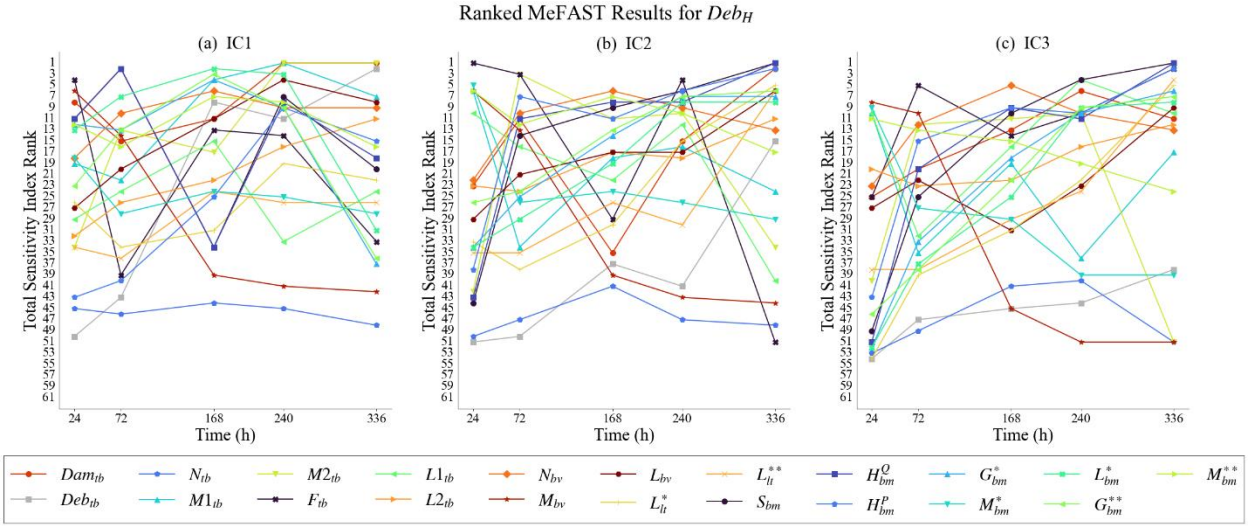


Figure 39. Ranked total sensitivity indices for Deb_H across all 105 MeFAST outputs for (a) IC1, superficial thermal burn; (b) IC2, superficial partial thickness thermal burn; and (c) IC3, deep partial thickness thermal burn.

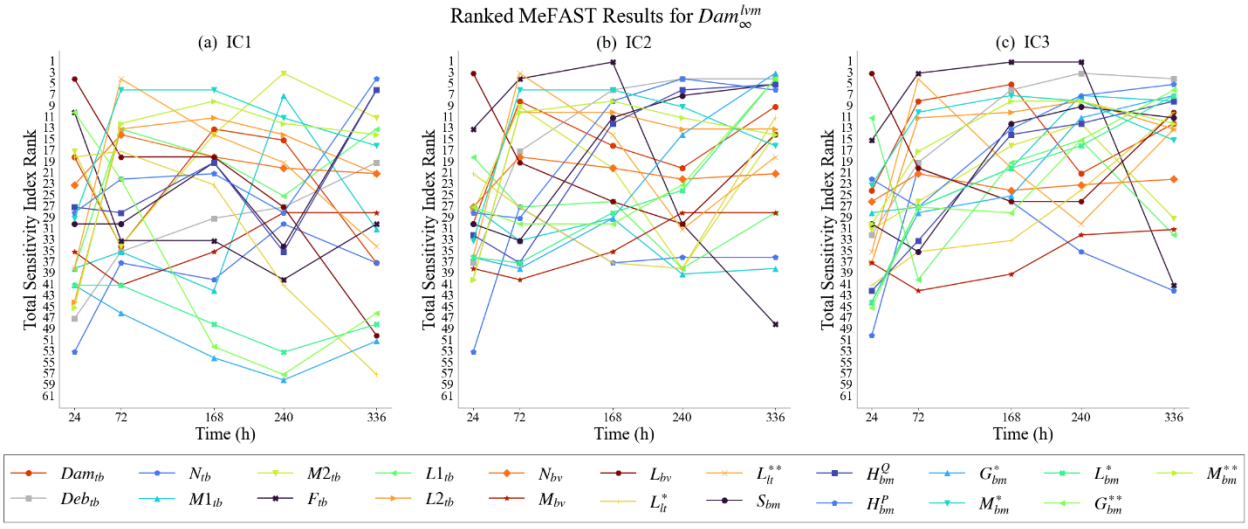


Figure 40. Ranked total sensitivity indices for $Dam^{\infty}{}_{lvm}$ across all 105 MeFAST outputs for (a) IC1, superficial thermal burn; (b) IC2, superficial partial thickness thermal burn; and (c) IC3, deep partial thickness thermal burn.

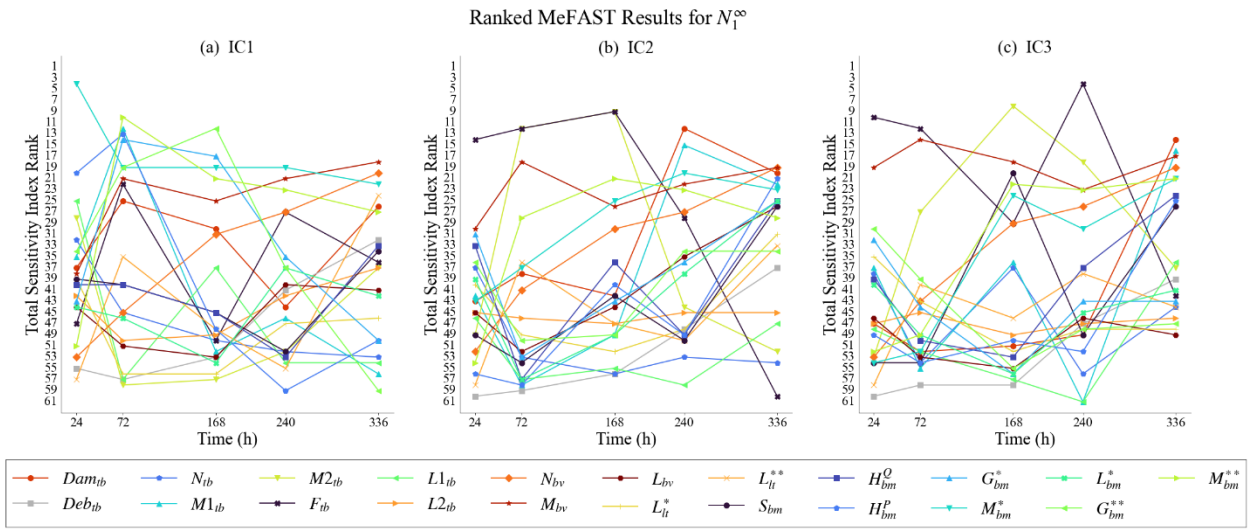


Figure 41. Ranked total sensitivity indices for N_1^{∞} across all 105 MeFAST outputs for (a) IC1, superficial thermal burn; (b) IC2, superficial partial thickness thermal burn; and (c) IC3, deep partial thickness thermal burn.

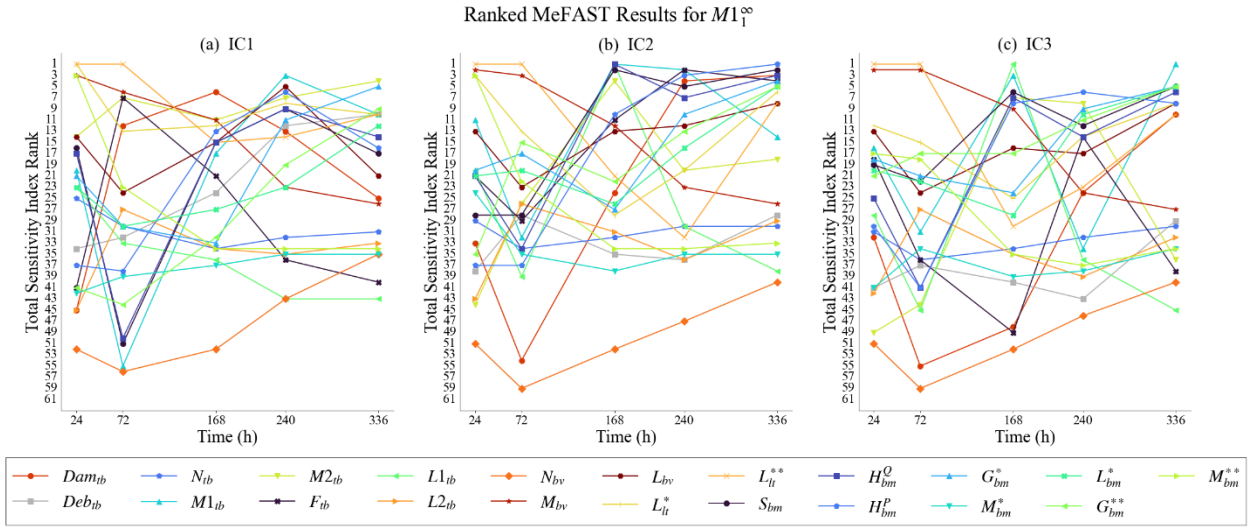


Figure 42. Ranked total sensitivity indices for $M1_1^{\infty}$ across all 105 MeFAST outputs for (a) IC1, superficial thermal burn; (b) IC2, superficial partial thickness thermal burn; and (c) IC3, deep partial thickness thermal burn.

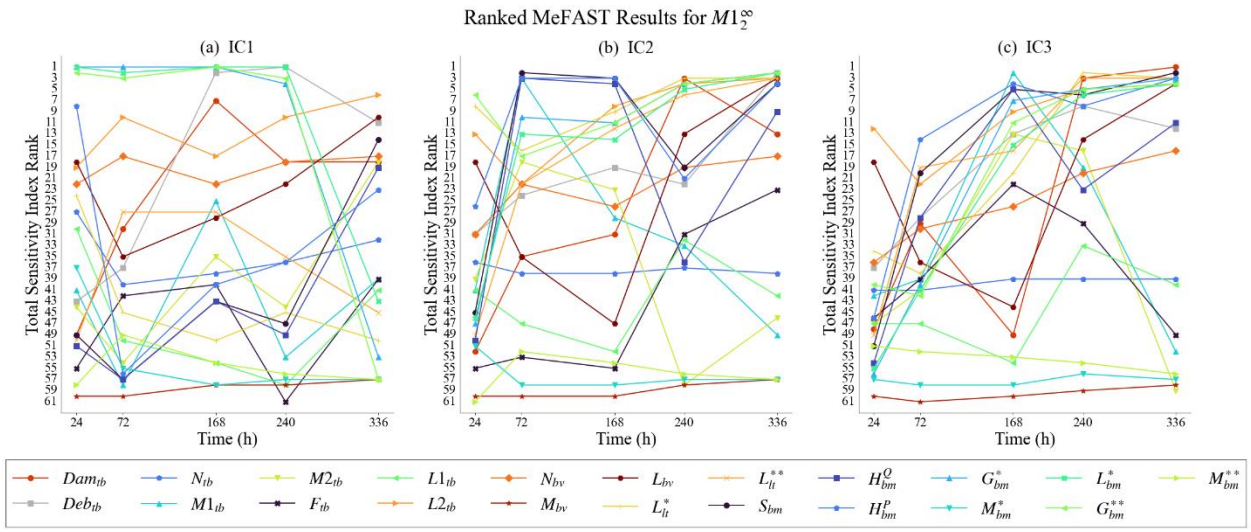


Figure 43. Ranked total sensitivity indices for $M2_1^{\infty}$ across all 105 MeFAST outputs for (a) IC1, superficial thermal burn; (b) IC2, superficial partial thickness thermal burn; and (c) IC3, deep partial thickness thermal burn.

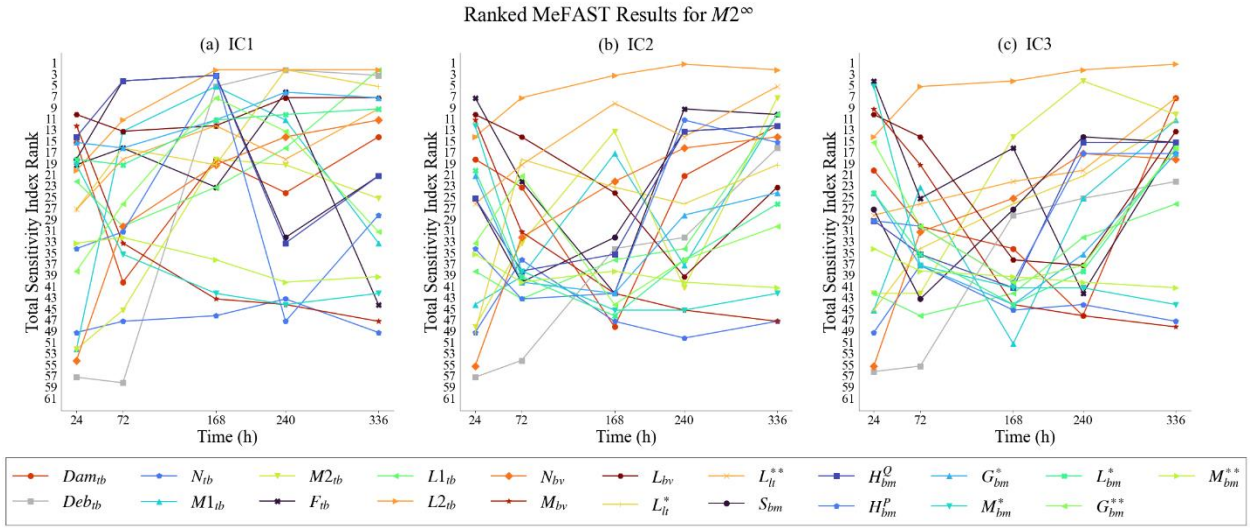


Figure 44. Ranked total sensitivity indices for $M2^{\infty}$ across all 105 MeFAST outputs for (a) IC1, superficial thermal burn; (b) IC2, superficial partial thickness thermal burn; and (c) IC3, deep partial thickness thermal burn.

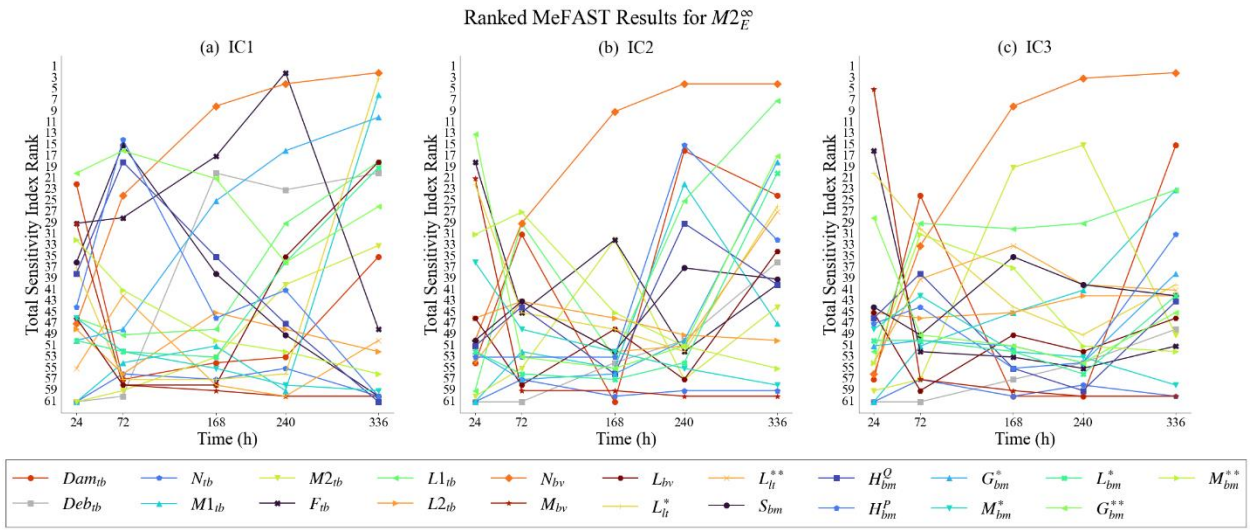


Figure 45. Ranked total sensitivity indices for $M2_E^{\infty}$ across all 105 MeFAST outputs for (a) IC1, superficial thermal burn; (b) IC2, superficial partial thickness thermal burn; and (c) IC3, deep partial thickness thermal burn.

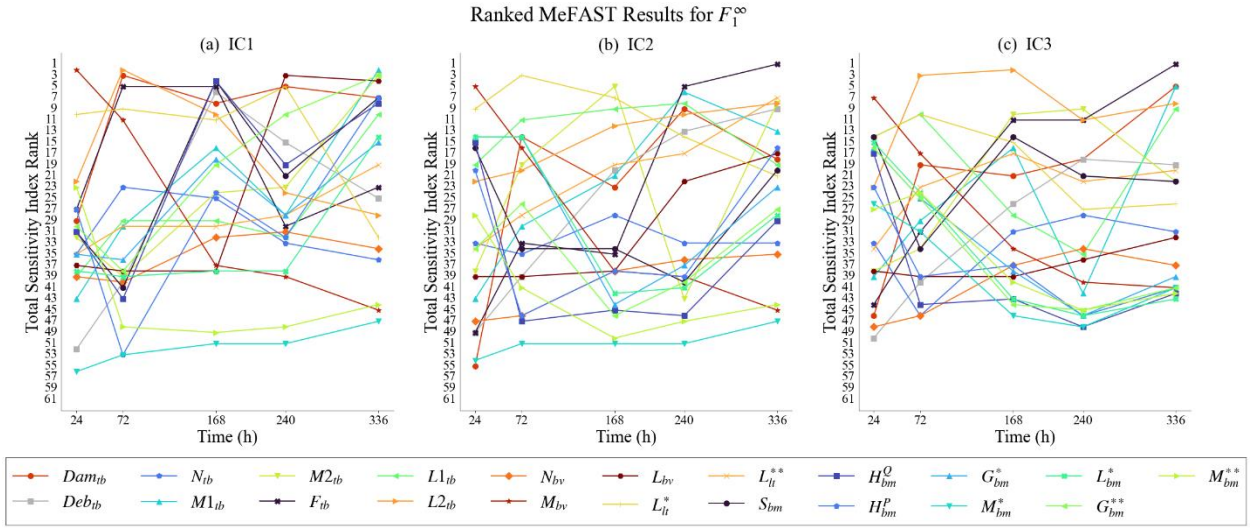


Figure 46. Ranked total sensitivity indices for F_1^{∞} across all 105 MeFAST outputs for (a) IC1, superficial thermal burn; (b) IC2, superficial partial thickness thermal burn; and (c) IC3, deep partial thickness thermal burn.

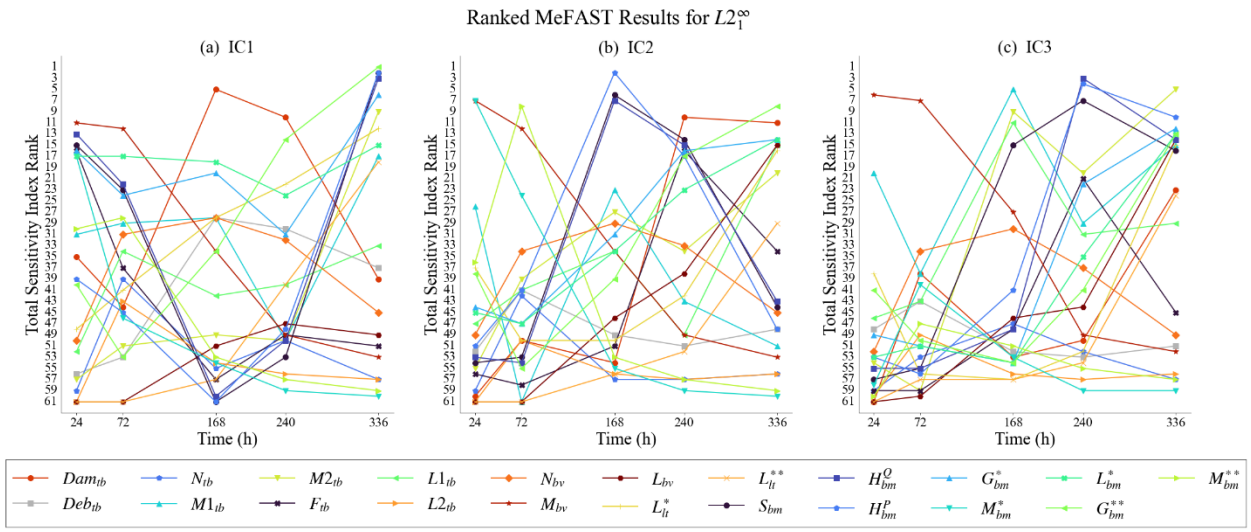


Figure 47. Ranked total sensitivity indices for $L2_1^{\infty}$ across all 105 MeFAST outputs for (a) IC1, superficial thermal burn; (b) IC2, superficial partial thickness thermal burn; and (c) IC3, deep partial thickness thermal burn.

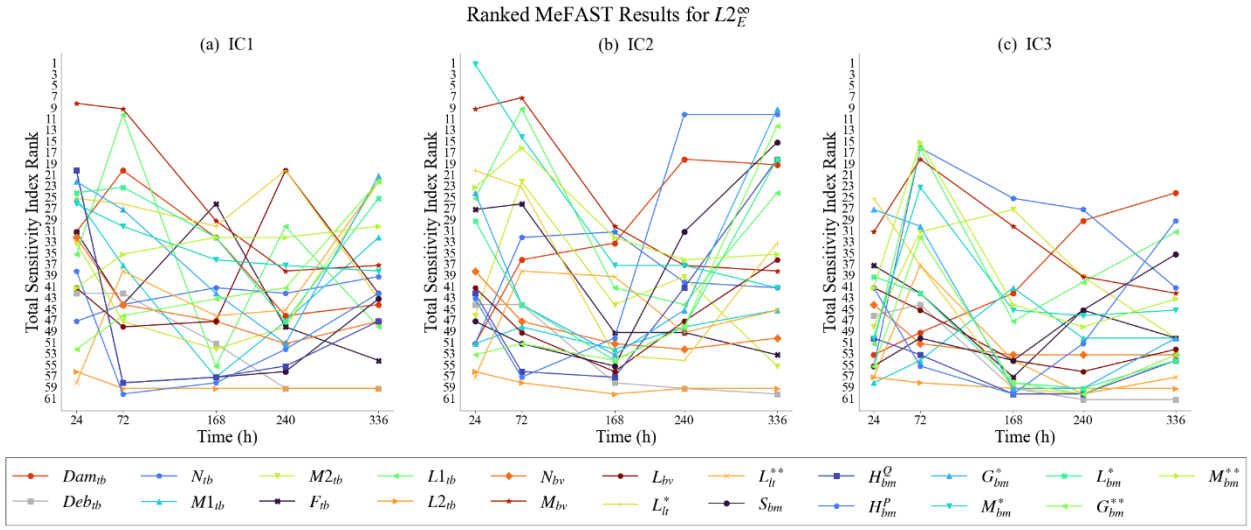


Figure 48. Ranked total sensitivity indices for $L2_E^{\infty}$ across all 105 MeFAST outputs for (a) IC1, superficial thermal burn; (b) IC2, superficial partial thickness thermal burn; and (c) IC3, deep partial thickness thermal burn.

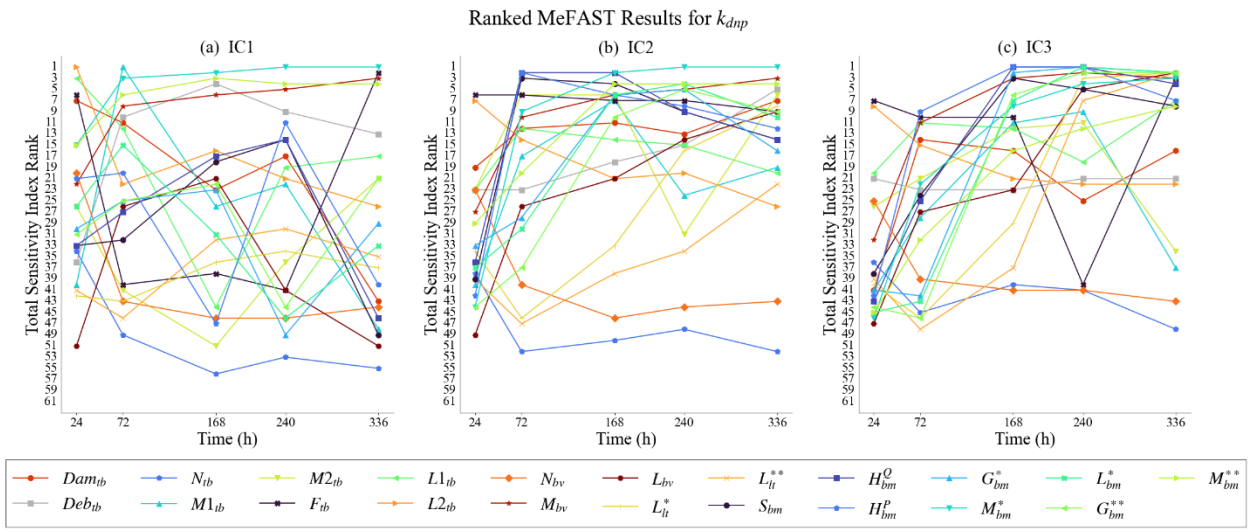


Figure 49. Ranked total sensitivity indices for k_{dnp} across all 105 MeFAST outputs for (a) IC1, superficial thermal burn; (b) IC2, superficial partial thickness thermal burn; and (c) IC3, deep partial thickness thermal burn.

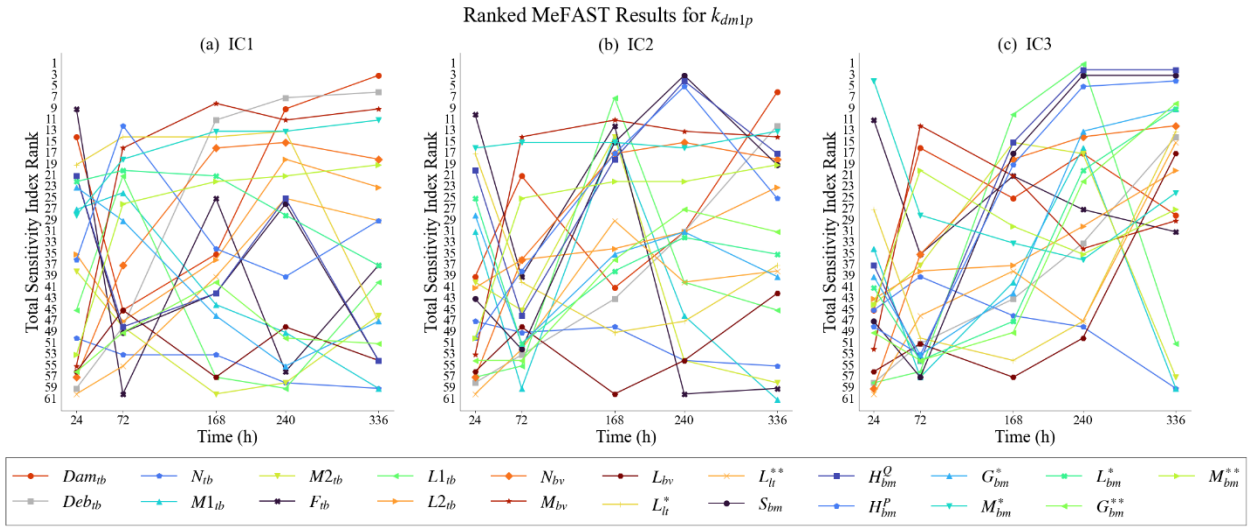


Figure 50. Ranked total sensitivity indices for k_{dm1p} across all 105 MeFAST outputs for (a) IC1, superficial thermal burn; (b) IC2, superficial partial thickness thermal burn; and (c) IC3, deep partial thickness thermal burn.

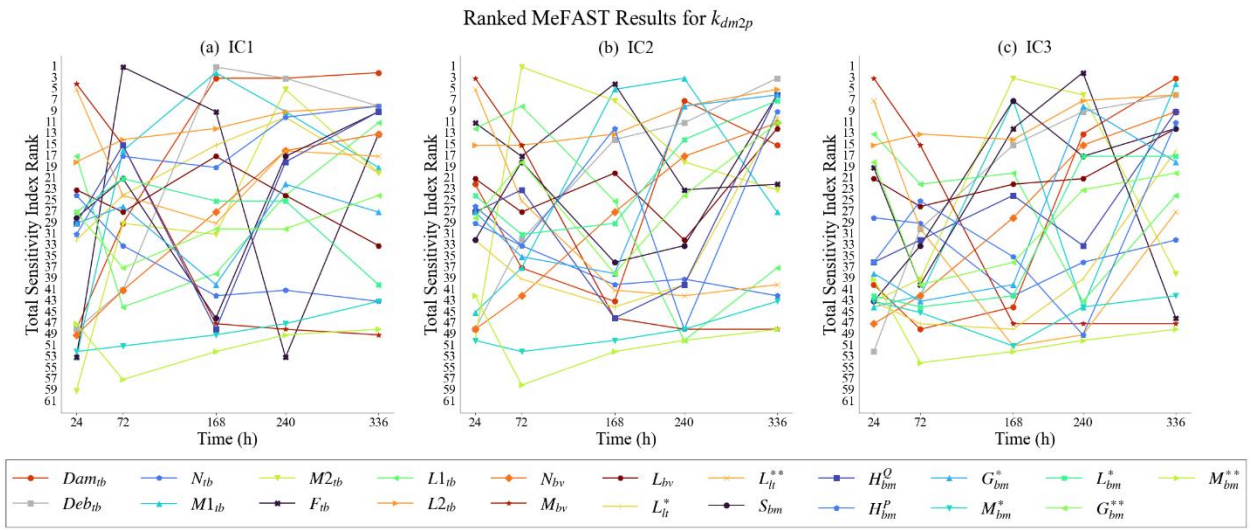


Figure 51. Ranked total sensitivity indices for k_{dm2p} across all 105 MeFAST outputs for (a) IC1, superficial thermal burn; (b) IC2, superficial partial thickness thermal burn; and (c) IC3, deep partial thickness thermal burn.

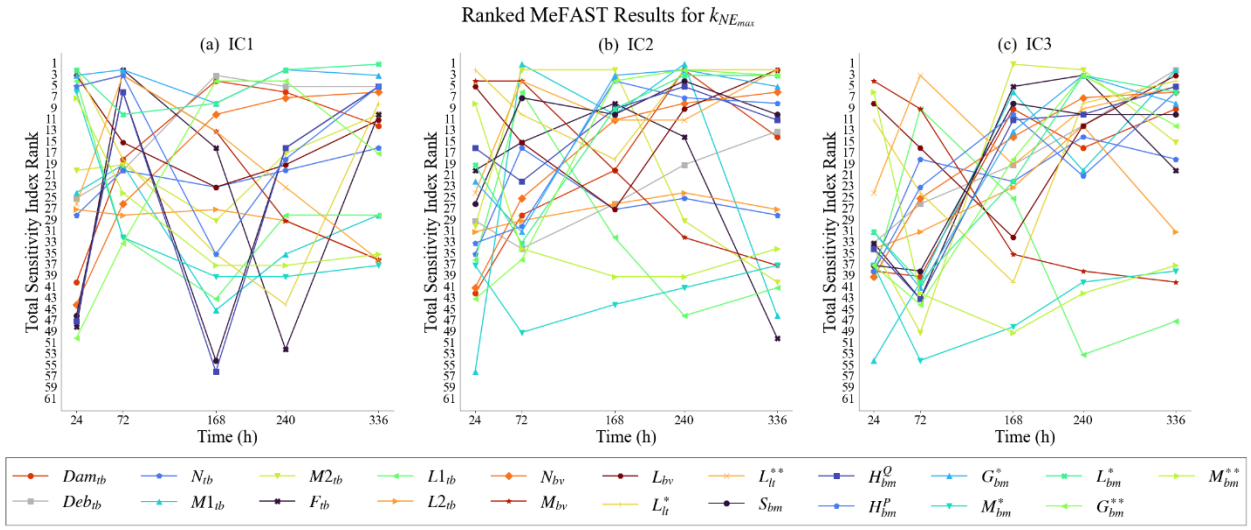


Figure 52. Ranked total sensitivity indices for k_{NEmax} across all 105 MeFAST outputs for (a) IC1, superficial thermal burn; (b) IC2, superficial partial thickness thermal burn; and (c) IC3, deep partial thickness thermal burn.

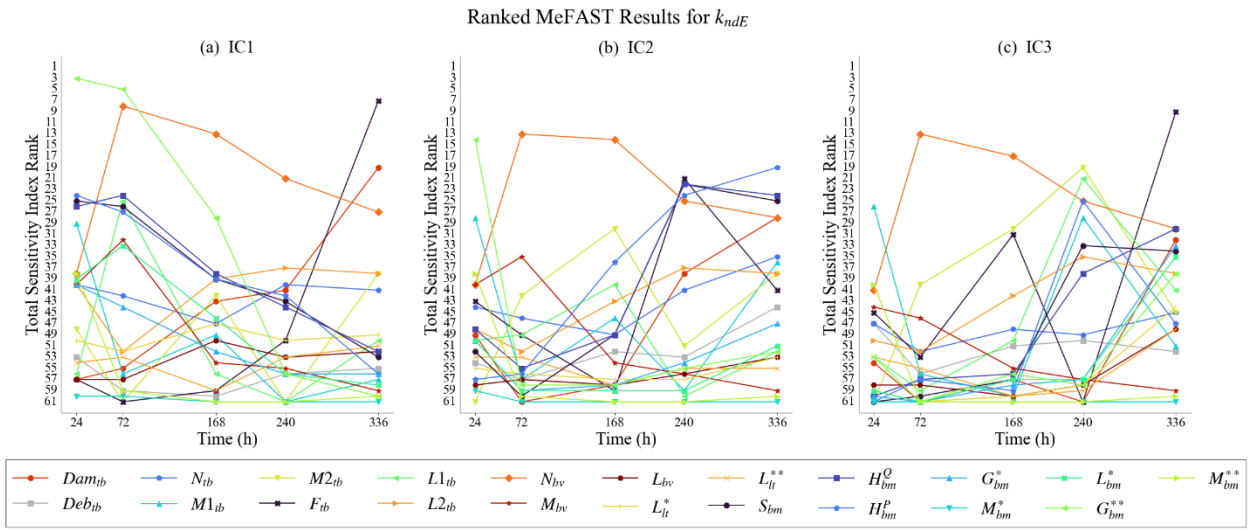


Figure 53. Ranked total sensitivity indices for k_{mdE} across all 105 MeFAST outputs for (a) IC1, superficial thermal burn; (b) IC2, superficial partial thickness thermal burn; and (c) IC3, deep partial thickness thermal burn.

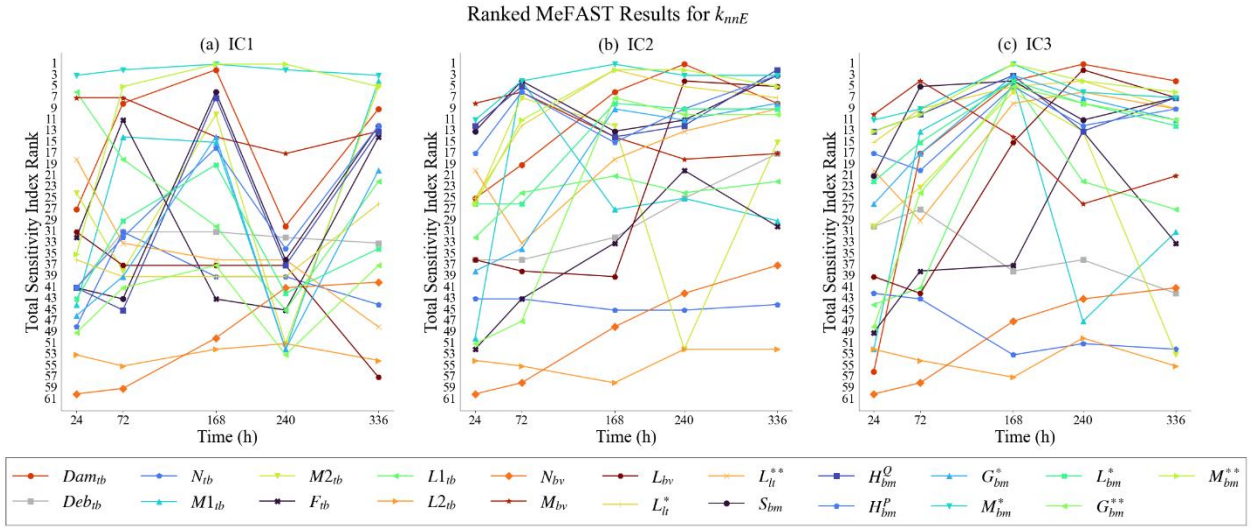


Figure 54. Ranked total sensitivity indices for k_{nnE} across all 105 MeFAST outputs for (a) IC1, superficial thermal burn; (b) IC2, superficial partial thickness thermal burn; and (c) IC3, deep partial thickness thermal burn.

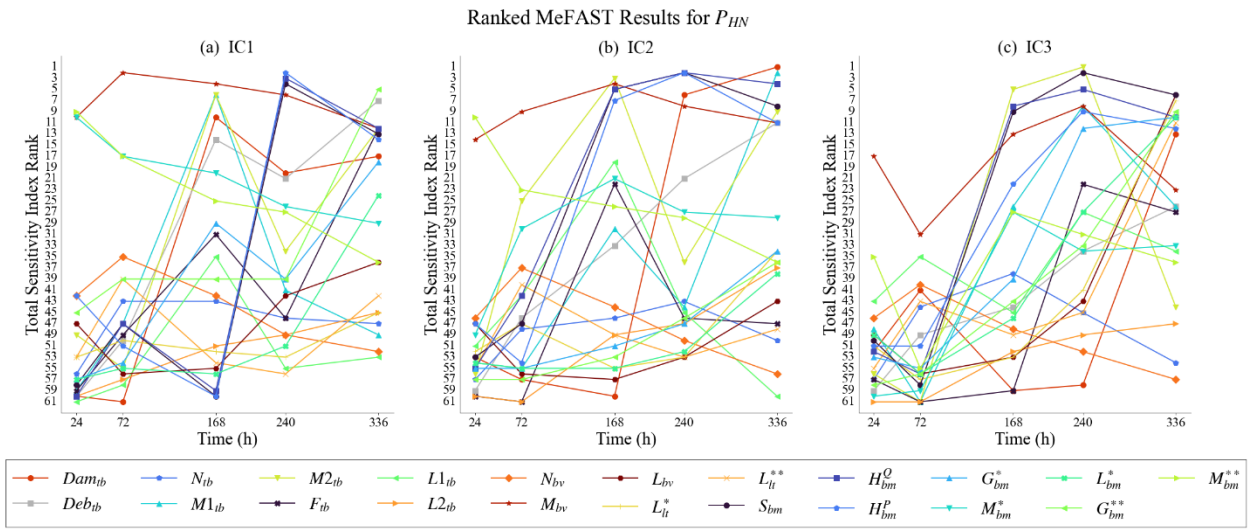


Figure 55. Ranked total sensitivity indices for P_{HN} across all 105 MeFAST outputs for (a) IC1, superficial thermal burn; (b) IC2, superficial partial thickness thermal burn; and (c) IC3, deep partial thickness thermal burn.

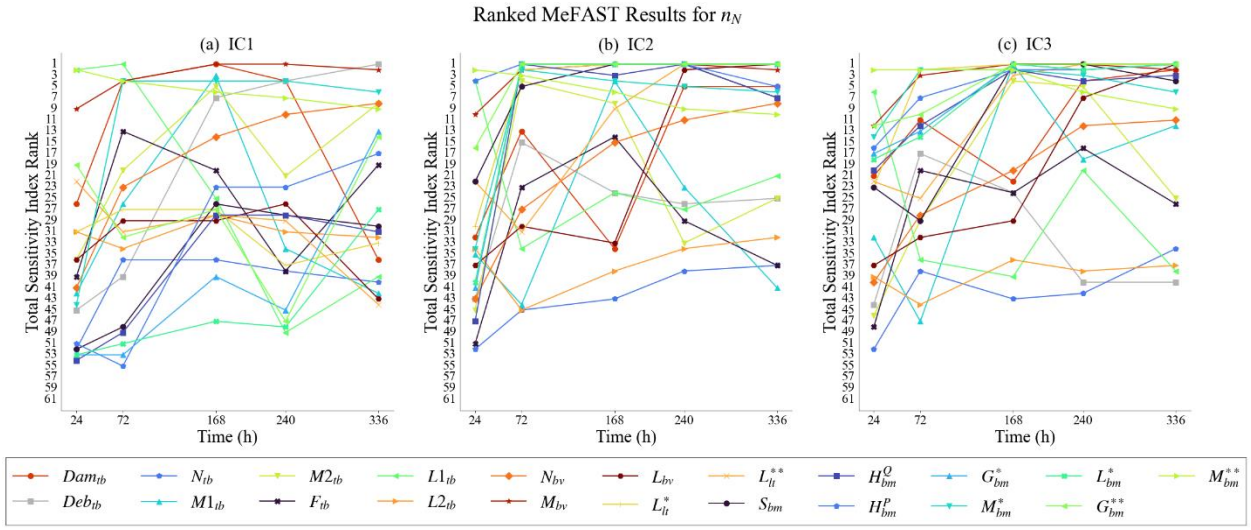


Figure 56. Ranked total sensitivity indices for n_N across all 105 MeFAST outputs for (a) IC1, superficial thermal burn; (b) IC2, superficial partial thickness thermal burn; and (c) IC3, deep partial thickness thermal burn.

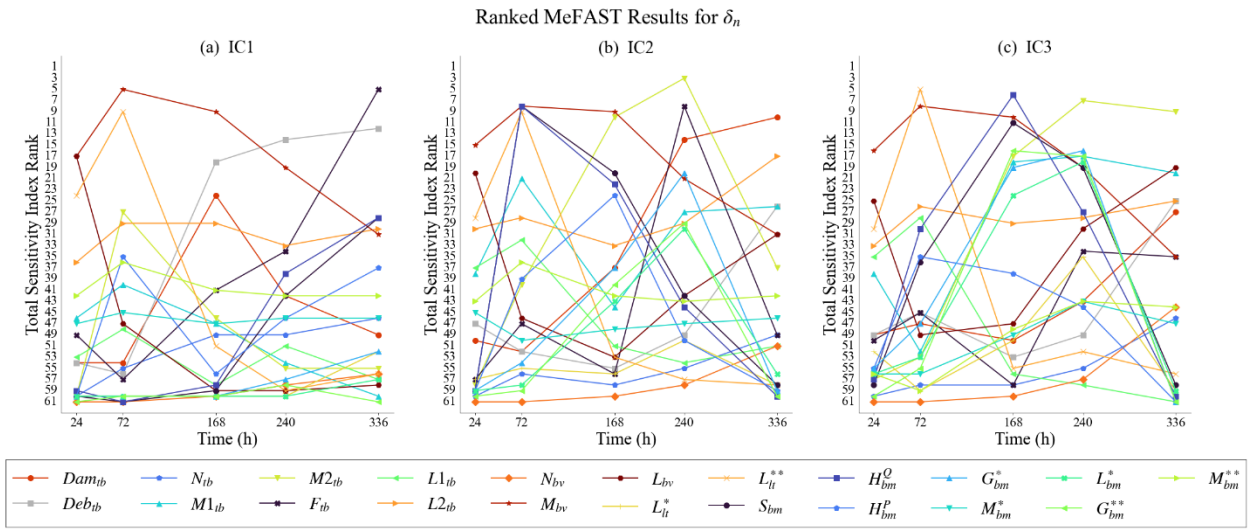


Figure 57. Ranked total sensitivity indices for δ_n across all 105 MeFAST outputs for (a) IC1, superficial thermal burn; (b) IC2, superficial partial thickness thermal burn; and (c) IC3, deep partial thickness thermal burn.

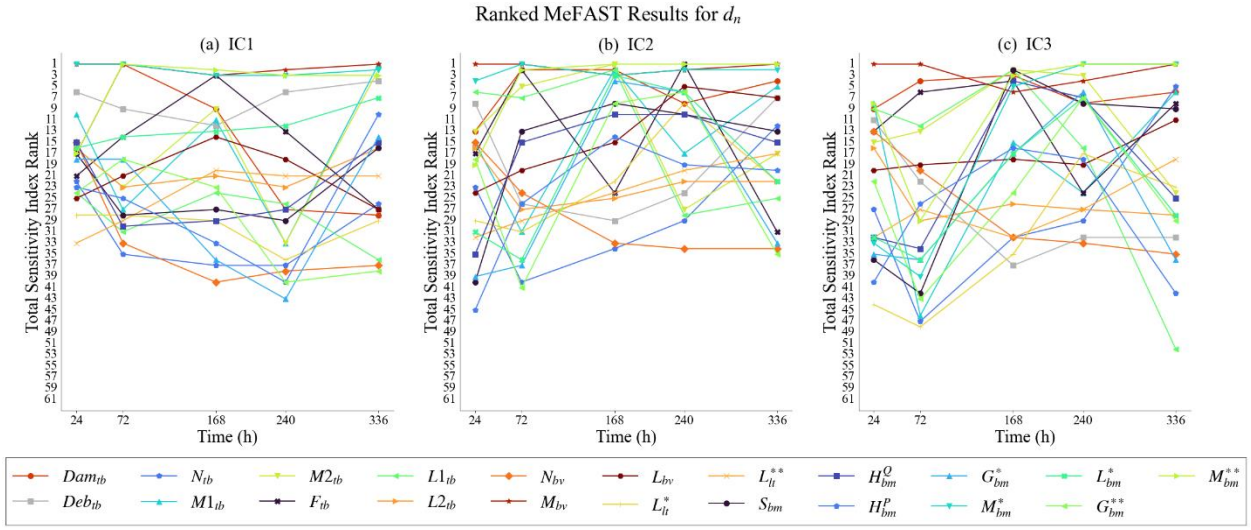


Figure 58. Ranked total sensitivity indices for d_n across all 105 MeFAST outputs for (a) IC1, superficial thermal burn; (b) IC2, superficial partial thickness thermal burn; and (c) IC3, deep partial thickness thermal burn.

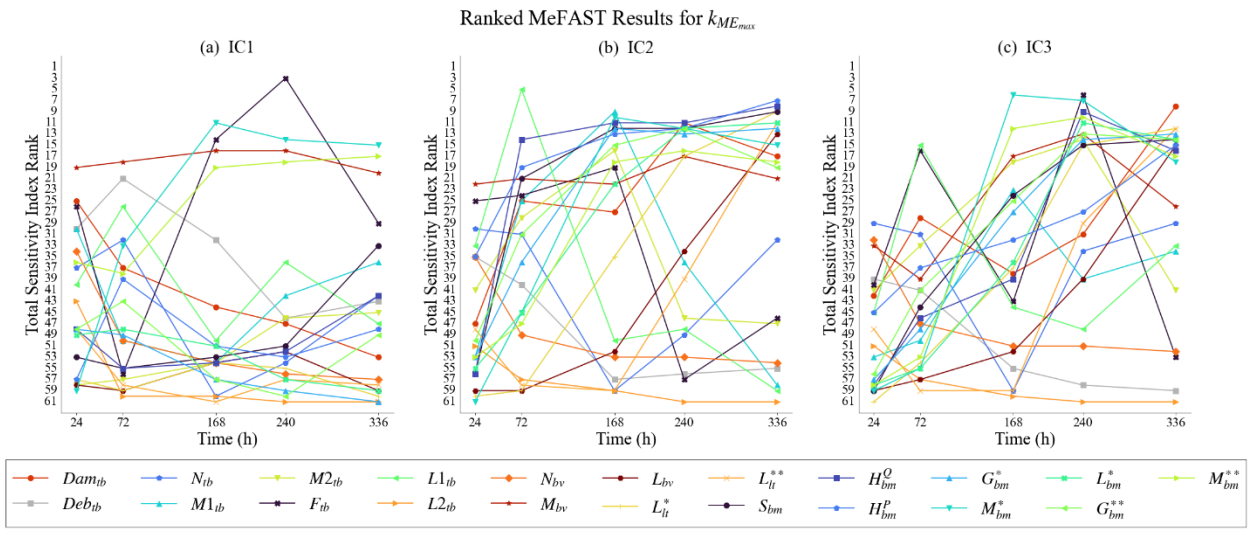


Figure 59. Ranked total sensitivity indices for k_{MEmax} across all 105 MeFAST outputs for (a) IC1, superficial thermal burn; (b) IC2, superficial partial thickness thermal burn; and (c) IC3, deep partial thickness thermal burn.

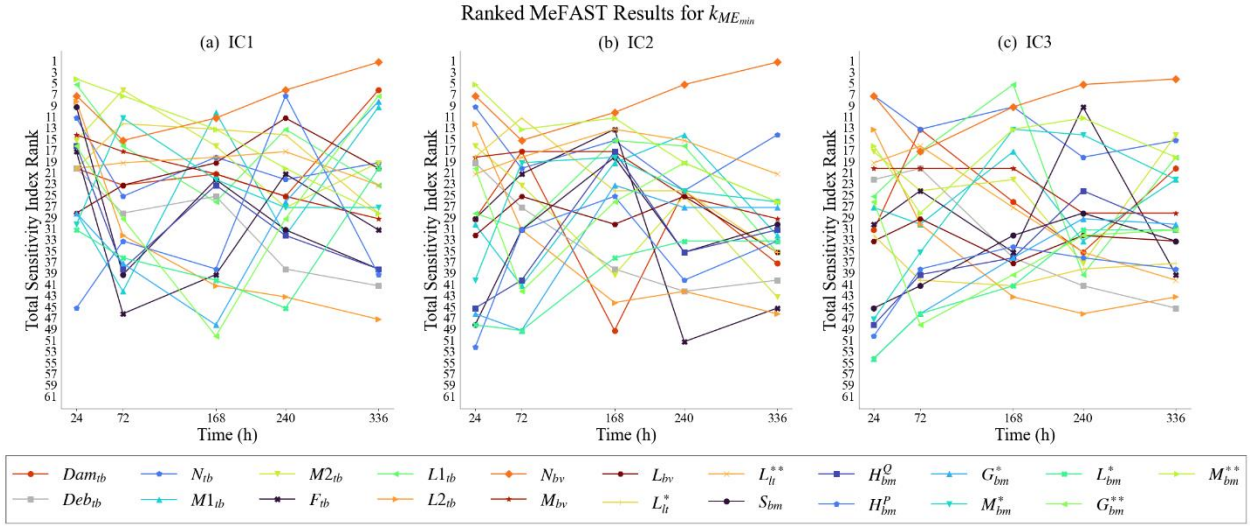


Figure 60. Ranked total sensitivity indices for k_{MEmin} across all 105 MeFAST outputs for (a) IC1, superficial thermal burn; (b) IC2, superficial partial thickness thermal burn; and (c) IC3, deep partial thickness thermal burn.

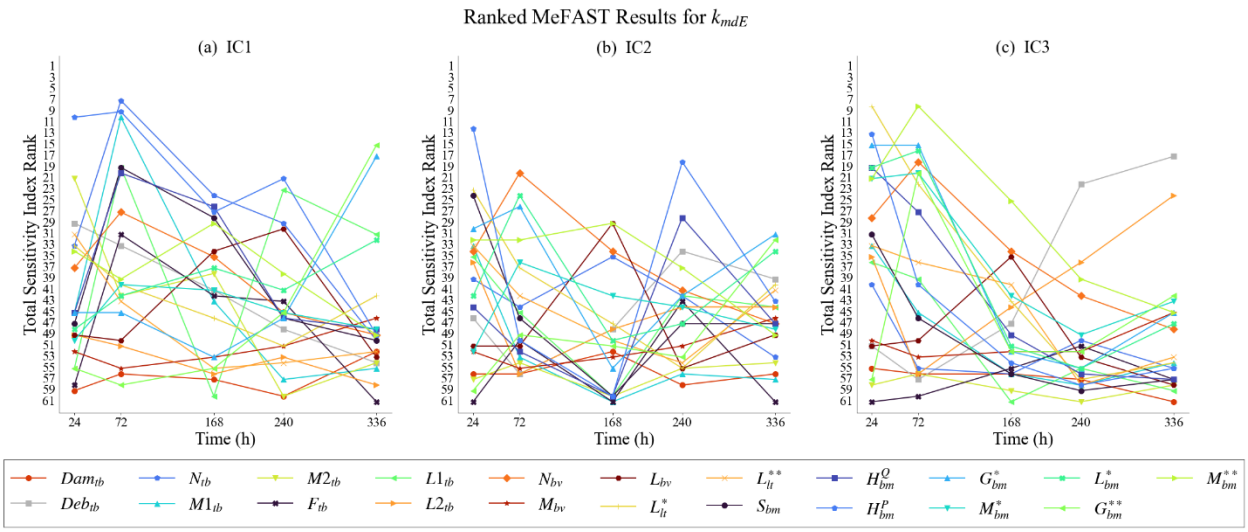


Figure 61. Ranked total sensitivity indices for k_{mdE} across all 105 MeFAST outputs for (a) IC1, superficial thermal burn; (b) IC2, superficial partial thickness thermal burn; and (c) IC3, deep partial thickness thermal burn.

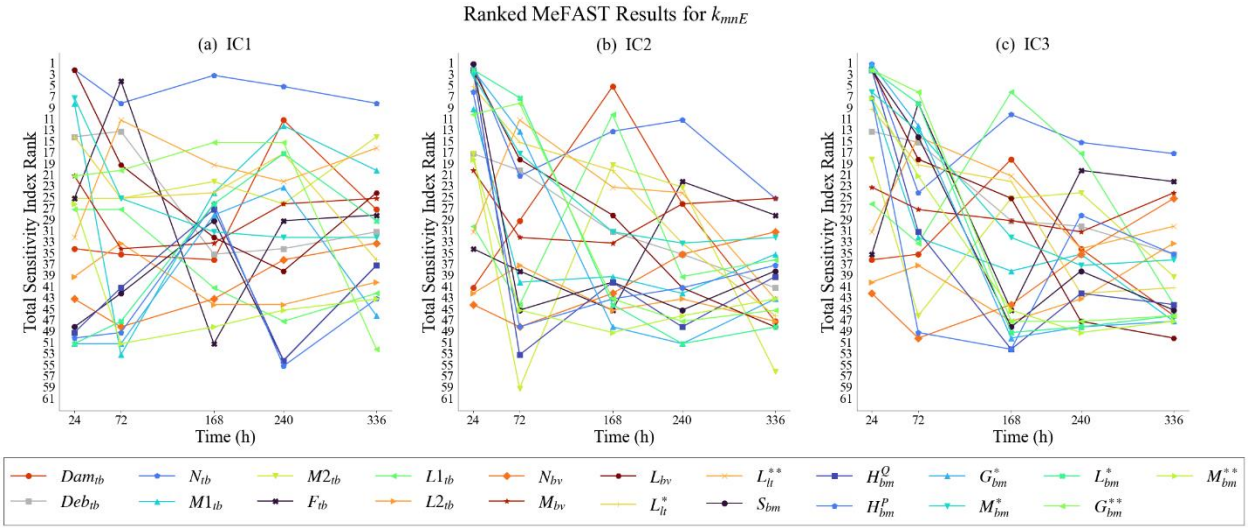


Figure 62. Ranked total sensitivity indices for k_{mnE} across all 105 MeFAST outputs for (a) IC1, superficial thermal burn; (b) IC2, superficial partial thickness thermal burn; and (c) IC3, deep partial thickness thermal burn.

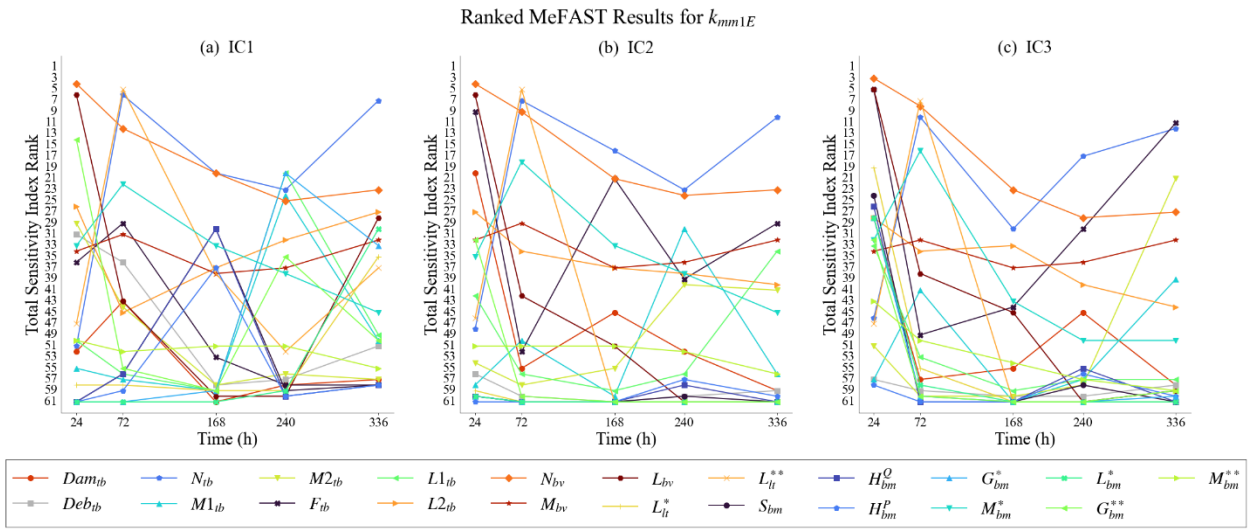


Figure 63. Ranked total sensitivity indices for k_{mm1E} across all 105 MeFAST outputs for (a) IC1, superficial thermal burn; (b) IC2, superficial partial thickness thermal burn; and (c) IC3, deep partial thickness thermal burn.

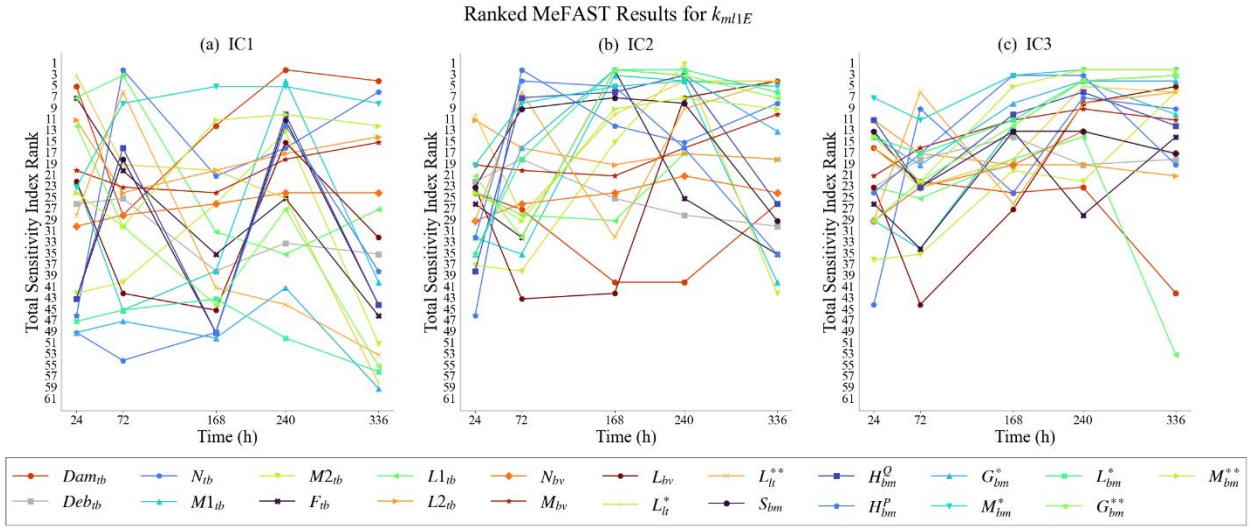


Figure 64. Ranked total sensitivity indices for k_{ml1E} across all 105 MeFAST outputs for (a) IC1, superficial thermal burn; (b) IC2, superficial partial thickness thermal burn; and (c) IC3, deep partial thickness thermal burn.

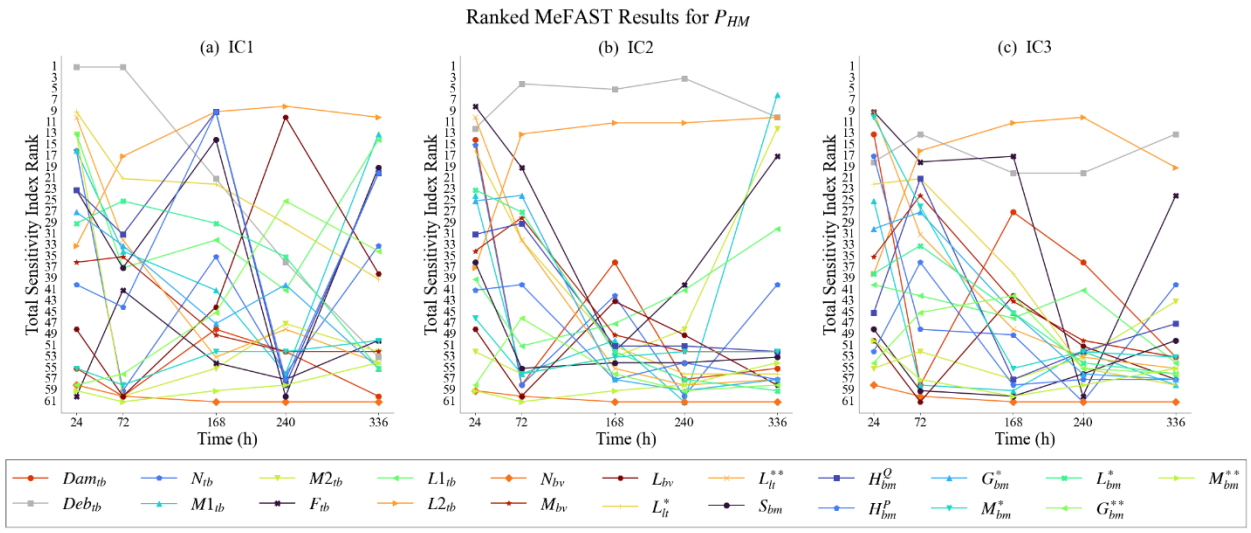


Figure 65. Ranked total sensitivity indices for P_{HM} across all 105 MeFAST outputs for (a) IC1, superficial thermal burn; (b) IC2, superficial partial thickness thermal burn; and (c) IC3, deep partial thickness thermal burn.

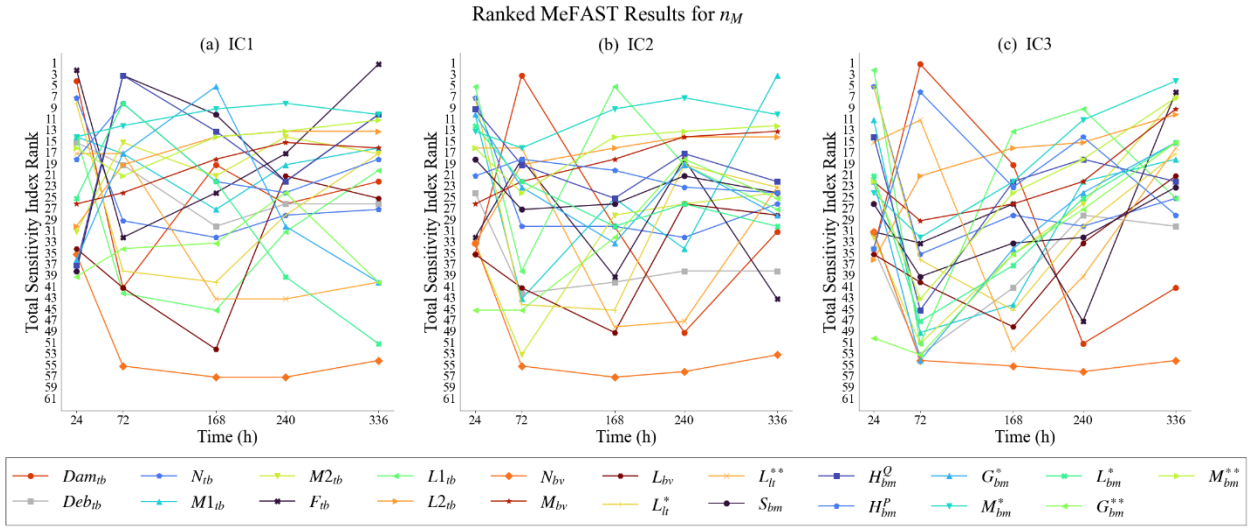


Figure 66. Ranked total sensitivity indices for n_M across all 105 MeFAST outputs for (a) IC1, superficial thermal burn; (b) IC2, superficial partial thickness thermal burn; and (c) IC3, deep partial thickness thermal burn.

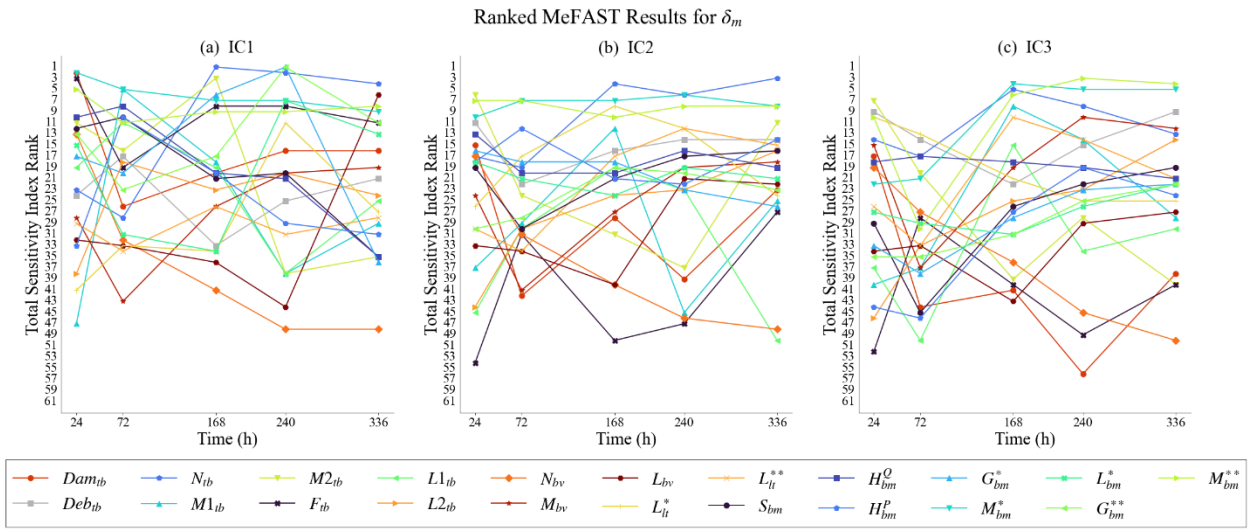


Figure 67. Ranked total sensitivity indices for δ_m across all 105 MeFAST outputs for (a) IC1, superficial thermal burn; (b) IC2, superficial partial thickness thermal burn; and (c) IC3, deep partial thickness thermal burn.

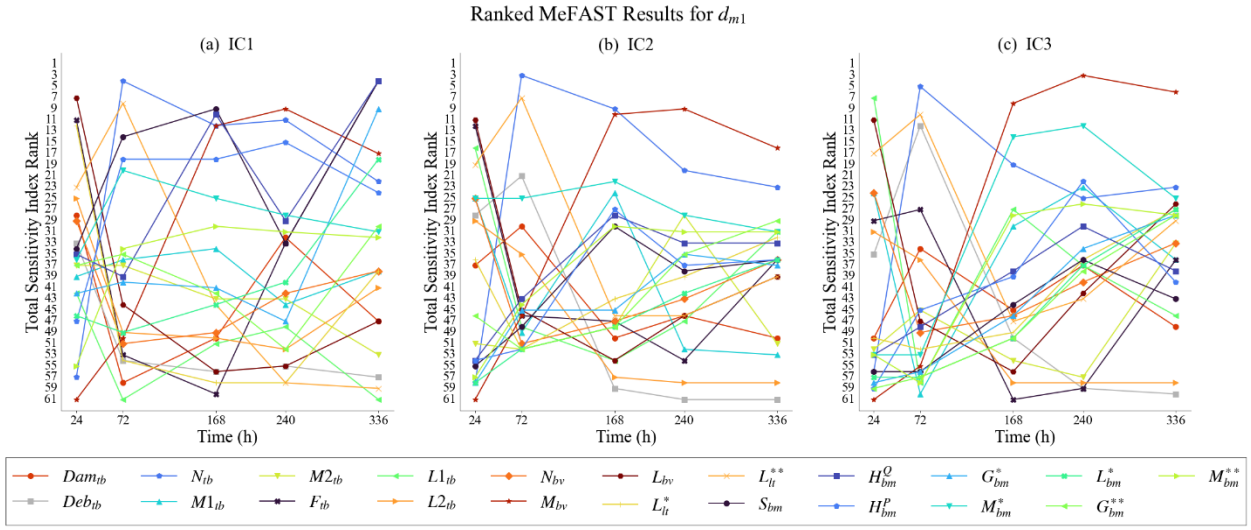


Figure 68. Ranked total sensitivity indices for d_{m1} across all 105 MeFAST outputs for (a) IC1, superficial thermal burn; (b) IC2, superficial partial thickness thermal burn; and (c) IC3, deep partial thickness thermal burn.

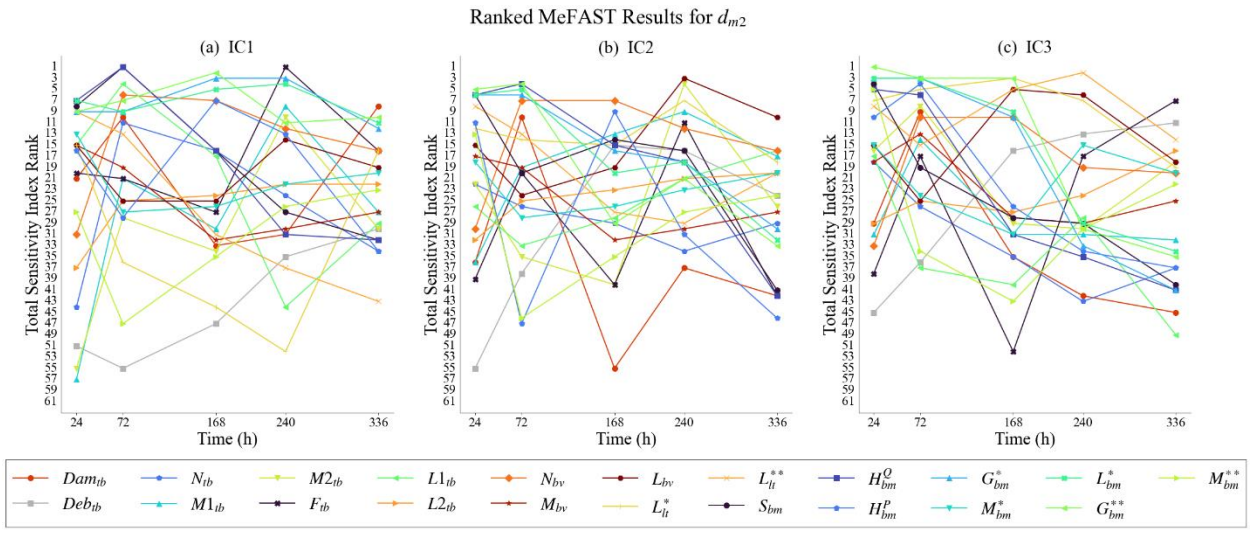


Figure 69. Ranked total sensitivity indices for d_{m2} across all 105 MeFAST outputs for (a) IC1, superficial thermal burn; (b) IC2, superficial partial thickness thermal burn; and (c) IC3, deep partial thickness thermal burn.

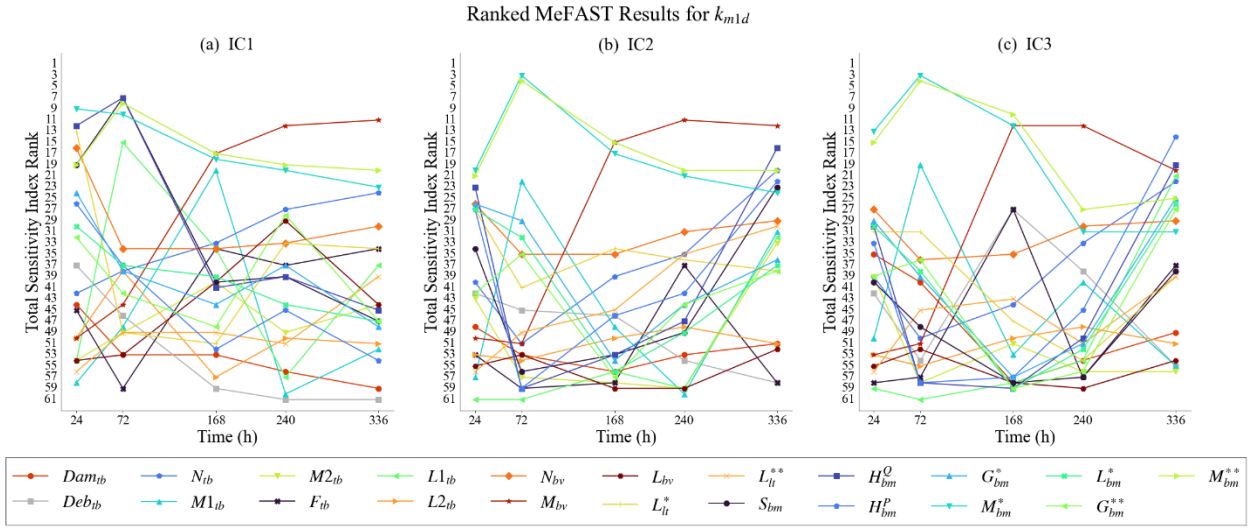


Figure 70. Ranked total sensitivity indices for k_{m1d} across all 105 MeFAST outputs for (a) IC1, superficial thermal burn; (b) IC2, superficial partial thickness thermal burn; and (c) IC3, deep partial thickness thermal burn.

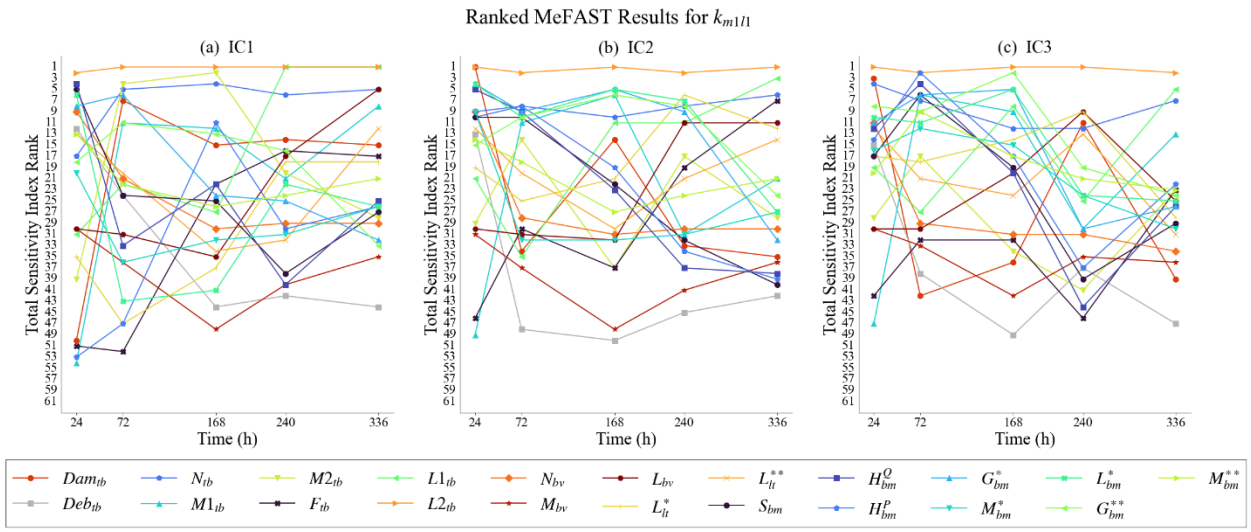


Figure 71. Ranked total sensitivity indices for k_{m1l1} across all 105 MeFAST outputs for (a) IC1, superficial thermal burn; (b) IC2, superficial partial thickness thermal burn; and (c) IC3, deep partial thickness thermal burn.

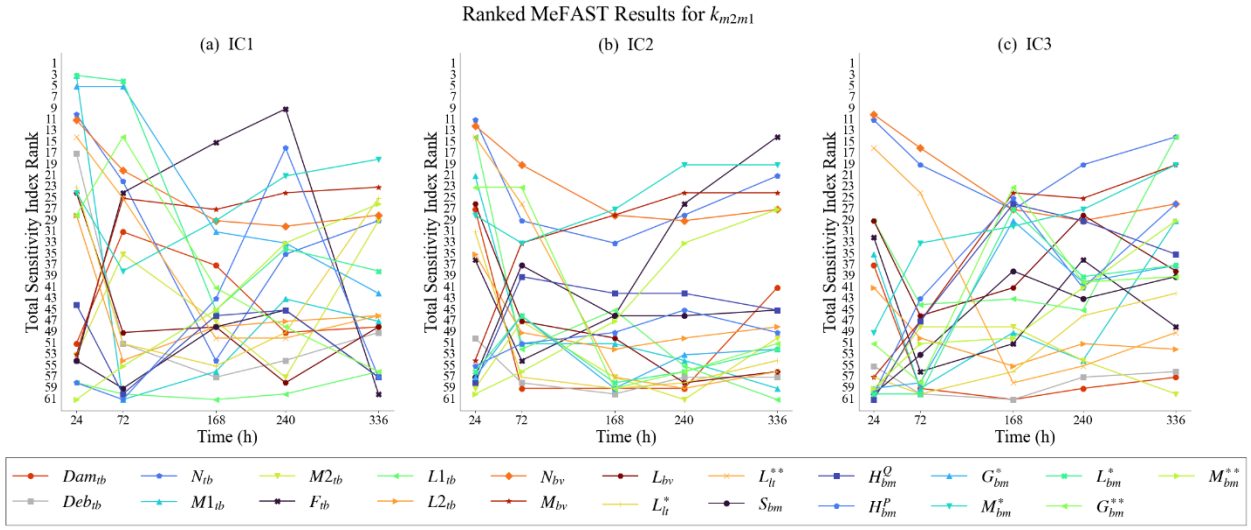


Figure 72. Ranked total sensitivity indices for k_{m2m1} across all 105 MeFAST outputs for (a) IC1, superficial thermal burn; (b) IC2, superficial partial thickness thermal burn; and (c) IC3, deep partial thickness thermal burn.

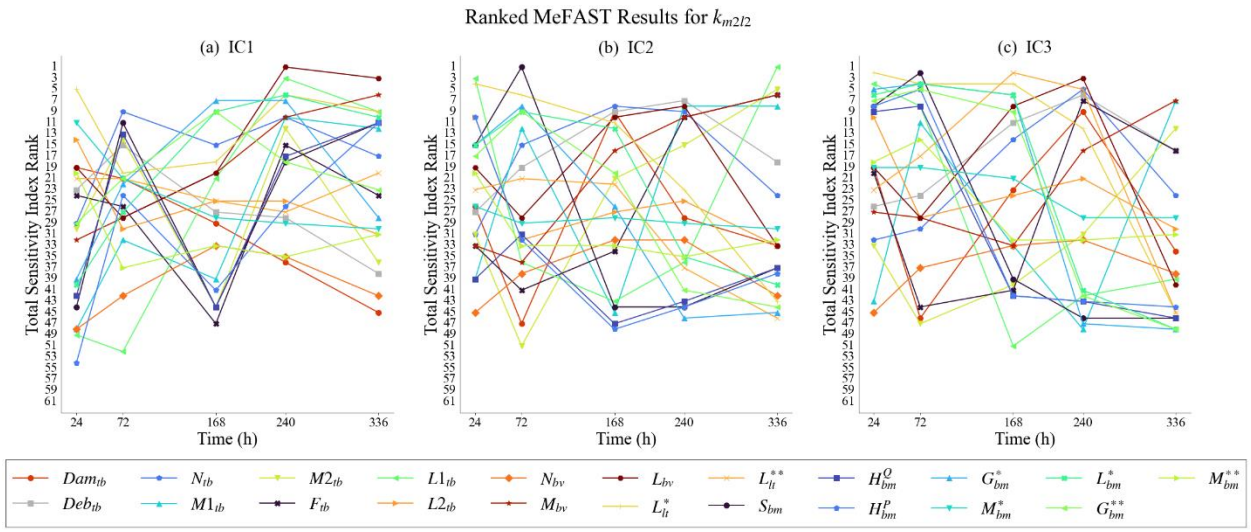


Figure 73. Ranked total sensitivity indices for k_{m2l2} across all 105 MeFAST outputs for (a) IC1, superficial thermal burn; (b) IC2, superficial partial thickness thermal burn; and (c) IC3, deep partial thickness thermal burn.

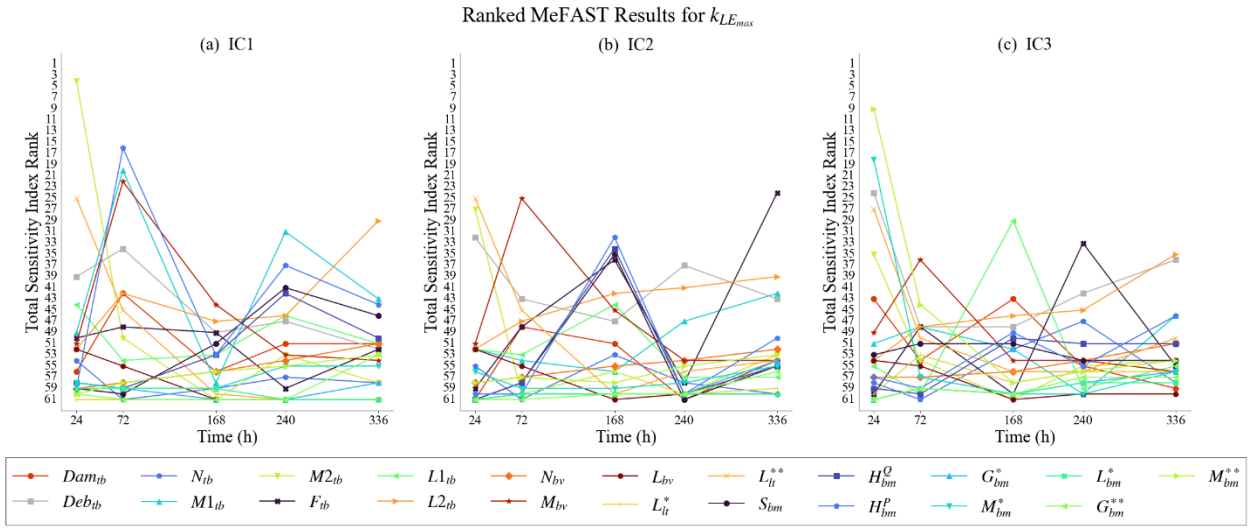


Figure 74. Ranked total sensitivity indices for k_{LEmax} across all 105 MeFAST outputs for (a) IC1, superficial thermal burn; (b) IC2, superficial partial thickness thermal burn; and (c) IC3, deep partial thickness thermal burn.

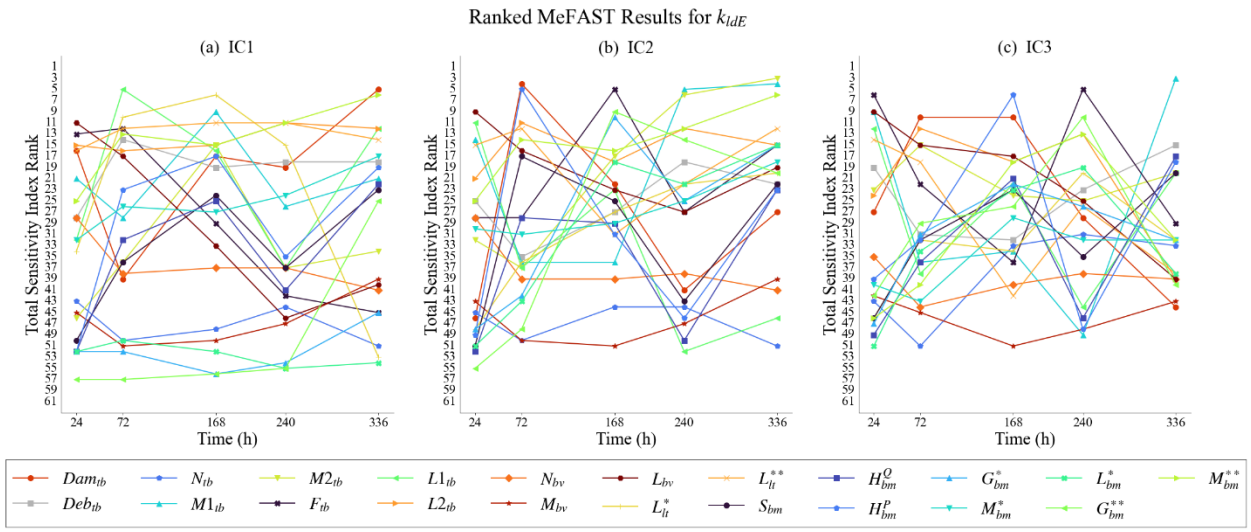


Figure 75. Ranked total sensitivity indices for k_{ldE} across all 105 MeFAST outputs for (a) IC1, superficial thermal burn; (b) IC2, superficial partial thickness thermal burn; and (c) IC3, deep partial thickness thermal burn.

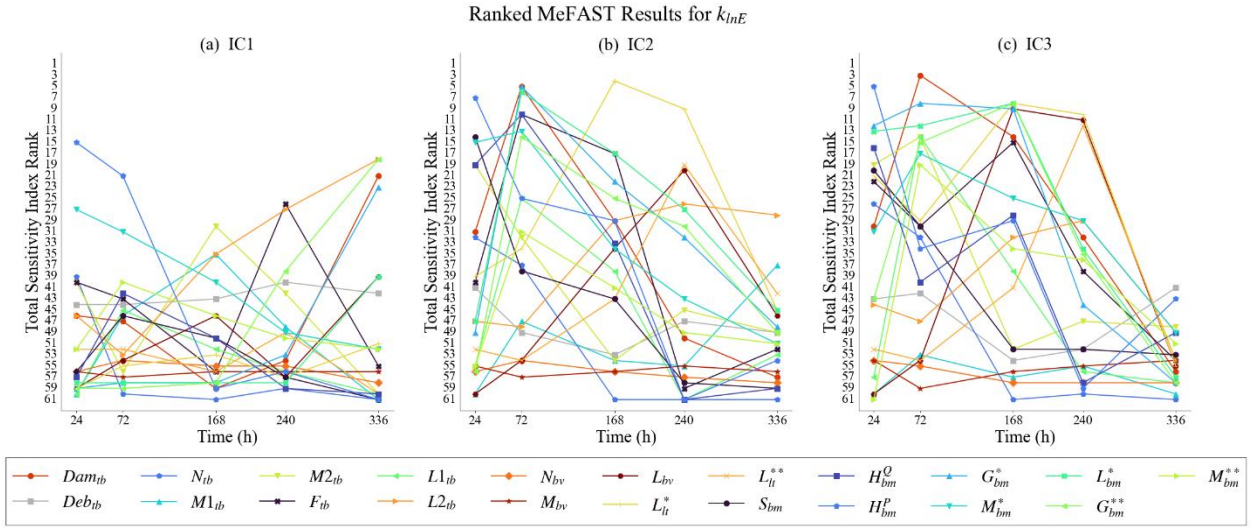


Figure 76. Ranked total sensitivity indices for k_{lnE} across all 105 MeFAST outputs for (a) IC1, superficial thermal burn; (b) IC2, superficial partial thickness thermal burn; and (c) IC3, deep partial thickness thermal burn.

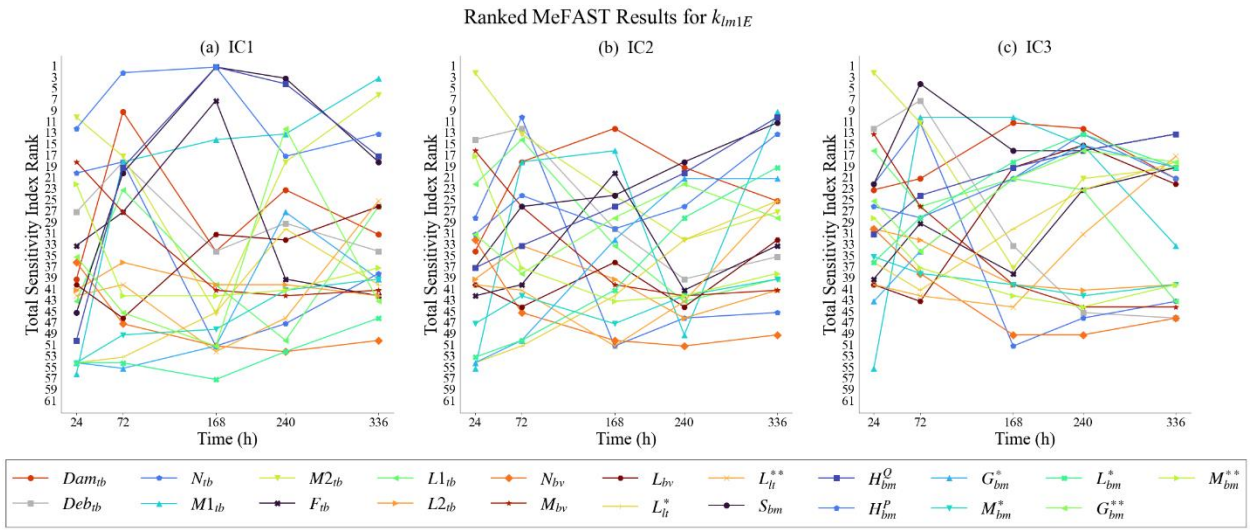


Figure 77. Ranked total sensitivity indices for k_{lm1E} across all 105 MeFAST outputs for (a) IC1, superficial thermal burn; (b) IC2, superficial partial thickness thermal burn; and (c) IC3, deep partial thickness thermal burn.

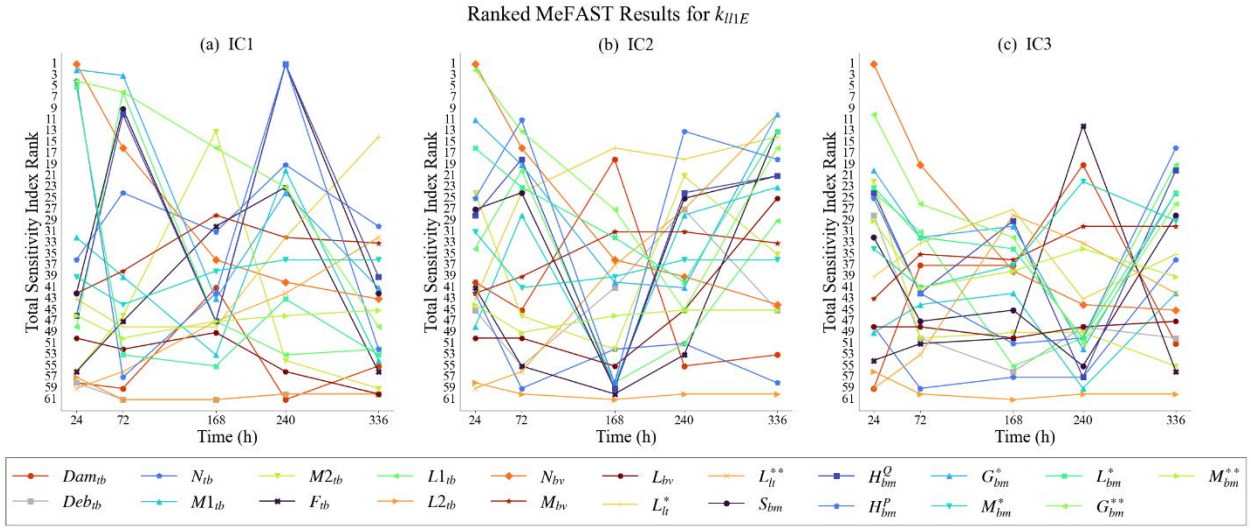


Figure 78. Ranked total sensitivity indices for k_{ll1E} across all 105 MeFAST outputs for (a) IC1, superficial thermal burn; (b) IC2, superficial partial thickness thermal burn; and (c) IC3, deep partial thickness thermal burn.

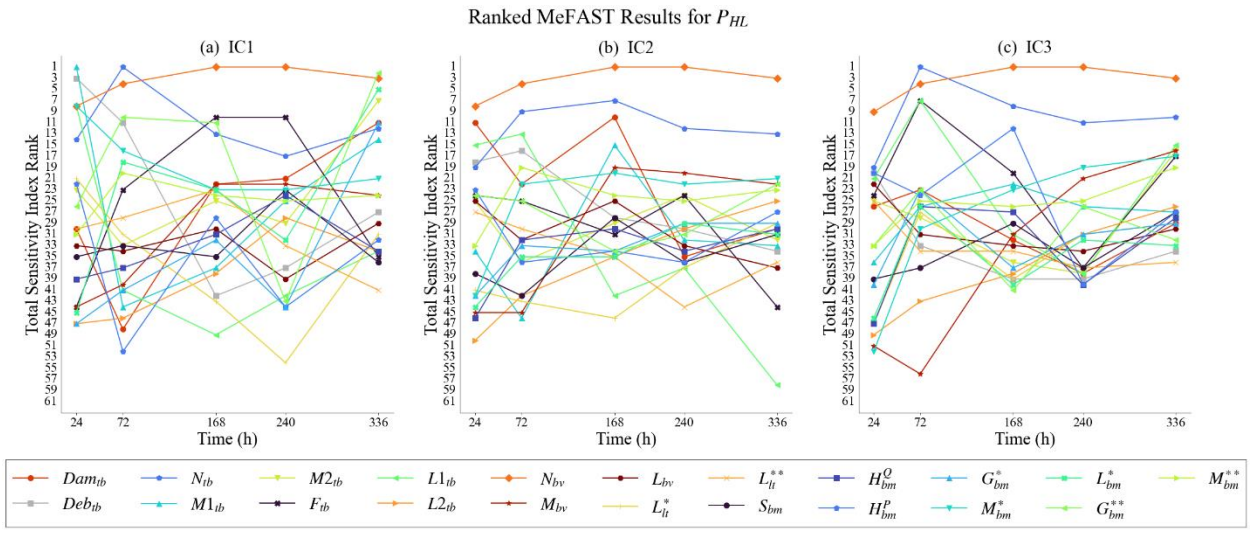


Figure 79. Ranked total sensitivity indices for P_{HL} across all 105 MeFAST outputs for (a) IC1, superficial thermal burn; (b) IC2, superficial partial thickness thermal burn; and (c) IC3, deep partial thickness thermal burn.

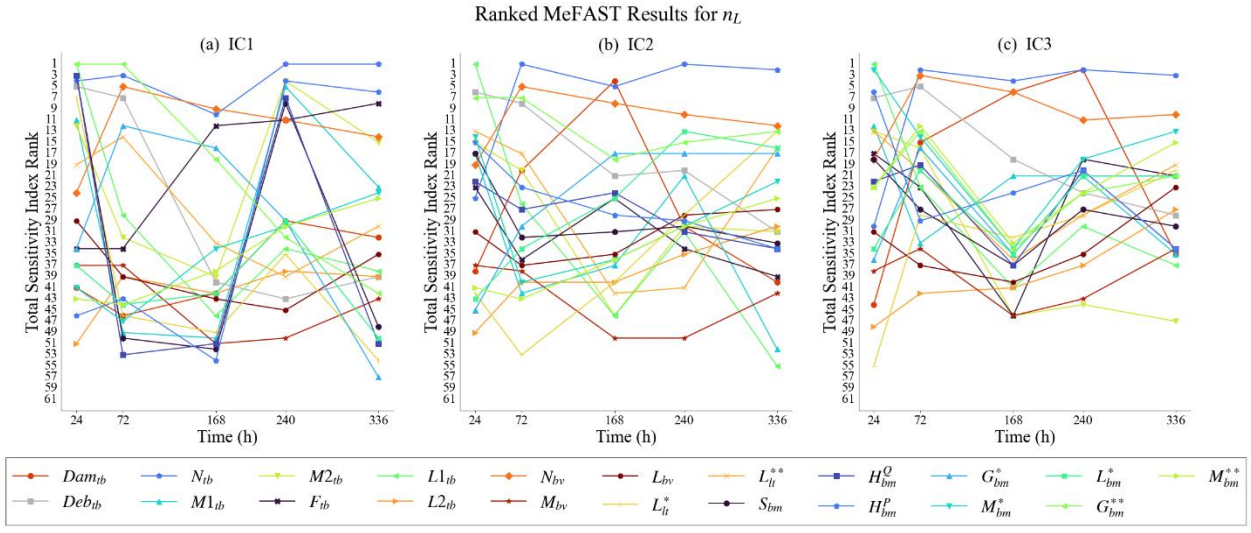


Figure 80. Ranked total sensitivity indices for n_L across all 105 MeFAST outputs for (a) IC1, superficial thermal burn; (b) IC2, superficial partial thickness thermal burn; and (c) IC3, deep partial thickness thermal burn.

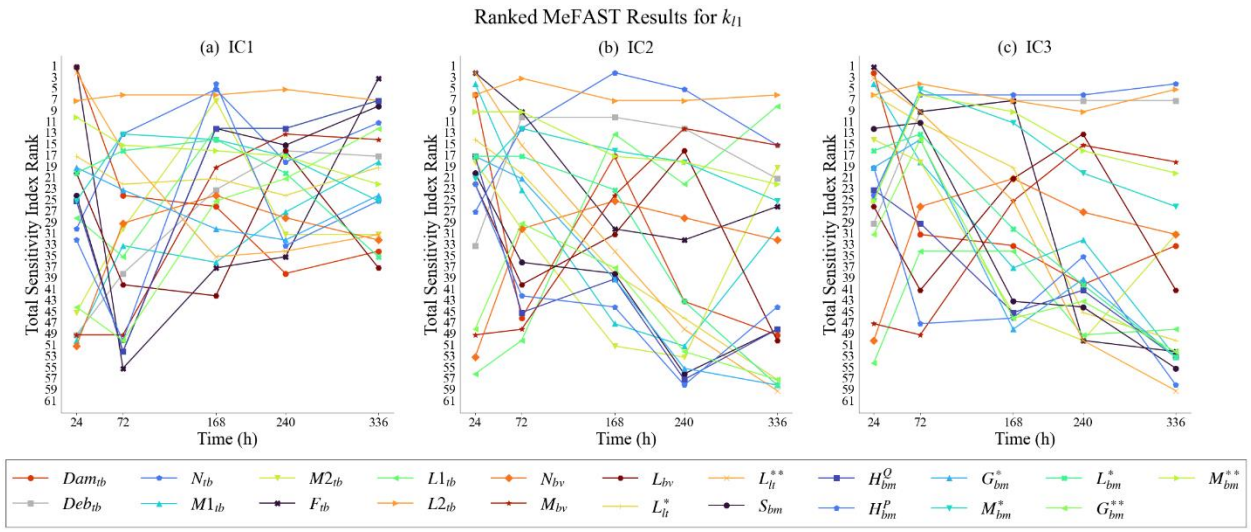


Figure 81. Ranked total sensitivity indices for k_{I1} across all 105 MeFAST outputs for (a) IC1, superficial thermal burn; (b) IC2, superficial partial thickness thermal burn; and (c) IC3, deep partial thickness thermal burn.

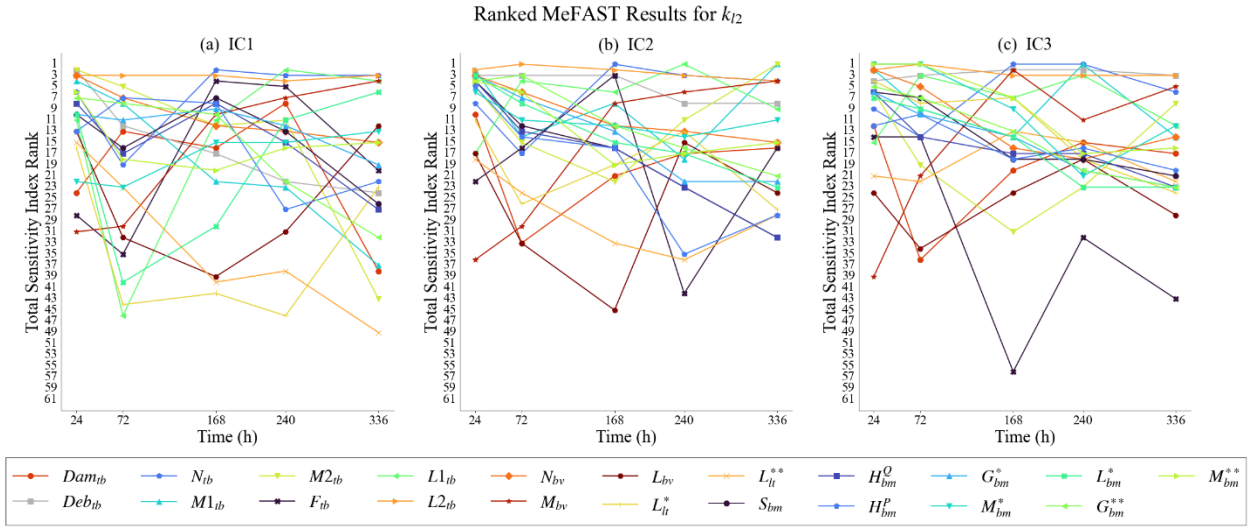


Figure 82. Ranked total sensitivity indices for k_{I2} across all 105 MeFAST outputs for (a) IC1, superficial thermal burn; (b) IC2, superficial partial thickness thermal burn; and (c) IC3, deep partial thickness thermal burn.

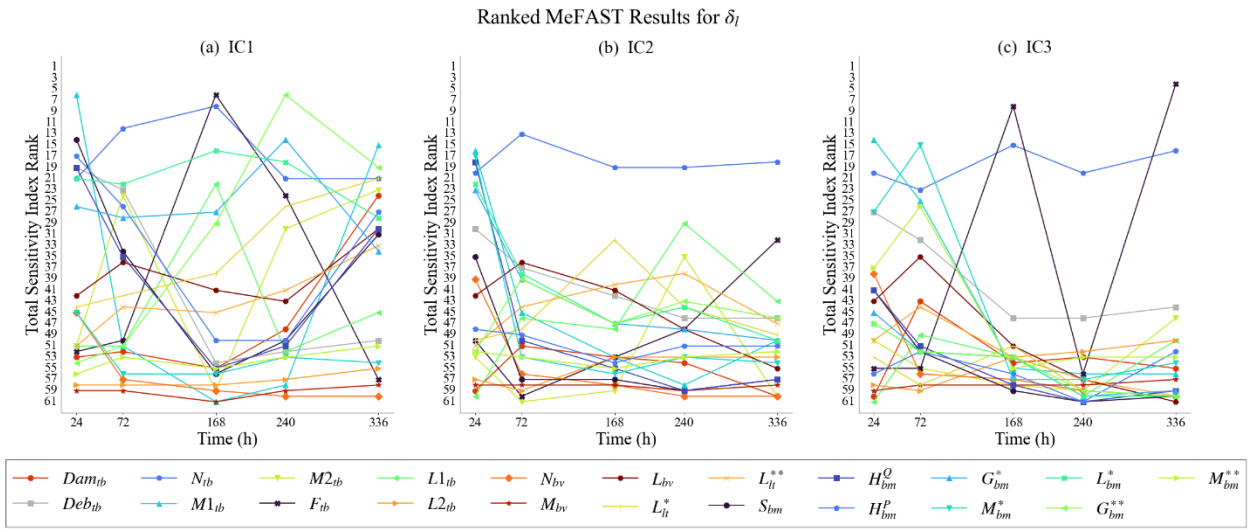


Figure 83. Ranked total sensitivity indices for δ_I across all 105 MeFAST outputs for (a) IC1, superficial thermal burn; (b) IC2, superficial partial thickness thermal burn; and (c) IC3, deep partial thickness thermal burn.

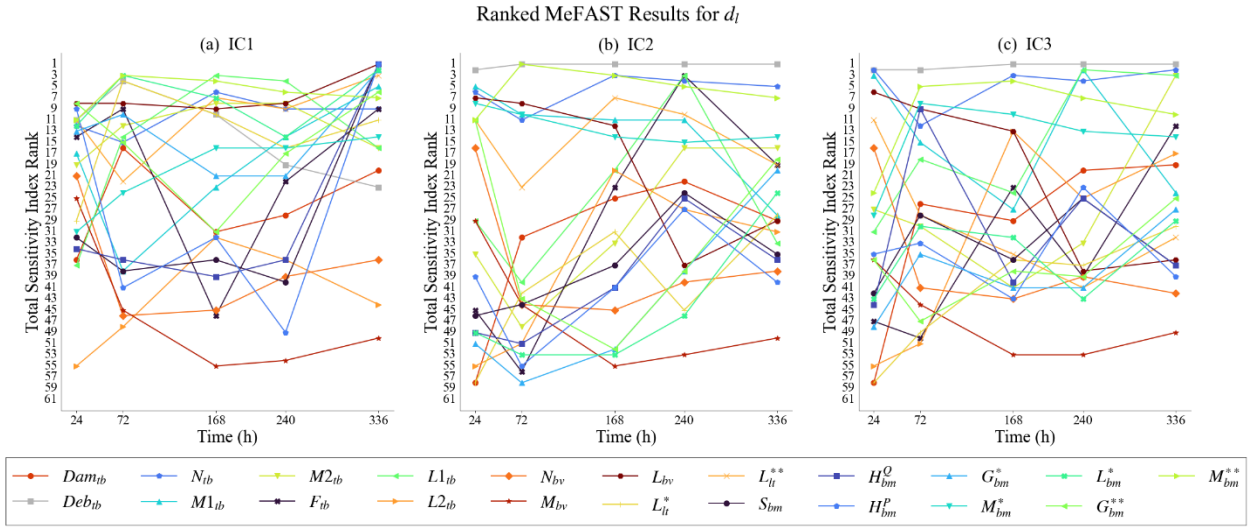


Figure 84. Ranked total sensitivity indices for d_I across all 105 MeFAST outputs for (a) IC1, superficial thermal burn; (b) IC2, superficial partial thickness thermal burn; and (c) IC3, deep partial thickness thermal burn.

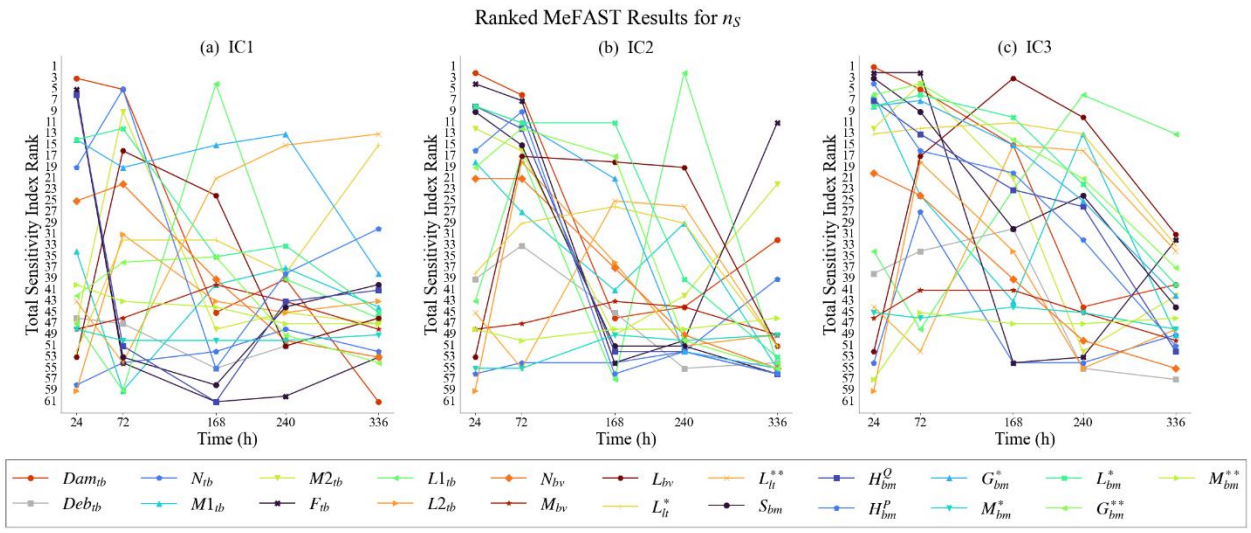


Figure 85. Ranked total sensitivity indices for n_S across all 105 MeFAST outputs for (a) IC1, superficial thermal burn; (b) IC2, superficial partial thickness thermal burn; and (c) IC3, deep partial thickness thermal burn.

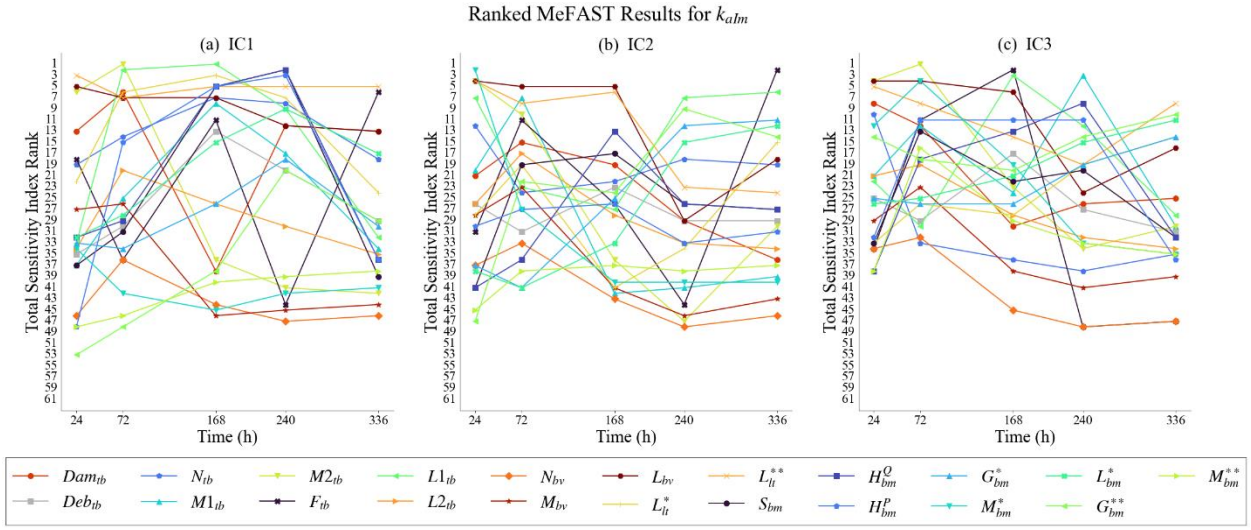


Figure 86. Ranked total sensitivity indices for k_{alm} across all 105 MeFAST outputs for (a) IC1, superficial thermal burn; (b) IC2, superficial partial thickness thermal burn; and (c) IC3, deep partial thickness thermal burn.

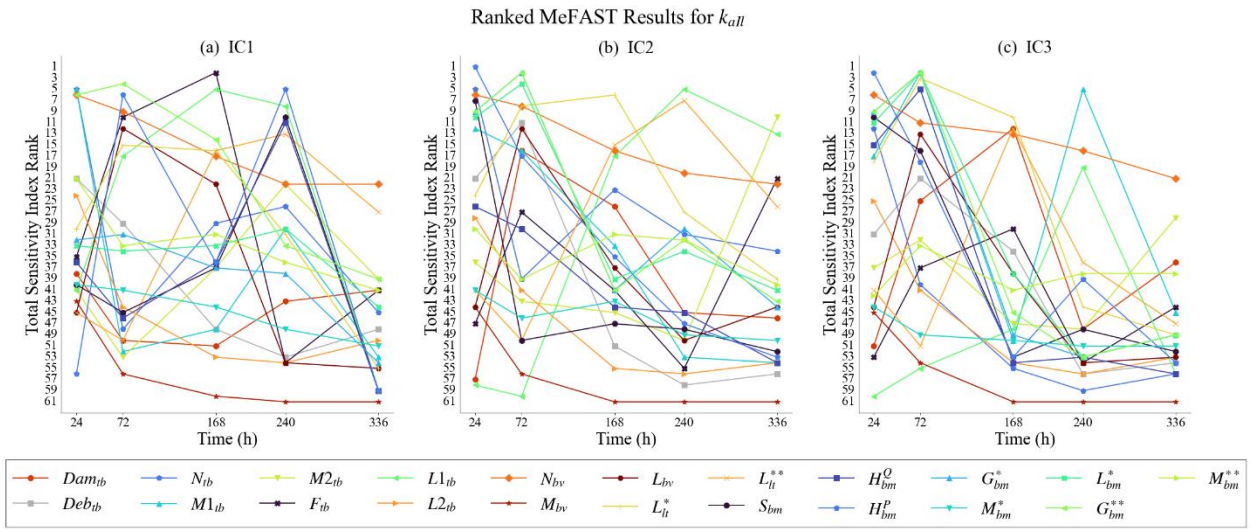


Figure 87. Ranked total sensitivity indices for k_{all} across all 105 MeFAST outputs for (a) IC1, superficial thermal burn; (b) IC2, superficial partial thickness thermal burn; and (c) IC3, deep partial thickness thermal burn.

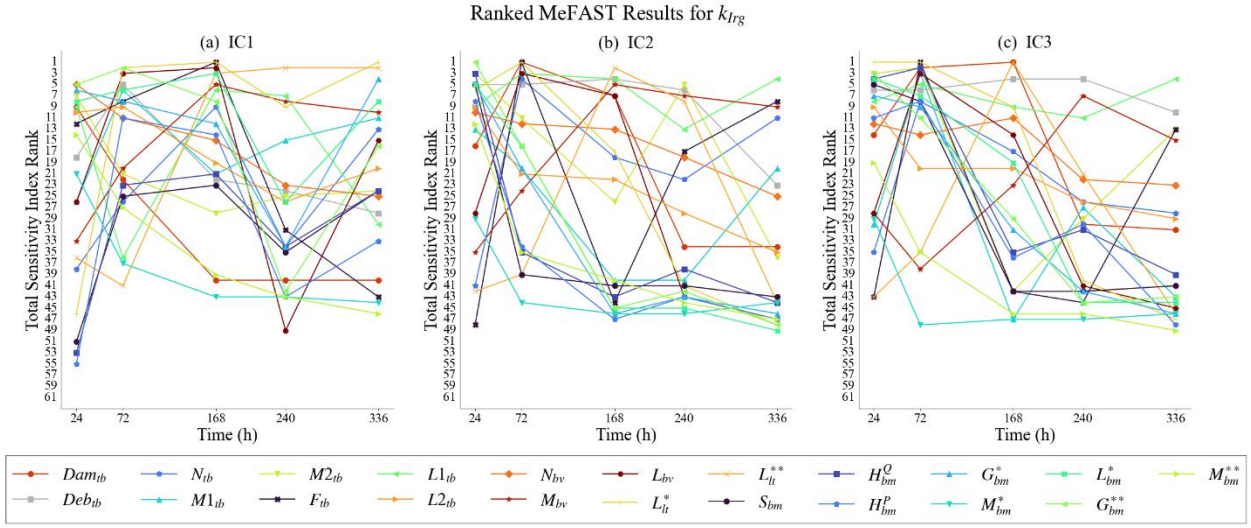


Figure 88. Ranked total sensitivity indices for k_{Irg} across all 105 MeFAST outputs for (a) IC1, superficial thermal burn; (b) IC2, superficial partial thickness thermal burn; and (c) IC3, deep partial thickness thermal burn.

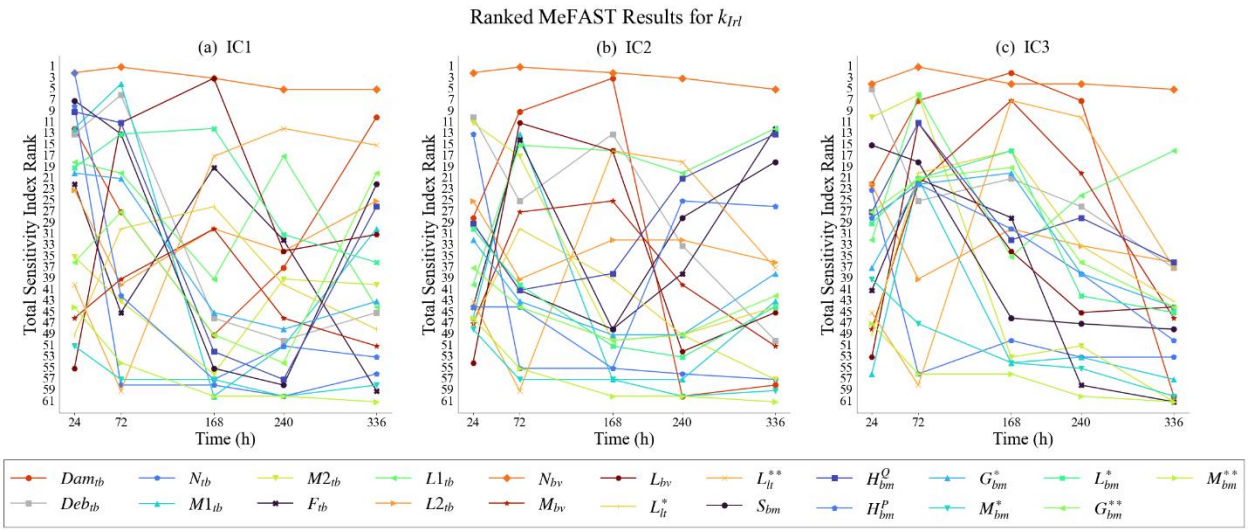


Figure 89. Ranked total sensitivity indices for k_{Irl} across all 105 MeFAST outputs for (a) IC1, superficial thermal burn; (b) IC2, superficial partial thickness thermal burn; and (c) IC3, deep partial thickness thermal burn.

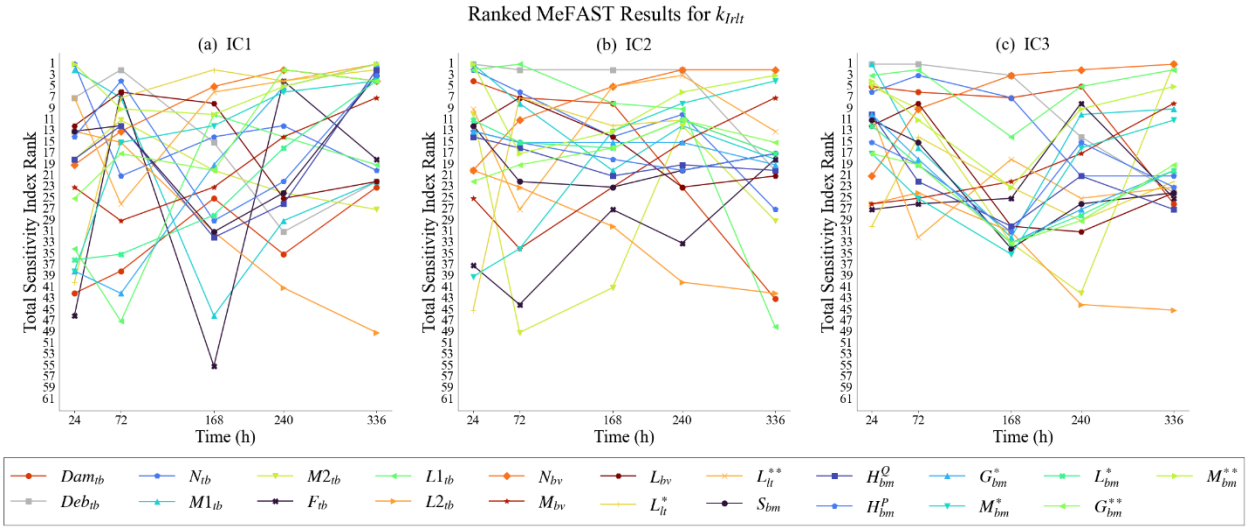


Figure 90. Ranked total sensitivity indices for k_{Irlt} across all 105 MeFAST outputs for (a) IC1, superficial thermal burn; (b) IC2, superficial partial thickness thermal burn; and (c) IC3, deep partial thickness thermal burn.

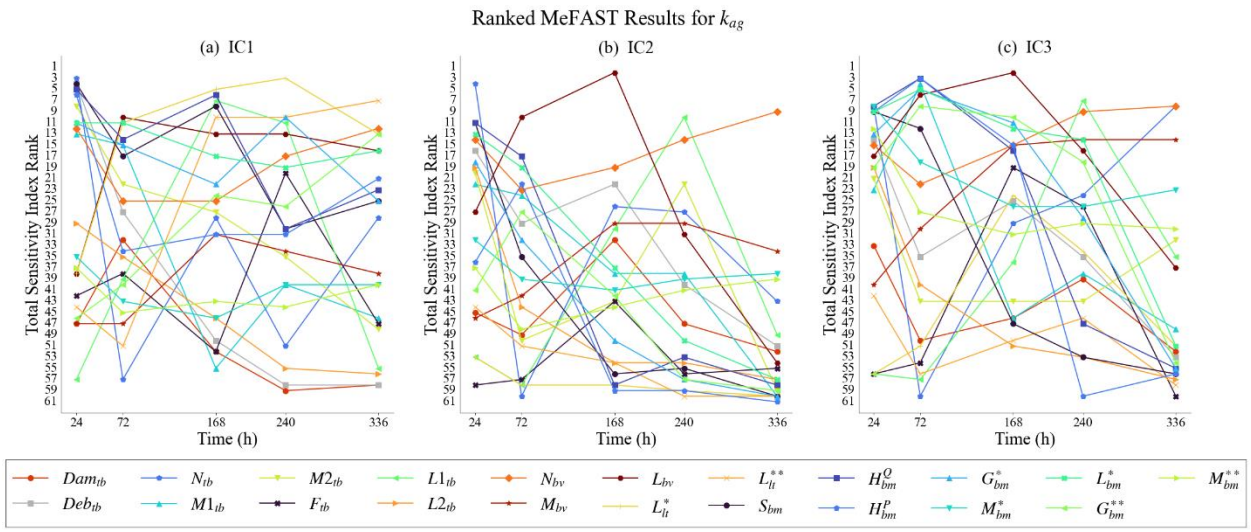


Figure 91. Ranked total sensitivity indices for k_{ag} across all 105 MeFAST outputs for (a) IC1, superficial thermal burn; (b) IC2, superficial partial thickness thermal burn; and (c) IC3, deep partial thickness thermal burn.

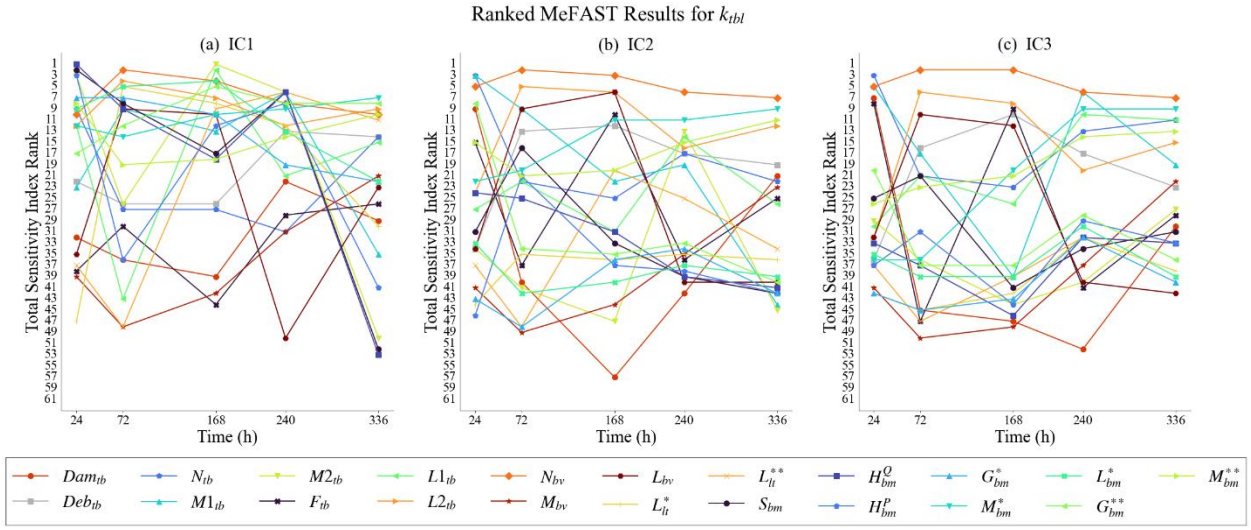


Figure 92. Ranked total sensitivity indices for k_{tbl} across all 105 MeFAST outputs for (a) IC1, superficial thermal burn; (b) IC2, superficial partial thickness thermal burn; and (c) IC3, deep partial thickness thermal burn.

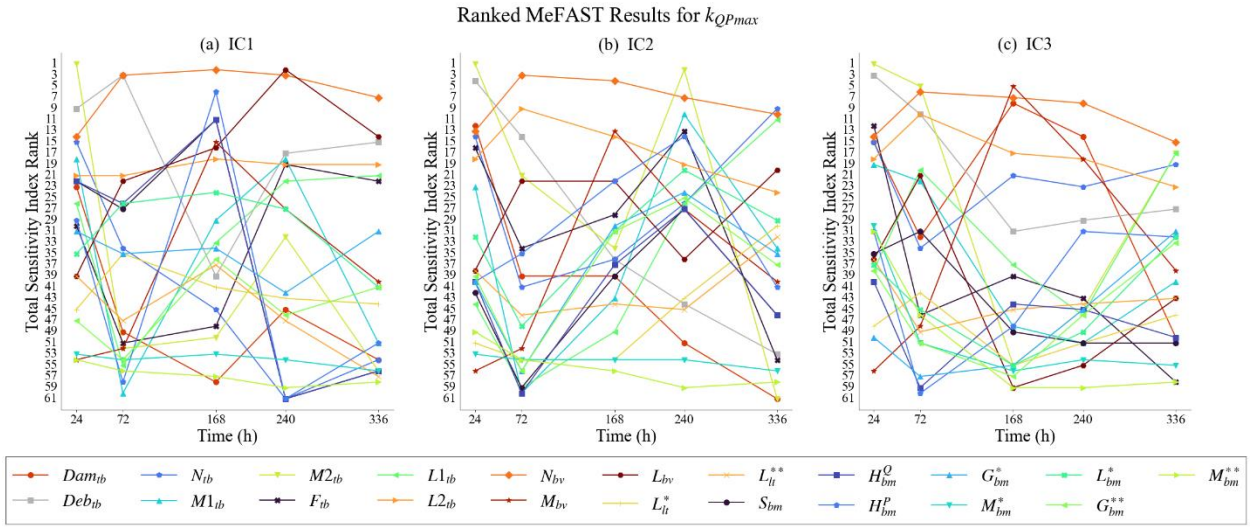


Figure 93. Ranked total sensitivity indices for k_{QPmax} across all 105 MeFAST outputs for (a) IC1, superficial thermal burn; (b) IC2, superficial partial thickness thermal burn; and (c) IC3, deep partial thickness thermal burn.

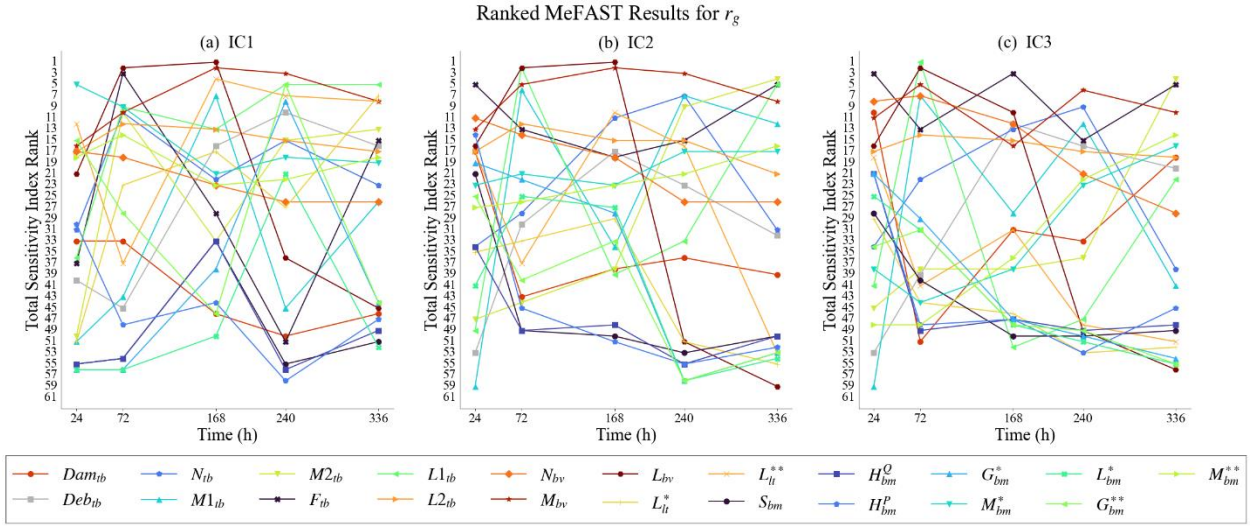


Figure 94. Ranked total sensitivity indices for r_g across all 105 MeFAST outputs for (a) IC1, superficial thermal burn; (b) IC2, superficial partial thickness thermal burn; and (c) IC3, deep partial thickness thermal burn.

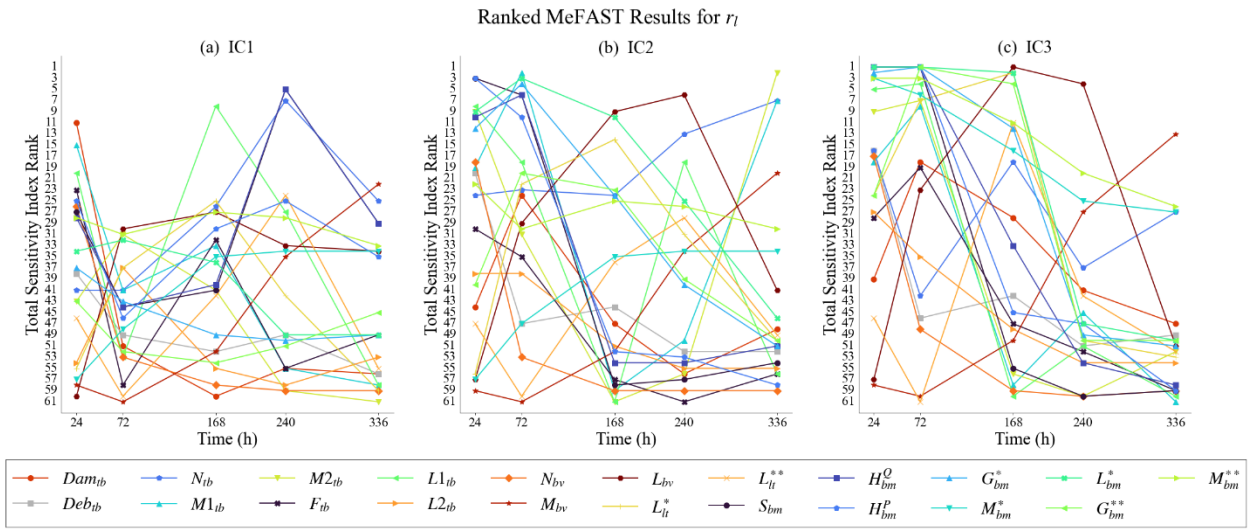


Figure 95. Ranked total sensitivity indices for r_I across all 105 MeFAST outputs for (a) IC1, superficial thermal burn; (b) IC2, superficial partial thickness thermal burn; and (c) IC3, deep partial thickness thermal burn.

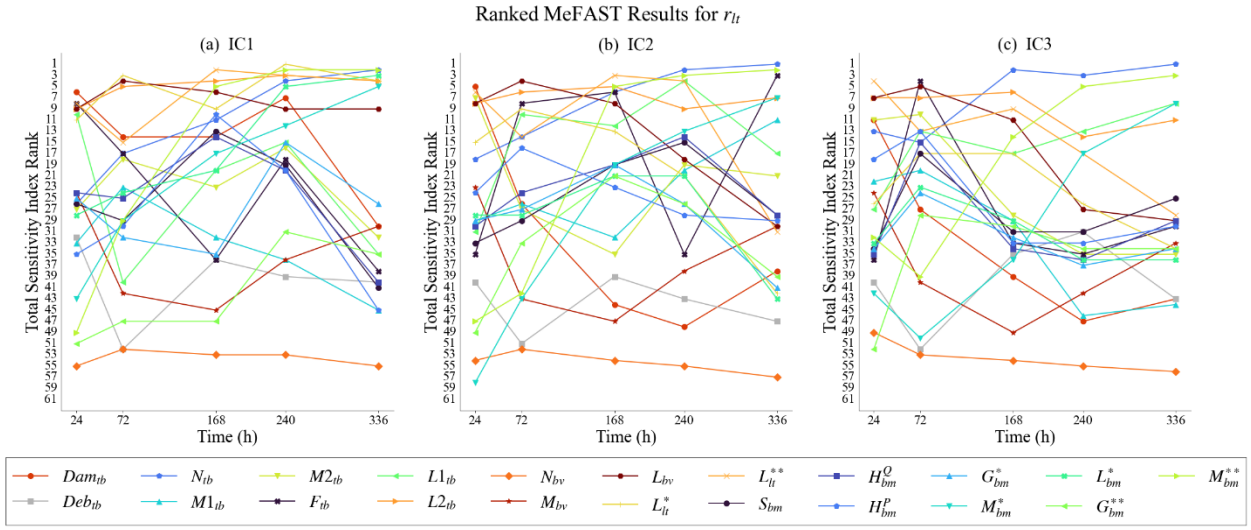


Figure 96. Ranked total sensitivity indices for r_{lt} across all 105 MeFAST outputs for (a) IC1, superficial thermal burn; (b) IC2, superficial partial thickness thermal burn; and (c) IC3, deep partial thickness thermal burn.

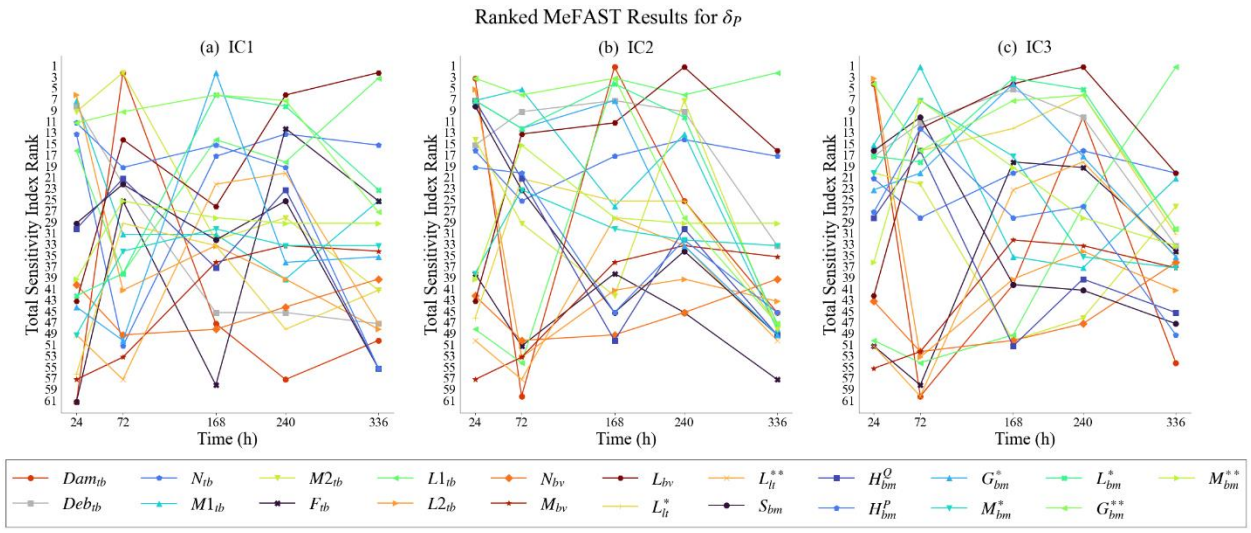


Figure 97. Ranked total sensitivity indices for δ_P across all 105 MeFAST outputs for (a) IC1, superficial thermal burn; (b) IC2, superficial partial thickness thermal burn; and (c) IC3, deep partial thickness thermal burn.

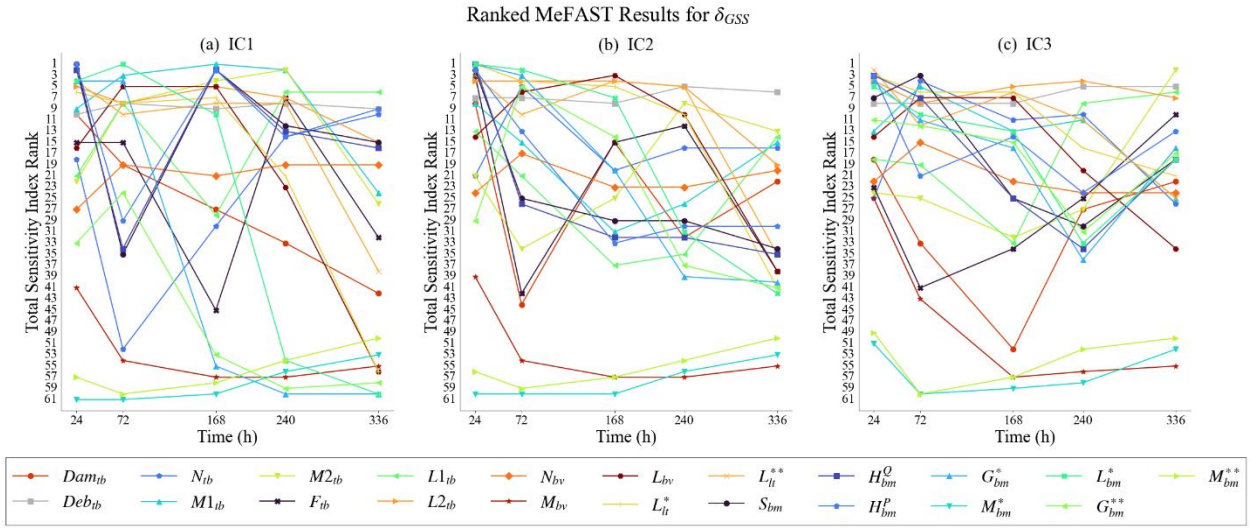


Figure 98. Ranked total sensitivity indices for δ_{GSS} across all 105 MeFAST outputs for (a) IC1, superficial thermal burn; (b) IC2, superficial partial thickness thermal burn; and (c) IC3, deep partial thickness thermal burn.

C.2.2. Heatmaps of Statistical Significance

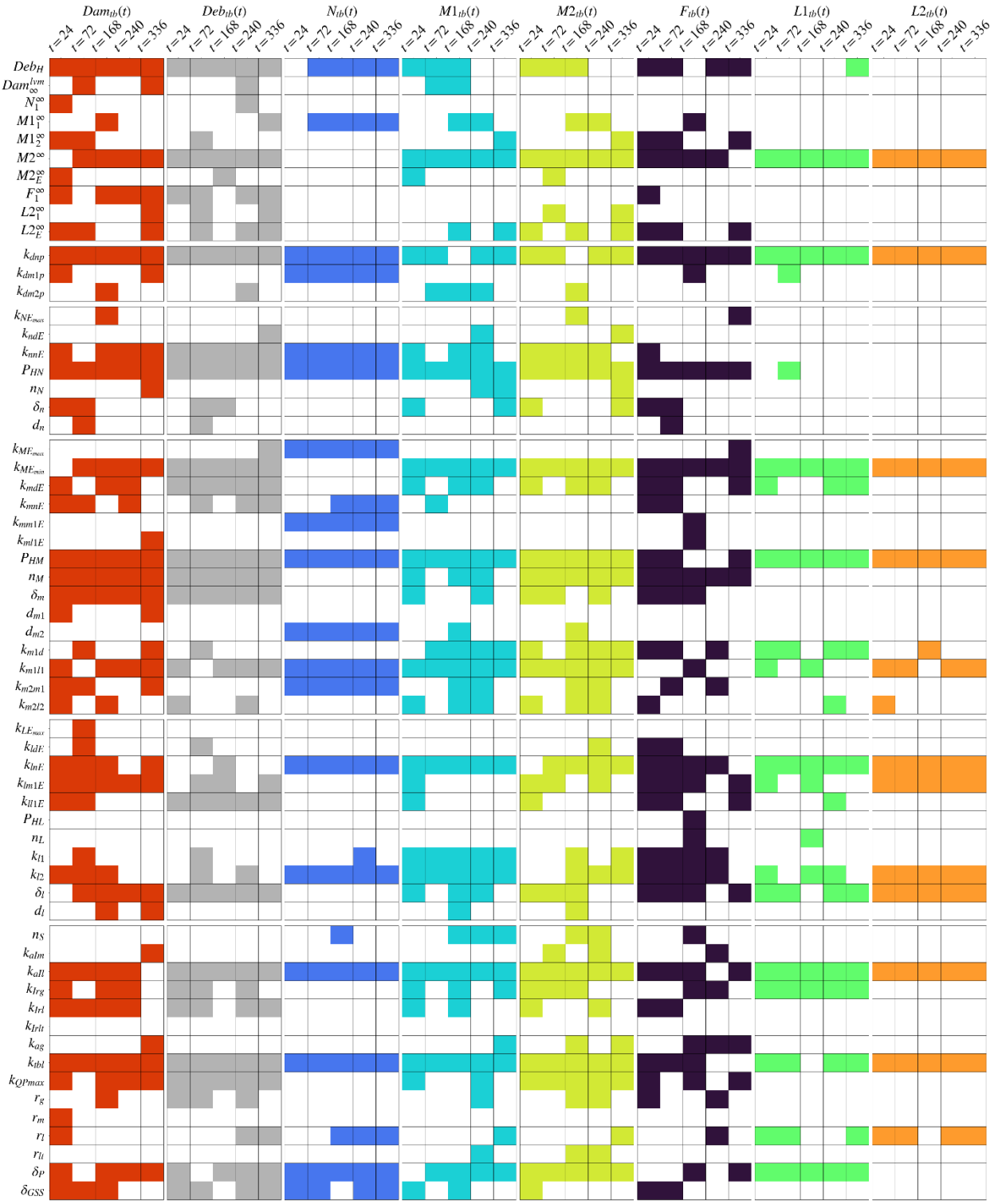


Figure 99. Significance results of MeFAST for parameters of the systemic TDPM with respect to the state variables of the thermal burn compartment for IC1 at days one, three, five, seven, and ten post-injury. A shaded box indicates that the parameter was flagged as statistically significant at the respective state variable and time point by at least two of the three tests performed during MeFAST. These significance results were passed through the algorithm presented in Section 3.1.3 to determine whether each parameter should be estimated or fixed during parameterization.

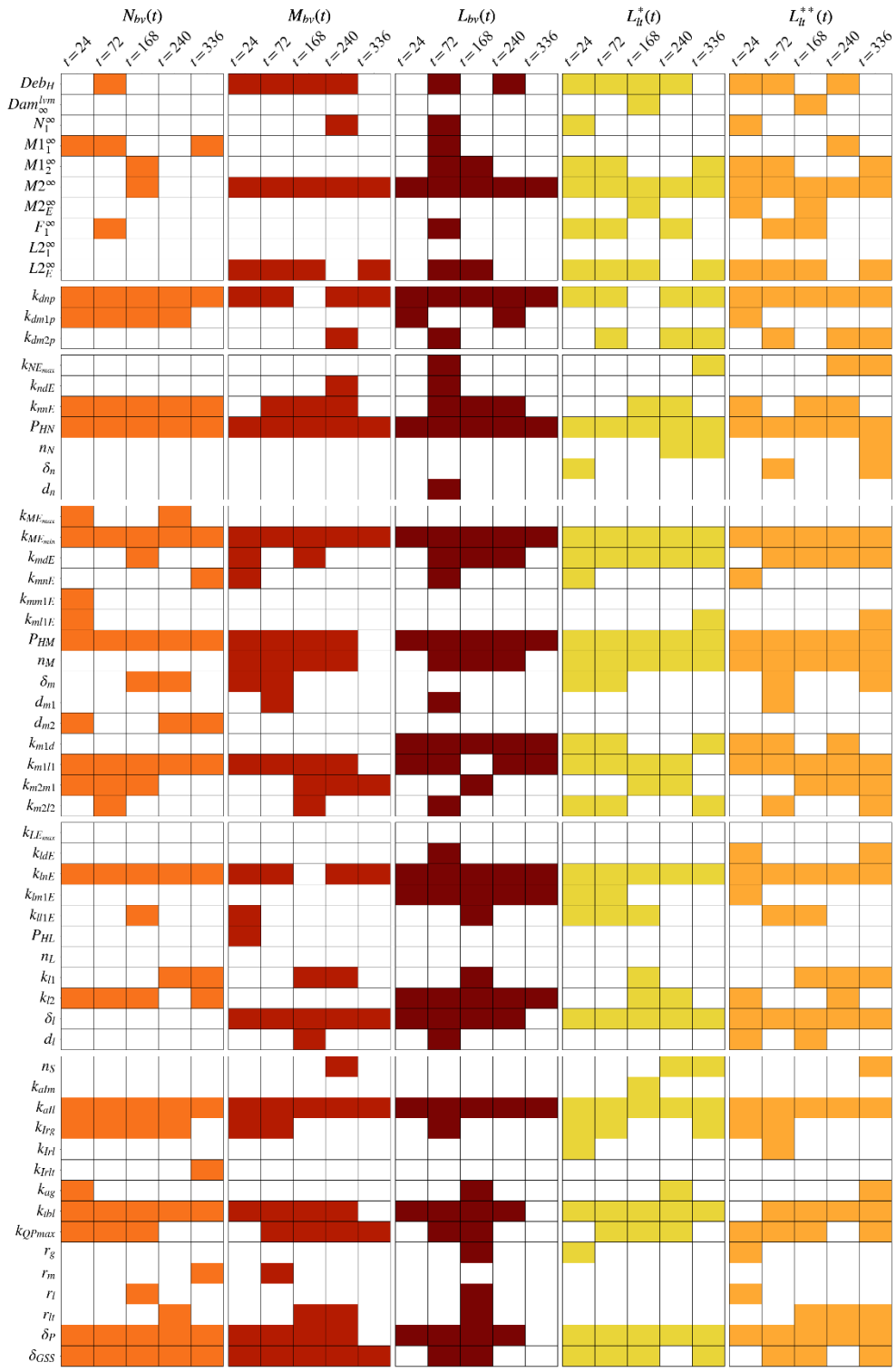


Figure 100. Significance results of MeFAST for parameters of the systemic TDPM with respect to the state variables of the blood vessel and lymphatic tissue compartments for IC1 at days one, three, five, seven, and ten post-injury. A shaded box indicates that the parameter was flagged as statistically significant at the respective state variable and time point by at least two of the three tests performed during MeFAST. These significance results were passed through the algorithm presented in Section 3.1.3 to determine whether each parameter should be estimated or fixed during parameterization.

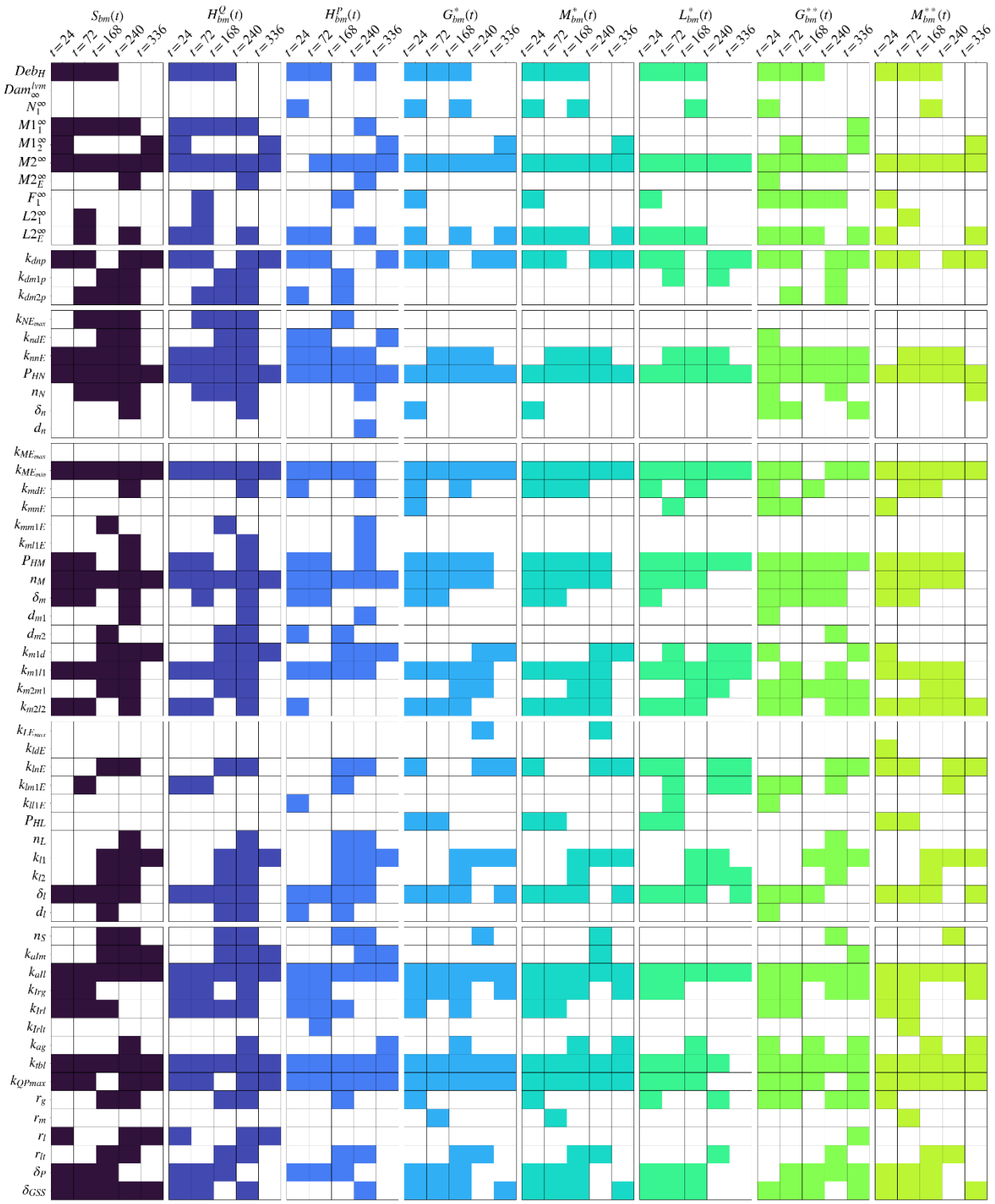


Figure 101. Significance results of MeFAST for parameters of the systemic TDPM with respect to the state variables of the bone marrow compartment for IC1 at days one, three, five, seven, and ten post-injury. A shaded box indicates that the parameter was flagged as statistically significant at the respective state variable and time point by at least two of the three tests performed during MeFAST. These significance results were passed through the algorithm presented in Section 3.1.3 to determine whether each parameter should be estimated or fixed during parameterization.

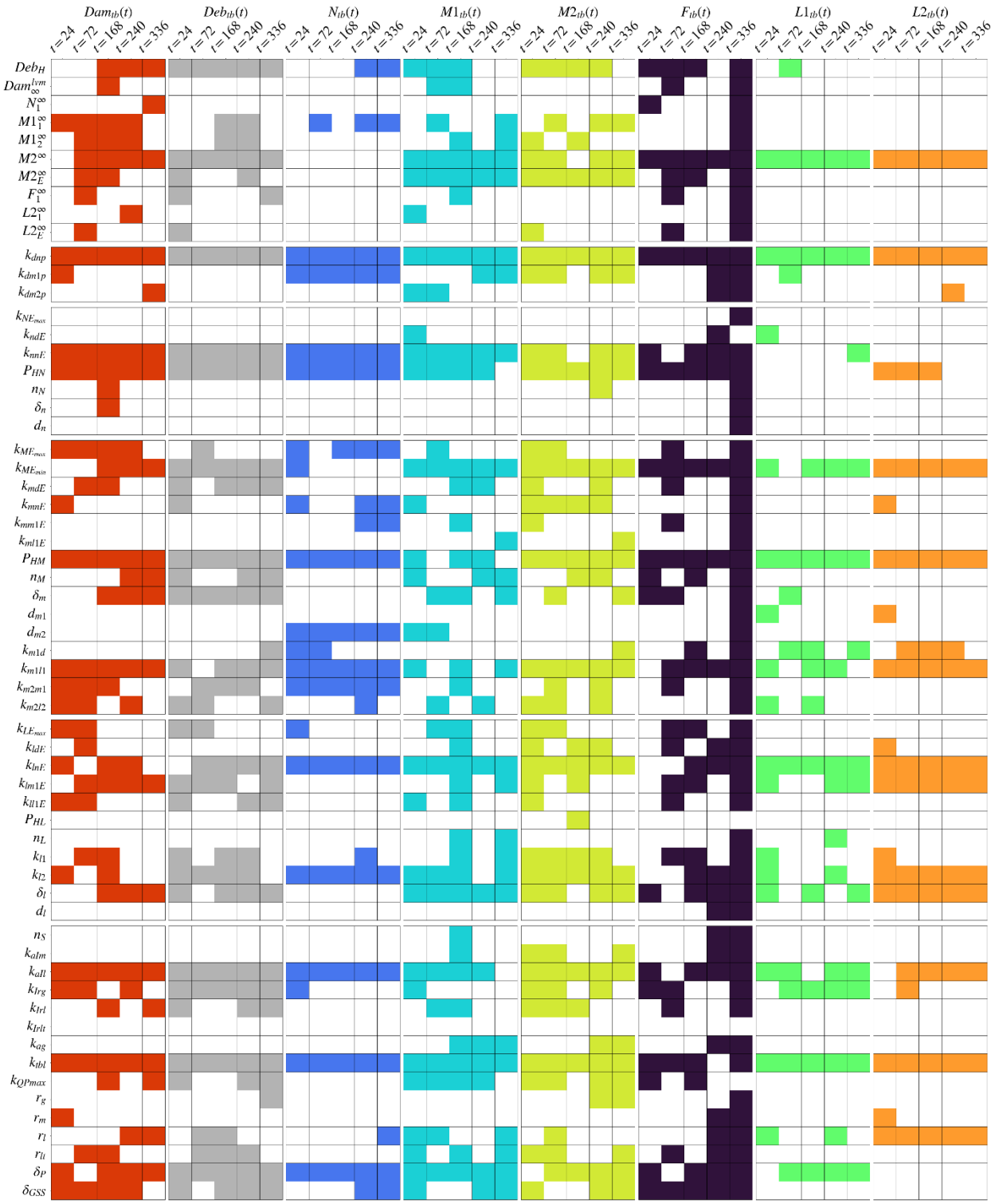


Figure 102. Significance results of MeFAST for parameters of the systemic TDPM with respect to the state variables of the thermal burn compartment for IC2 at days one, three, five, seven, and ten post-injury. A shaded box indicates that the parameter was flagged as statistically significant at the respective state variable and time point by at least two of the three tests performed during MeFAST. These significance results were passed through the algorithm presented in Section 3.1.3 to determine whether each parameter should be estimated or fixed during parameterization.

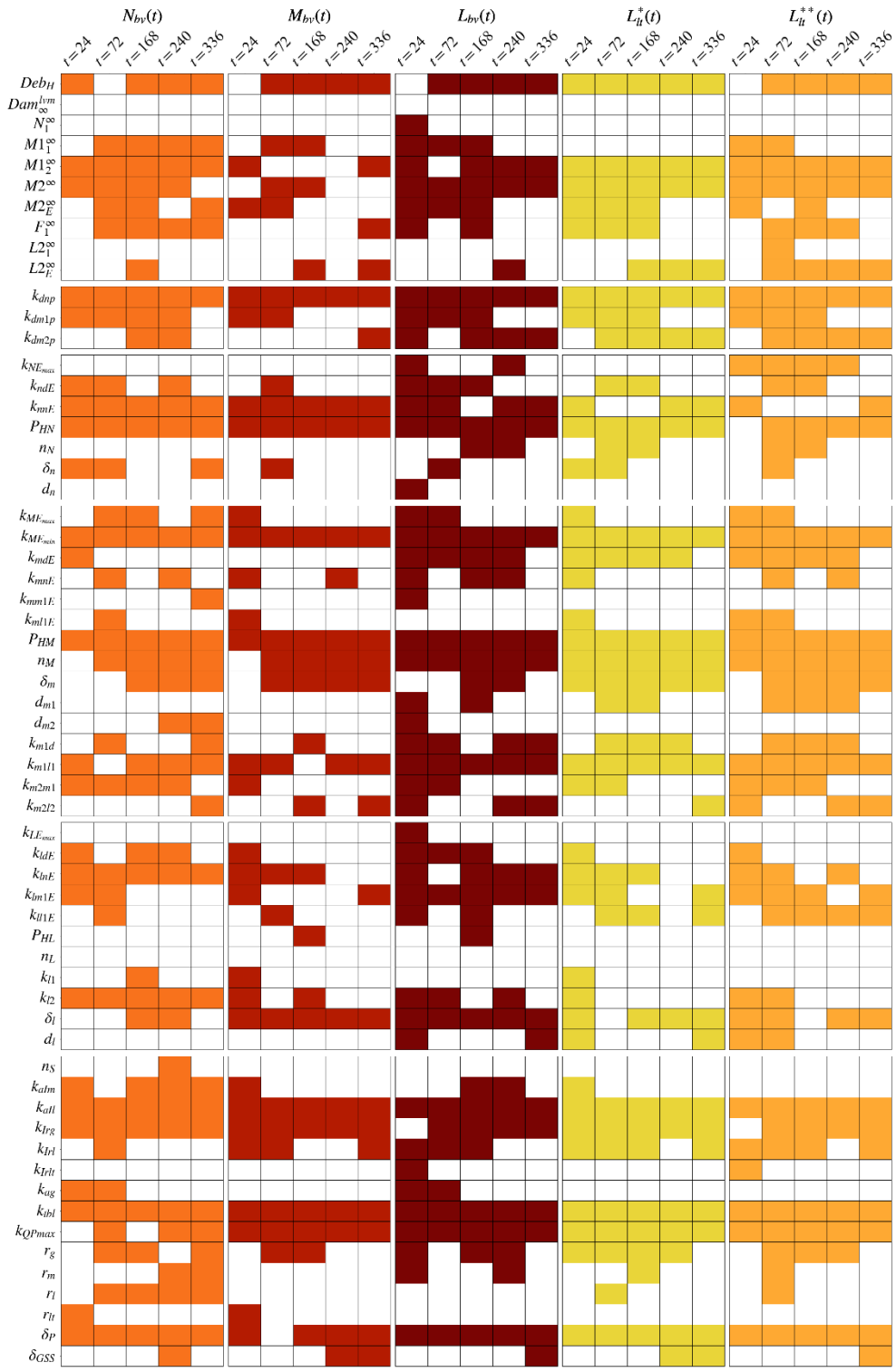


Figure 103. Significance results of MeFAST for parameters of the systemic TDPM with respect to the state variables of the blood vessel and lymphatic tissue compartments for IC2 at days one, three, five, seven, and ten post-injury. A shaded box indicates that the parameter was flagged as statistically significant at the respective state variable and time point by at least two of the three tests performed during MeFAST. These significance results were passed through the algorithm presented in Section 3.1.3 to determine whether each parameter should be estimated or fixed during parameterization.

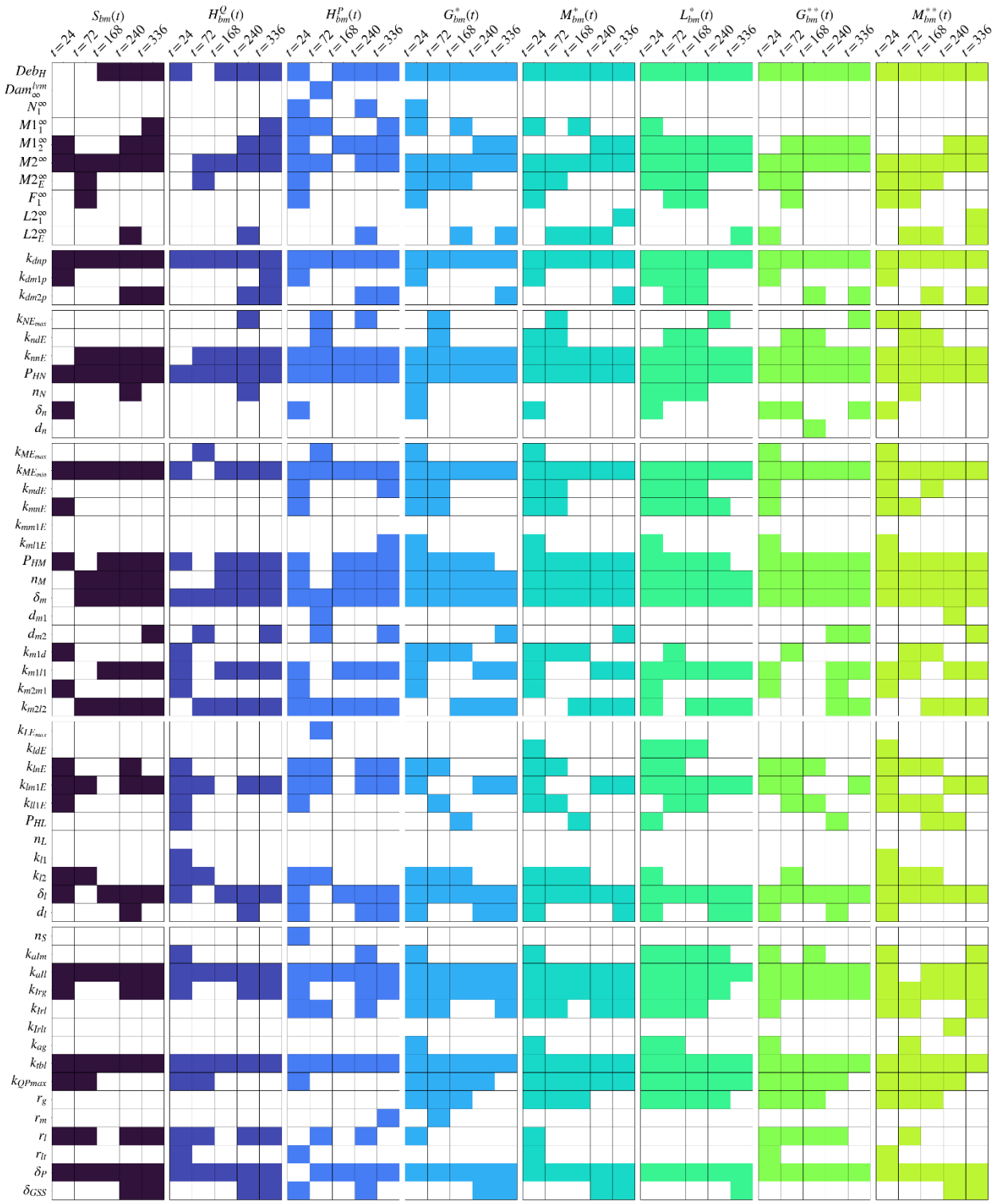


Figure 104. Significance results of MeFAST for parameters of the systemic TDPM with respect to the state variables of the bone marrow compartment for IC2 at days one, three, five, seven, and ten post-injury. A shaded box indicates that the parameter was flagged as statistically significant at the respective state variable and time point by at least two of the three tests performed during MeFAST. These significance results were passed through the algorithm presented in Section 3.1.3 to determine whether each parameter should be estimated or fixed during parameterization.

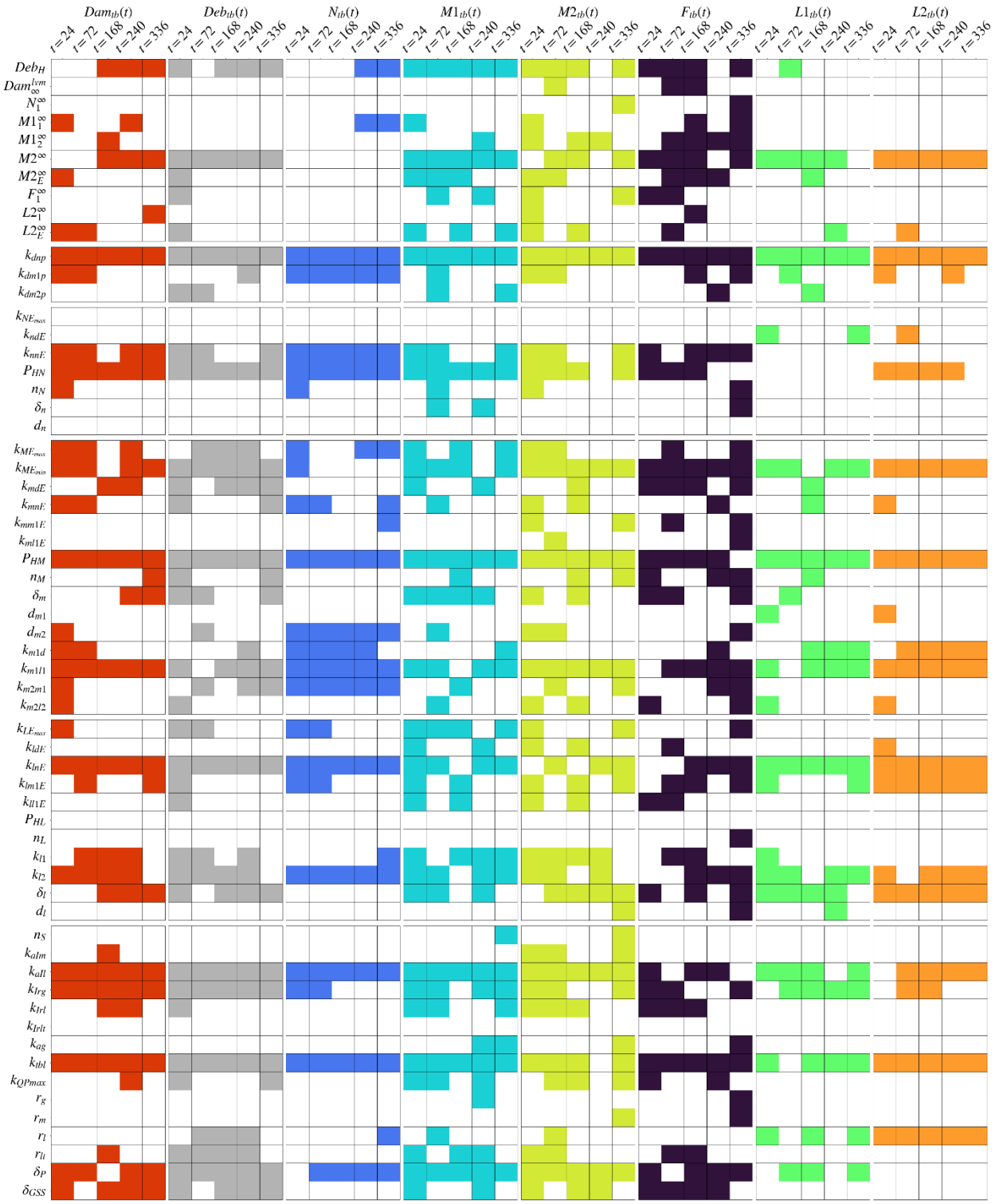


Figure 105. Significance results of MeFAST for parameters of the systemic TDPM with respect to the state variables of the thermal burn compartment for IC3 at days one, three, five, seven, and ten post-injury. A shaded box indicates that the parameter was flagged as statistically significant at the respective state variable and time point by at least two of the three tests performed during MeFAST. These significance results were passed through the algorithm presented in Section 3.1.3 to determine whether each parameter should be estimated or fixed during parameterization.

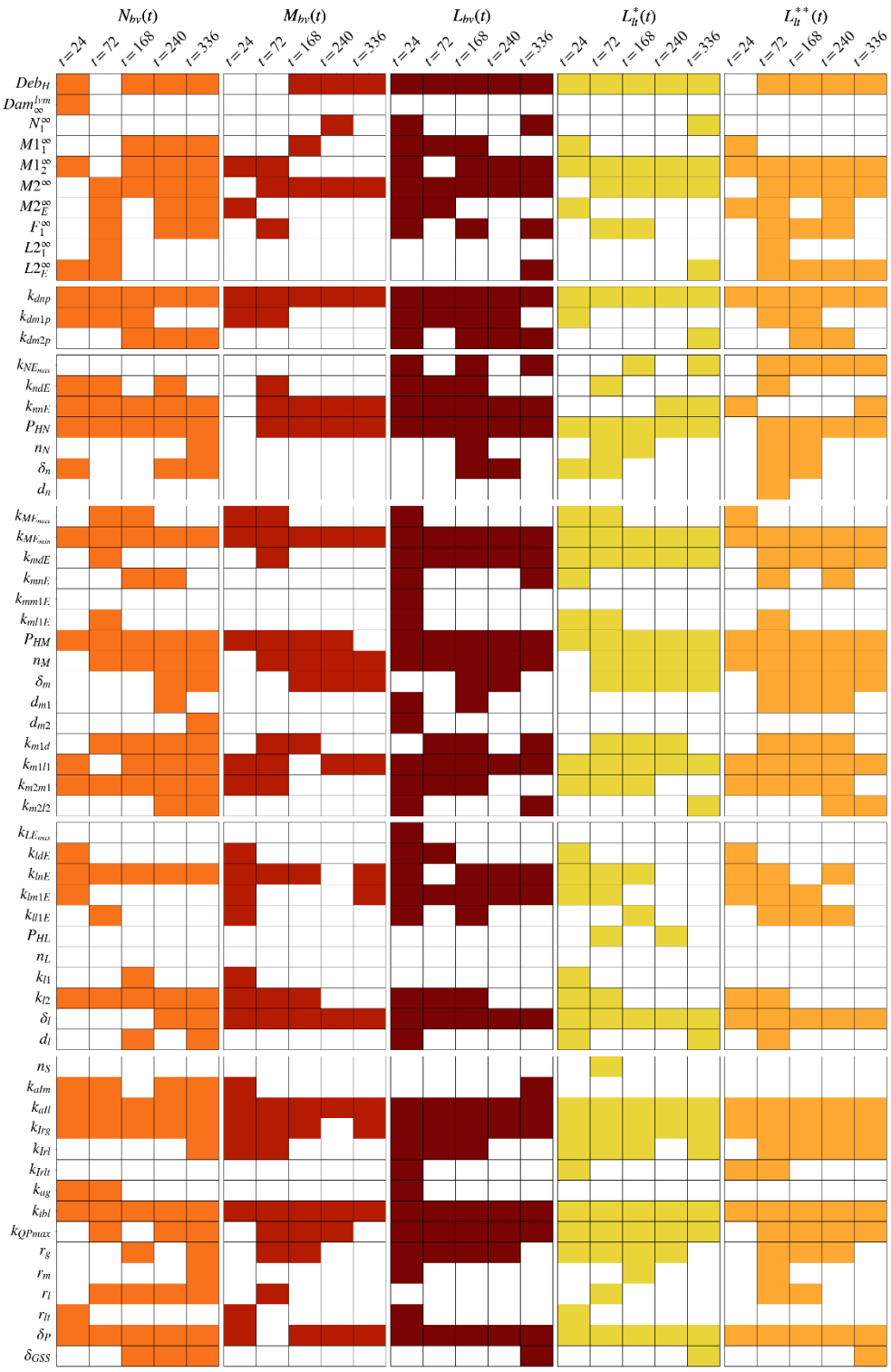


Figure 106. Significance results of MeFAST for parameters of the systemic TDPM with respect to the state variables of the blood vessel and lymphatic tissue compartments for IC3 at days one, three, five, seven, and ten post-injury. A shaded box indicates that the parameter was flagged as statistically significant at the respective state variable and time point by at least two of the three tests performed during MeFAST. These significance results were passed through the algorithm presented in Section 3.1.3 to determine whether each parameter should be estimated or fixed during parameterization.

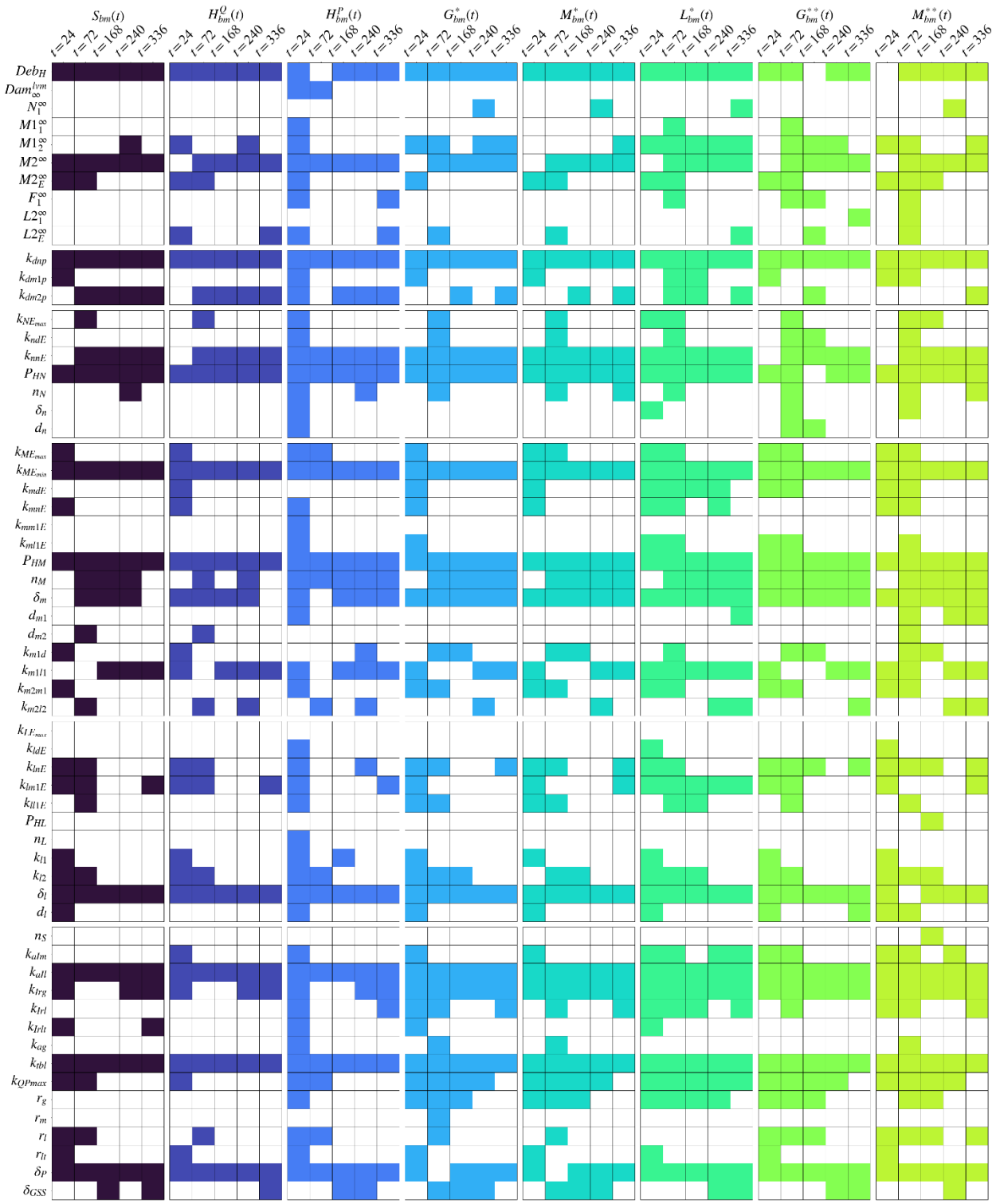


Figure 107. Significance results of MeFAST for parameters of the systemic TDPM with respect to the state variables of the bone marrow compartment for IC3 at days one, three, five, seven, and ten post-injury. A shaded box indicates that the parameter was flagged as statistically significant at the respective state variable and time point by at least two of the three tests performed during MeFAST. These significance results were passed through the algorithm presented in Section 3.1.3 to determine whether each parameter should be estimated or fixed during parameterization.

Appendix D. Acronyms and Abbreviations

AC	Acceptability criteria
ARA	Applied Research Associates, Inc.
DTRA	Defense Threat Reduction Agency
eFAST	Extended Fourier amplitude sensitivity test
GSA	Global sensitivity analysis
HENRE	Health Effects from Nuclear Radiological Environments
IC	Initial condition
LHS	Latin hypercube sampling
LITBM	Locally irradiated thermal burn model
NUDET	Nuclear Detonation Event
MeFAST	Multi-test extended Fourier amplitude sensitivity test
ODE	Ordinary differential equation
SA	Sensitivity Analysis
STBM	Superficial thermal burn model
TDPM	Time-dependent physiological model
TR	Technical report
WITBM	Widespread irradiated thermal burn model (i.e., time-dependent physiological model for combined injury following thermal burn and widespread radiation exposure)